

https://dspace.org/

# Kinetics and mechanism of the reduction of Mamatwan manganese ore fines by solid carbon

**Burucu, E**

**1991**

http://hdl.handle.net/10539/22033

Burucu, E. (1991) Kinetics and mechanism of the reduction of Mamatwan manganese ore fines by solid carbon, University of he Witwatersrand, Johannesburg <http://wiredspace.wits.ac.za/handle/10539/22033>

Downloaded from a DSpace repository. https://dspace.org/

# KINETICS AND MECHANISM OF THE REDUCTION OF MAMATWAN MANGANESE ORE FINES BY SOLID CARBON

E. Burucu

A dissertation submitted to the Faculty of Engineering, University of Witwatersrand, Johannesburg, in fulfilment of the requirements for the degree of Master of Science in Engineering

Johannesburg, 1991

DECLARATION

I declare that this dissertation is my own, unaided work. It is being submitted for the degree of Master of Science in Engineering in the University of the Witwatersrand, Johannesburg. It has not been submitted before for any degree or examination in any other university.

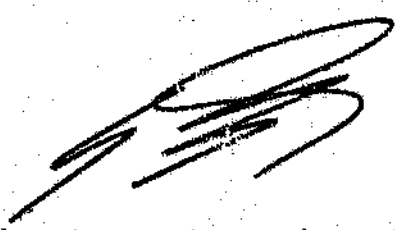

(Signature of candidate)

22 th day of February, 1991

**ABSTRACT**

The kinetics of reduction of the manganese ore from the Mamatwan mine has been studied by thermogravimetric (TGA) analysis, X-ray diffraction analysis (XRD), optical microscopy, and energy dispersive analysis of x-rays (EDAX) between 1100 and 1350°C with pure graphite under argon atmosphere. It has been observed that the rate and degree of reduction increased with increasing temperature and decreasing particle size.

The effect of the different reaction atmosphere has also been investigated by replacing argon atmosphere with carbonmonoxide (CO) and carbondioxide ($CO_2$). The results clarified importance of some reactions in the reduction mechanism of the ore.

In early stages of reduction, up to about 4 minutes of reaction time, carbothermic reduction of higher oxides of manganese and iron ($Mn_2O_3$ and $Fe_2O_3$) to manganeous oxide (MnO) and metallic iron respectively was observed which was controlled by diffusional process across the boundary layer between the solid phases. Apparent activation energy is calculated as 61.03 kJ for this stage which corresponds to about 30 percent reduction.

Metallization started as random nucleation of iron rich carbides around MnO grains inside the particle. After 30 percent reduction the formation of a silicate phase was observed. Up to 70 percent reduction at 1350°C, reduction rate was controlled by chemical reaction between oxide phase and gaseous phase with an apparent activation energy of 153.32 kJ.

**ABSTRACT**

The kinetics of reduction of the manganese ore from the Mamatwan mine has been studied by thermogravimetric (TGA) analysis, X-ray diffraction analysis (XRD), optical microscopy, and energy dispersive analysis of x-rays (EDAX) between 1100 and 1350°C with pure graphite under argon atmosphere. It has been observed that the rate and degree of reduction increased with increasing temperature and decreasing particle size.

The effect of the different reaction atmosphere has also been investigated by replacing argon atmosphere with carbonmonoxide (CO) and carbondioxide ($CO_2$). The results clarified importance of some reactions in the reduction mechanism of the ore.

In early stages of reduction, up to about 4 minutes of reaction time, carbothermic reduction of higher oxides of manganese and iron ($Mn_2O_3$ and $Fe_2O_3$) to manganeous oxide (MnO) and metallic iron respectively was observed which was controlled by diffusional process across the boundary layer between the solid phases. Apparent activation energy is calculated as 61.03 kJ for this stage which corresponds to about 30 percent reduction.

Metallization started as random nucleation of iron rich carbides around MnO grains inside the particle. After 30 percent reduction the formation of a silicate phase was observed. Up to 70 percent reduction at 1350°C, reduction rate was controlled by chemical reaction between oxide phase and gaseous phase with an apparent activation energy of 153.32 kJ.

The later part of the reduction proceeded by the reduction of MnO covered by either the carbide or silicate phase by carbon dissolved in carbide phase $(Mn, Fe)_5C_2$. Diffusion of $Mn^{+2}$ ions in oxide phase is the most likely rate determining phase for this stage. Apparent activation energy was found to be as 310.40 kJ.

## ACHIEVEMENTS

It has been shown that the low grade Mamatwan manganese ore could be upgraded to yield a material with suitable manganese and iron content by a carbothermic reduction process, prior to smelting. Since the prereduced material contained no volatiles and considerably less oxygen compared to the ore, it may result smoother smelting operation, reduction in the energy cost and efficiency increase in the ferromanganese production.

The prereduction caused sintering in the material at temperatures particularly above 1200°C. Therefore it would be more convenient in the industrial practice to reduce manganese oxides in the ore to the MnO rather than metallic level which could be achieved at temperatures both 1100°C and 1200°C.

This dissertation is dedicated to my family,

(* Bedrettin Burucu *)
Aysel Burucu
Esma Konuk
(* Fazil Burucu *)

**ACKNOWLEDGEMENTS**

The author would like to express his appreciation and thanks to:

a) His supervisor, Prof. R.H. Eric, whose help and advice made this work possible.

b) The Council for Mineral Technology, (MINTEK), for sponsoring this work.

c) Ferro Alloy Producer' Association of South Africa (FAPA) which supplied a grant towards the work on ferroalloys of the Pyrometallurgy Research Group.

d) Charlotte Swanepoel for her support during this period.

e) Guven Akdogan for his suggestions

CONTENTS


| | | Page |
|---|---|---|
| DECLARATION | | ii |
| ABSTRACT | | iii |
| ACHIEVEMENTS | | iv |
| DEDICATION | | v |
| ACKNOWLEDGEMENTS | | vi |
| CONTENTS | | vii |
| LIST OF FIGURES | | ix |
| LIST OF TABLES | | xv |
| 1. | INTRODUCTION | 1.1 |
| 1.1 | Statement of the Problem | 1.1 |
| 1.2 | Manganese Metal | 1.3 |
| 1.3 | Manganese Ore in South Africa | 1.4 |
| 2. | LITERATURE SURVEY | 2.1 |
| 2.1 | The Studies on Reduction of MnO and Mamatwan Ore | 2.1 |
| 2.2 | The Studies on Manganese Oxides | 2.18 |
| 2.3 | Thermodyanamic Data on Manganese Oxide Reduction | 2.19 |
| 2.4 | The System C-Mn and C-Fe-Mn | 2.39 |
| 3. | EXPERIMENTAL PROCEDURE | 3.1 |
| 3.1 | Raw Materials | 3.1 |
| 3.2 | Description of Equipment | 3.2 |

| | | |
|---|---|---|
| 3.3 | Reduction Runs | 3.6 |
| 3.4 | Definition of the Degree of Reduction | 3.8 |
| 3.5 | X-ray Diffraction Analysis | 3.12 |
| 3.6 | Optical Examination and Energy Dispersive Analysis of X-rays (EDAX) | 3.12 |
| 3.7 | Chemical Analysis | 3.12 |
| **4.** | **EXPERIMENTAL RESULTS AND DISCUSSIONS** | **4.1** |
| 4.1 | Kinetic Results | 4.1 |
| 4.2 | Investigation of Reaction Products | 4.19 |
| 4.3 | Reduction Mechanism | 4.48 |
| 4.3.1 | Theory of Oxide Reduction by Graphite | 4.48 |
| 4.3.2 | First Stage of Reduction | 4.52 |
| 4.3.3 | Second Stage of Reduction | 4.55 |
| 4.3.4 | Third Stage of Reduction | 4.58 |
| **5.** | **MATHEMATICAL ANALYSIS OF KINETIC DATA** | **5.1** |
| 5.1 | Introduction | 5.1 |
| 5.2 | Review of Some Solid State Models | 5.2 |
| 5.2.1 | Diffusion Model | 5.2 |
| 5.2.2 | Phase Boundary Model | 5.4 |
| 5.2.3 | Nuclei-Growth Model | 5.5 |
| 5.3 | Analysis of Experimental Data | 5.6 |
| **6.** | **CONCLUSION** | **6.1** |
| **7.** | **REFERENCES** | **7.1** |

## LIST OF FIGURES


| Figure | | Page |
|---|---|---|
| 2.1 | Effect of MnO-to-C ratio on the reduction of MnO by graphite (after Rankin) | 2.10 |
| 2.2 | Effect of temperature on the reduction of MnO by graphite (after Rankin) | 2.11 |
| 2.3 | Effect of particle size on the reduction of MnO by graphite (After Rankin) | 2.12 |
| 2.4 | Effect of temperature on the reduction of MnO by graphite (after Terayama) | 2.13 |
| 2.5 | Effect of particle size on the reduction of MnO by graphite (after Terayama) 2.7 | 2.14 |
| 2.6 | Effect of MnO-to-C ratio on the reduction of MnO by graphite (after Terayama) 2.8 | 2.15 |
| 2.7 | Effect of temperature on the reduction of Mamatwan ore by graphite (after Grimsley) | 2.16 |
| 2.8 | Effect of carbon amount on the reduction of Mamatwan ore by graphite (after Grimsley) | 2.17 |
| 2.9 | Equilibrium curve between $MnO_2$ and $Mn_2O_3$ | 2.25 |
| 2.10 | Equilibrium curve between $Mn_2O_3$ and $Mn_3O_4$ | 2.26 |

| | | |
|---|---|---|
| 2.11 | The system $Mn_2O_3$ - $Mn_3O_4$ | 2.27 |
| 2.12 | The system MnO - $Mn_3O_4$ | 2.28 |
| 2.13 | Free energy change of MnO reduction reactions | 2.29 |
| 2.14 | Entalphy change of MnO reduction reactions | 2.30 |
| 2.15 | Free energy change of reduction reactions of $Mn_2O_3$ and $Mn_3O_4$ | 2.31 |
| 2.16 | Entalphy change of reduction reactions of $Mn_2O_3$ and $Mn_3O_4$ | 2.32 |
| 2.17 | Free energy change of dissociation reactions of manganese oxides | 2.33 |
| 2.18 | Entalphy change of dissociation reactions of manganese oxides | 2.34 |
| 2.19 | CaO - $Mn_2O_3$ phase diagram | 2.35 |
| 2.20 | The system CaO - MnO - $SiO_2$ (below 1000$^oC$) | 2.36 |
| 2.21 | The system CaO - MnO - $SiO_2$ (above 1000$^oC$) | 2.37 |
| 2.22 | Ternary phase diagram of CaO - MnO - $SiO_2$ | 2.38 |
| 2.23 | Binary Mn-C phase diagram | 2.41 |
| 2.24 | The system C-Fe-Mn | 2.42 |
| 2.25 | Pourbaix diagram for the Mn-O-C system | 2.43 |

| | | |
|---|---|---|
| 3.1 | Molybdenum-wound resistance furnace | 3.4 |
| 3.2 | Experimental Apparatus | 3.5 |
| 4.1 | Effect of preheating on the Mamatwan ore at 1000°C | 4.7 |
| 4.2 | Effect of temperature on the reduction of Mamatwan ore (ore is - 0.420 mm) | 4.8 |
| 4.3 | Effect of temperature on the mass loss of the Mamatwan ore. | 4.9 |
| 4.4 | Effect of particle size on the reduction (1100°C) | 4.10 |
| 4.5 | Effect of particle size on the reduction (1200°C) | 4.11 |
| 4.6 | Effect of particle size on the reduction (1300°C) | 4.12 |
| 4.7 | Effect of particle size on the reduction (1350°C) | 4.13 |
| 4.8 | Reduction versus particle size curves | 4.14 |
| 4.9 | Effect of carbon amount on reduction at 1300°C | 4.15 |
| 4.10 | Effect of carbon particle size on reduction at 1300°C | 4.16 |
| 4.11 | Reduction versus time curves for pure $Mn_3O_4$ at 1300°C and 1350°C | 4.17 |

| | | |
|---|---|---|
| 4.12 | Reduction of Mamatwan ore under $CO_2$ and CO atmospheres at 1300°C | 4.18 |
| 4.13 | Microstructure of a manganese ore grain subjected to 26.64 % reduction at 1350 °C | 4.28 |
| 4.14 | Microstructure of a manganese ore grain subjected to 38.14 % reduction at 1350 °C | 4.29 |
| 4.15 | Microstructure of a manganese ore grain subjected to 45.54 % reduction at 1350 °C | 4.30 |
| 4.16 | Microstructure of a manganese ore grain subjected to 68.09 % reduction at 1350 °C | 4.31 |
| 4.17 | Microstructure of a manganese ore grain subjected to 78.03 % reduction at 1350 °C | 4.32 |
| 4.18 | Microstructure of a manganese ore grain subjected to 86.83 % reduction at 1350 °C | 4.33 |
| 4.19 | Microstructure of a manganese ore grain subjected to 92.15 % reduction at 1350 °C | 4.34 |
| 4.20 | Microstructure of a manganese ore grain subjected to 94.01 % reduction at 1350 °C | 4.35 |
| 4.21 | Microstructure of a manganese ore grain subjected to 52.61 % reduction at 1300 °C | 4.36 |
| 4.22 | Microstructure of a manganese ore grain subjected to 82.45 % reduction at 1300 °C | 4.37 |
| 4.23 | Microstructure of a manganese ore grain subjected to 53.09 % reduction at 1200 °C | 4.38 |

| | | |
|---|---|---|
| 4.24 | Microstructure of a manganese ore grain subjected to 37.81 % reduction at 1100 $^{o}$C | 4.39 |
| 4 25 | Microstructure of a manganese ore grain subjected to 50 minutes reduction at 1350 $^{o}$C | 4.40 |
| 4.26 | Microstructure of a manganese ore grain subjected to 10 minutes reduction at 1350 $^{o}$C | 4.41 |
| 4.27 | Microstructure of a cracked grain reduced at 1300$^{o}$C for 25 minutes | 4.42 |
| 4.28 | Microstructure showing the formation of oxide layer around ore grain (1350$^{o}$C, 2 minutes) | 4.43 |
| 4.29 | Carbon content of reaction mixture versus time curve at 1350$^{o}$C | 4.44 |
| 4.30 | Oxygen content of reaction mixture versus time curve at 1350$^{o}$C | 4.45 |
| 4.31 | Manganese content of reaction mixture versus time curve at 1350$^{o}$C. | 4.46 |
| 4.32 | Iron content of reaction mixture versus time curve at 1350$^{o}$C. | 4.47 |
| 5.1 | Arrhenius plot of the first stage data | 5.13 |
| 5.2 | Replotting of kinetic data by equation 5.9 | 5.14 |
| 5.3 | Regression analysis of Second stage data | 5.15 |
| 5.4 | Arrhenius plot of second stage data | 5.16 |

5.5 Application of equation 5.8 to the third stage data 5.17

5.6 Arrhenius plot of the third stage data. 5.18

## LIST OF TABLES


| Table | | Page |
|---|---|---|
| 1.1 | Manganese ore world production | 1.7 |
| 1.2 | Estimate of reserves in the Kalahari manganese deposit | 1.8 |
| 1.3 | Typical chemical analysis of manganese ore from Kalahari deposit | 1.8 |
| 1.4 | The major minerals found in the kalahari deposit and their physical properties | 1.9 |
| 2.1 | Free energy changes for the manganese oxides reduction reactions by carbon and CO | 2.22 |
| 2.2 | Free energy changes for the manganese oxides reduction reactions by iron carbide | 2.23 |
| 2.3 | Properties of manganese carbides | 2.24 |
| 3.1 | Screen analysis of Mamatwan ore | 3.10 |
| 3.2 | Chemical analysis of Mamatwan ore | 3.11 |
| 4.1 | Linear relationship between reduction and particle size | 4.4 |
| 4.2 | Mineralogical Analysis of Mamatwan ore | 4.24 |

| | | |
|---|---|---|
| 4.3 | X-ray Analysis of Reaction products at 1300 $^{o}$C and 1350$^{o}$C | 4.25 |
| 4.4 | EDAX Analysis of Metal Phase in reaction products at 1350 $^{o}$C | 4.26 |
| 4.5 | Variations of iron, manganese, carbon and oxygen of reaction mixture at 1350$^{o}$C | 4.27 |
| 5.1 | Tabulation of regression analysis of second stage kinetic data | 5.10 |
| 5.2 | Tabulation of diffusion values for third stage | 5.11 |

# 1 INTRODUCTION

## 1.1 Statement of the Problem

From a theoretical smelting balance, Featherstone (1975) concludes that Mamatwan ore can not be regarded as a suitable source on its own for the production of high grade ferromanganase. Another problem which is causing increasing concern among ferroalloy producers is the high percentage of fines present in the furnace feed. These fines, which originate mainly from the ore, reduce the porosity of the furnace bed resulting in unstable operating conditions characterized by frequent blow-outs and eruptions (Maruse, 1975). More efficient methods for the treatment of fines involve screening, with subsequent agglomeration by briquetting, pelletizing or sintering. At its Mamatwan mine Samancor has recently established a plant for sintering of manganese ore (Geyicke, 1989). It is expected that this plant should significantly improve the cost effectiveness or Samancor's manganese alloy operations. As can be understood from the efforts in establishing the sintering plant by Samancor, methods currently in use by South Africa producers of ferromanganese and metal may not be optimum for the processing of lower grade ores & fines. Since it is becoming more important for the large reserves of lower-grade manganese ores like Mamatwan manganese ore to be utilised for the production of ferromanganese and manganese metal, more efficient techniques should be sought. One such technique is the prereduction of manganese ore with carbon to yield material with a suitable manganese

content. Prereduction of ores/concentrates, prior to smelting offers several advantages over the direct smelting such as:

a) Less carbon is required during smelting and therefore the overall operation and slag viscosity are more easily controlled with less sulphur or ash impurities introduced into the system.
b) More oxygen and volatiles are removed prior to smelting.
c) Prereduction can effectively use more readily available and much cheaper solid carbonaceous reductants for partial reduction of the ore so that less electrical energy is required in the submerged arc smelting furnaces.
d) Preheated material can be charged directly into the smelting furnace effectively using the heat generated in the reduction process.
e) Productivity is increased for a given furnace size.
f) Lower electrode consumption is possible.
g) Smoother smelting operation may be possible.
h) Higher recoveries are realized.

The current investigation was aimed at the determination of the kinetics, nature and extent of the reactions occurring during the reduction of Mamatwan manganese ore by carbon. Knowledge of the rate-controlling mechanism and the kinetics of the reduction of the manganese ore by carbon is also important in the prediction of the reduction reactions that may take place in upper portions of ferromanganese furnace and in rotary kilns.

The degree and mechanism of reduction of Mamatwan manganese ore by solid carbon was determined at temperatures from 1100°C to 1350°C, the reduction being carried out in a resistance furnace in an argon atmosphere. The change in mass of the sample during reaction was measured with a thermobalance, and the products of reaction were examined by X-ray diffraction, optical microscopy and EDAX. Mathematical analysis of the kinetic data was done to clarify the rate controlling steps and calculate activation energies.

## 1.2 Manganese Metal

Manganese is probably the most versatile additive in the steel industry and has the added advantages of low cost and easy availability. A major use is as an alloy addition to steel where it acts as a desulphurizer and deoxidizer as well as providing improved strength and hardenability via suppressing the hardening transformation of steel on quenching. It is also added to silver, aluminum, copper, magnesium, nickel, titanium, and zinc alloys as an alloying element. In some alloys special properties are developed, such as high damping capacity, high permanent magnet characteristics (BiMn, AlMn) low expansion and high electrical resistivity (Morral, 1984).

Manganese can be added in the form of its ore during iron-making, or as ferromanganese in the steel-making stage. Various types and grades of ferromanganese, mostly containing from 70 to 90 percent manganese, are produced in large submerged arc furnaces.

In chemical industry manganese is used as an oxidizing agent in chemical processes and for the production of chemical compounds. Manganese compounds are used in pigments, colouring agents for glazes, glasses, and porcelains, bleaches for textiles, driers in paints, preservatives for wood and to increase tackiness in rubber as well as in the production of fireworks and matches. One of the most important single applications of manganese compounds is in the dry battery industry where manganese oxide is used as a depolarizing agent. Manganese is a constituent of medicines, fertilizers and fungicides as well as food stock additives since as a trace element it has nutritional value.

The manganese may be obtained from a number of sources which include manganiferous iron ore for use in the blast furnace, spiegeleisen or a low grade ferromanganese, medium-carbon ferromanganese, low-carbon ferromanganese, silicomanganese. However the high carbon ferromanganese has become the most widely produced and traded alloy in the world. Manganese metal is being increasely used instead of low-carbon ferromanganese in the production of stainless and alloy steels with very low carbon contents (Mikolajczak, 1974).

## 1.3 Manganese Ore in South Africa

The manganese ore production in South Africa is estimated to be the second largest in the world after those of the USSR ( See Table 1.1 ). The most important manganese occurrences in South Africa, which are located in the northern Cape province, extend from

Postmasburg northwards through Sishen, Hotazel, and Severn, virtually to the Botswana border, a distance of 350 Km. A gap of 55 Km separates them into the southern field and northern (Kalahari) field. While the ore in the Kalahari field is continuous from the Mamatwan mine to the Wessels mine in the north, only a few isolated erosion remnants occur as islands north of the Wessel mine. These fields differ in type of orebody, stratigraphic position and genesis (Kleyenstuber, 1982). Table 1.2 shows the estimate of reserves in the Kalahari manganese deposit

Mamatwan mine is the largest open-cast operation mining low-grade manganese ore within the Kalahari manganese field. This deposit was opened in 1963. Mamatwan type ore is a diagenetic to very low-grade metamorphic, carbonate-bearing braunitic manganolutite ore with a maximum manganese content of 38 to 40 percent ( See Table 1.3). Thrust faulting affected the strata to the west and in proximity to this zone of structural deformation Mamatwan-type ore has been hydrothermally upgraded to carbonate-poor, braunite, hausmannite, and bixbyite-bearing ore. This ore which has a manganese content of up to 60 percent is known as Wessel-type ore (Kleyenstuber, 1982).

Mamatwan ore is dark brown in colour and spotted throughout with white and/or light-brown ellipsoidal carbonate ooids. Braunite is the major manganese mineral present in the ore. Kutnahorite (manganese-dolomite) is representative of the carbonate ooids, but also occurs together with braunite in the

matrix. Typical values for the physical properties for the major minerals of the ore body are given in Table 1.4.

It may seem that with less than 40 mass percent manganese content, Mamatwan manganese ore is not suitable for smelting in electric furnace. However, the ores with favourable manganese-to-iron ratios, approximately 9 to 1, have been smelted successfully by Samancor at Meyerton in the Transvaal.

Table 1.1

Manganese ore : world production
(in million short tons gross weight (Moral, 1984))

| | | %Mn | 1980 | 1970 | 1960 |
|---|---|---|---|---|---|
| N.America | Mexico | 35 + | 0.493 | 0.302 | 0.171 |
| S.America | Cuba | 36-50 | | | 0.018 |
| | Argentina | 30-40 | 0.005 | 0.035 | |
| | Brazil | 38-50 | 2.601 | 2.071 | 1.101 |
| | Chile | 33-40 | 0.031 | 0.029 | 0.051 |
| Europe | Bulgaria | 30+ | 0.054 | 0.036 | |
| | Greece | 48-50 | 0.006 | 0.007 | |
| | Hungary | 30-33 | 0.097 | 0.186 | 0.136 |
| | Italy | 22+ | 0.010 | 0.055 | 0.055 |
| | U.S.S.R | 35 | 10.748 | 7.541 | 6.473 |
| | Rumania | | | | 0.193 |
| | Yugoslavia | 30+ | 0.033 | 0.016 | |
| Africa | Egypt | 28+ | | | |
| | Gabon | 50-53 | 2.366 | 1.602 | |
| | Ghana | 30-50 | 0.278 | 0.447 | 0.600 |
| | Morocco | 50-53 | 0.145 | 0.124 | 0.533 |
| | S.Africa | 30-48+ | 6.278 | 3.568 | 1.316 |
| | Sudan | 48 | | | |
| | Zaire | 30-57 | 0.018 | 0.382 | 0.420 |
| Asia | China | 20+ | 1.750 | 1.100 | 1.320 |
| | India | 10-54 | 1.814 | 1.820 | 1.321 |
| | Indonesia | 47-56 | 0.005 | 0.011 | |
| | Japan | 24-28 | 0.088 | 0.298 | 0.357 |
| | Pakistan | 35 | | | |
| | Philippines | 35-45 | 0.003 | 0.006 | |
| | Thailand | 46-50 | 0.060 | 0.026 | |
| | Turkey | 35-46 | 0.045 | 0.010 | |
| Oceania | Australia | 37-53 | 2.162 | 0.828 | 0.068 |
| | Fiji | 40+ | | 0.027 | 0.013 |
| Total | | | 29.091 | 20064 | 14959 |

Table 1.2

Estimate of Reserves in the Kalahari Manganese Deposit (after Taljaardt, 1982)

| Wessels Grade (Mt) | | Mamatwan Grade (Mt) | |
|---|---|---|---|
| +44 % Mn (60 % Mn + Fe) | = 330 | 38-40 % Mn | = 982 |
| 40-44 % Mn (60 % Mn + Fe) | = 30 | 30-38 % Mn | = 6284 |
| 36-40 % Mn (60 % Mn + Fe) | = 18 | 20-30 % Mn | = 5938 |
| 30-40 % Mn (5-10 % Fe) | = 31 | | |
| Subtotal | = 409 | Subtotal | = 13204 |
| Total Reserve = 13613 Mt (based on data from approximately 1337 boreholes) | | | |

Table 1.3

Typical Chemical Analysis of Manganese ore from the Kalahari Deposit ( in weight percent)

| | Mamatwan-type | | Wessels-type | |
|---|---|---|---|---|
| | Lumpy | Fines | Lumpy* | Lumpy |
| Mn | 37-38 | 35-37 | 38.09 | 47-48 |
| Fe | 4-6 | 7.0 | 2.15 | 11-14 |
| $SiO_2$ | 4-6 | 5-7 | 3.62 | 6-9 |
| CaO | 12-16 | 12-16 | 12-81 | 4-6 |
| MgO | 3-5 | 3-5 | 2.52 | 0.5-1.5 |
| $Al_2O_3$ | 1.0 | 1.0 max | N.A | 1.0 max |
| $Na_2O$ | 0.4 | 0.4 | N.A | 0.4 |
| $K_2O$ | 0.5 | 0.5 | N.A | 0.2 |
| P | 0.05 max | 0.05 | N.A | 0.05 max |
| S | 0.10 max | 0.10 | N.A | 0.15 |
| $CO_2$ | 15-17 | 15-17 | 16.08 | 1-3 |
| $H_2O$ | 3.5 | 5.0 | N.A | 2.3 |

* Analyses after Kleyenstuber (1979, 1984) others after SAMANCOR (1979)

Table 1.4

The More important of the major manganesc minerals found in the Kalahari manganese field

| Mineral | Colour | Hardness | Relative density | Other properties |
|---|---|---|---|---|
| Braunite | Brownish black | 6 | 4.8 | Non-magnetic |
| Braunite II | Brownish black | 6 | 4.8 | Non-magnetic |
| Hausmannite | Grey-black | 5.5 | 4.75 | Non-magnetic |
| Bixbyite | Dull-black | 6.5 | 4.9-5.0 | Non-magnetic |
| Cryptomelane | Dull-black | | 4.3 | Non-magnetic |
| Jacopsite | Iron-black | 6 | 4.75 | Magnetic |

## 2 LITERATURE SURVEY

### 2.1 The Studies on Reduction of MnO and Mamatwan Ore

Contrary to the importance to the ferromanganase industry, the amount of research carried out on the reduction of manganese ores, and of Mamatwan manganese ore in particular, is very limited. The literature pertinent to this work is summarised in the following.

The major mineral present in Mamatwan ore is braunite the composition of which is generally accepted as being $3Mn_2O_3.MnSiO_3$ (Kleyenstuber, 1982). De Villiers (1975 ) and Muan (1959) both point that this is the ideal composition. Muan showed that braunite is part of a continuous solid solution of $SiO_2$ in $Mn_2O_3$, varying from pure $Mn_2O_3$ to 40 mass per cent $SiO_2$. De Villiers (1975) explains the solid solution of $SiO_2$ and $Mn_2O_3$ proposed by Muan in terms of the substitution of silicon ions for manganese ions in the $Mn_2O_3$ lattice. The $Si^{4+}$ ion replaces a $Mn^{3+}$ ion and charge balance is regained by the opposite $Mn^{3+}$ ion in the octahedral cation arrangement being reduced to $Mn^{2+}$. This theory suggests that substitution by silica will reach a maximum when all the $Mn^{+3}$ ions have been replaced by $Si^{4+}$ and $Mn^{2+}$ ions. In this case the maximum theoretical $SiO_2$ content in the braunite is 44.05 mass per cent, which is in good agreement with the 40 mass per cent determined experimentally by Muan (1959).

The formula $3Mn_2O_3.MnSiO_3$, or $Mn^{2+}Mn^{3+}{}_6Si_{12}$, corresponds to a $SiO_2$ content of 9.98 mass per cent. De Villiers (1979) found that there was between 8 to 10

mass per cent $SiO_2$ in the Mamatwan braunite which is sufficiently close to the ideal composition to justify the use of this formula.

In literature, there are few studies on solid state reduction behaviour of manganese ores. Some of them involve the study of reactions in the production of high carbon ferromanganese from Mamatwan manganese ore (Koursaris and Finn, 1975). Featherstone (1975) states that Mamatwan ore is an excellent blending ore that is suitable for smelting to high carbon ferromanganese in a blast furnace. The high MgO and CaO contents are desirable in the ferromanganese blast furnace as they make the burden self fluxing. It is also possible to use high percentages of Mamatwan ore in silicomanganese production as high MgO contents enhance the reduction of MnO while at the same time not decreasing the activities of $SiO_2$ too much as high $SiO_2$ activities are essential in the furnace slag.

Pentz (1970) and De Villiers (1973) studied the effects of heat on Mamatwan ore. DTA, TGA, X-ray diffraction and microscopic examination showed that the following mineralogical changes take place during heating in air:

700 $^{o}$C --> Decomposition of dolomite

800 to 900 $^{o}$C --> Decomposition of calcite with the formation of $CaMnO_3$ and possibly some $Ca(OH)_2$.

900 $^{o}$C --> Beginning of the formation of $CaMn_2O_4$ and decomposition of braunite.

1000 °C --> Formation of Jacobsite when braunite decomposes to hausmannite(tetragonal) and $SiO_2$.

While heating in air from room temperature to 1000 °C Mamatwan ore loses water as well as small amount of oxygen and carbon dioxide from the carbonates. Pentz (1970) recommends preheating of the ore to at least 800 °C to promote decomposition of the carbonates prior to any reduction studies and prevent the loss in mass due to reduction from being masked by the loss in mass due to the thermal decomposition.

Koursaris, Kleyenstuber, and Finn ([illegible]) concluded that the early stages of reduction of Mamatwan ore by coal in temperature range between 1200 °C and 1600 °C for up to four hours in a argon atmosphere involve complex mineralogical changes which can be summarised as follows:

a) Breakdown of braunite and gangue minerals
b) Reduction of higher manganese oxides to manganous oxide and of hematite to metallic iron.
c) Formation of slag as a result of reaction between gangue and manganous oxide.
d) Finally, further reduction of the ore involves the carburisation of the metallic phase and the reduction of solid manganous oxide, or manganous oxide dissolved in the slag, by solid carbon or carbon dissolved in the metal.

McRae (1981) conducted a series of experiments on Mamatwan ores involving pretreatment of the ore, thermogravimetric analysis under reducing and oxidizing

conditions, reoxidation of heat treated samples which were 15 mm in size and x-ray diffraction analysis in the temperature range from 800 $^{o}$C to 1100 $^{o}$C. He showed that the thermal treatment in neutral atmosphere and in air resulted in a rapid loss of mass between 13 and 22 percent. An increase in temperature resulted in a considerable increase in the rate of mass loss under atmospheric conditions.

Another work was done by Koursaris and See (1975) to investigate the effects of temperature and retention time for charges of Mamatwan manganese ore and either Delmas coal or Iscor metallurgical coke in the temperature range between 1300 $^{o}$C and 1600 $^{o}$C. The experimental method was a variation of the stationary charge in controlled environment (SCICE) technique. The charges of Mamatwan ore which ranged in size from 2.83 to 12.7 mm and reducing agent were heated to temperatures between 1300 $^{o}$C and 1600 $^{o}$C and either cooled immediately after the required temperature had been reached or held at the temperature for periods of up to 4 hours. They found that the reactions which occur during the reduction of Mamatwan manganese ore with either Iscor coke or Delmas coal were not significantly different. They concluded that reduction of the ore involved the breakdown of silicates, carbonates, oxides, the formation of a primary slag, beads of iron and grains of a solid solution of manganous oxide and magnesia. The primary slag contained mainly calcium oxide and silica. Further reduction appeared to take place by dissolution of manganese into slag and reduction of solute by solid carbon or carbides. The final slag had a composition in the $Al_2O_3$-CaO-MgO-$SiO_2$ system.

Dewar and See (1978) investigated the influence of carbonaceous reducing agents on the rate of reduction of Mamatwan manganese and Winterfield chromite ore in the range 850°C to 1500°C under neutral atmosphere. The reducing agents Lurgi char, Rand char, gasworks coke, Iscor coke, anthracite and electrode graphite were used in experiments with the raw material having size fractions of 40 to 50, 100 to 140, and less than 270 mesh. The For Mamatwan ore microscopic and x-ray analysis revealed no differences in the mode of reduction with different reducing agents. It was found that the initial stages of reduction of higher oxides of manganese to manganous oxide in Mamatwan ore proceeded more rapidly as the reactivity of reducing agent towards $CO_2$ increases. In the second stage of reduction, manganese oxide is converted to manganese carbides and higher contents of fixed carbon in the reducing agents give higher final percentage reductions.

Pilter (1967) found that the reduction of the higher oxides of manganese to MnO with carbon monoxide and hydrogen occurs at low temperatures (320-400 °C) but the complete reduction to metal Mn cannot be obtained. Antonov and Chyfarov (1961) reduced MnO with graphite in CO atmosphere at temperatures between 1300 °C and 1380 °C. They stated that above 1360 °C, MnO can be reduced completely. Additions of $Fe_2O_3$ and $K_2CO_3$ accelerate the process of reduction, while with increased of addition of $Fe_2O_3$, the speed of reduction increases.

Rankin (1980) studied the reduction of MnO under argon atmosphere at temperature ranging from 1200 $^{o}$C to 1425 $^{o}$C by graphite. He found that the reduction product at this temperature range is $Mn_5C_2$ and the activation energy for the reaction is 240.6 kJ and gasification of the graphite is the rate controlling step in the reduction of MnO.

$$5MnO + 9CO = Mn_5C_2 + 7CO_2 \quad \ldots\ldots\ldots\ldots \quad 2.1$$

$$C + CO_2 = 2CO \quad \ldots\ldots\ldots\ldots \quad 2.2$$

Following conclusions were drawn from the study:
a) The rate of reduction of MnO by graphite is increased by an increase in the temperature and a decrease in the ratio of MnO to C. The effect of particle size of MnO and of graphite is very slight.
b) The rate of reduction of MnO by graphite at 1350 $^{o}$C is increased markedly by the addition of $Fe_2O_3$, uneffected by the addition of $Na_2CO_3$ and $K_2CO_3$, slightly increased by the addition of CaO, MgO and $Al_2O_3$ and decreased by the addition of $SiO_2$.

He stated that the apparent fractional reactions are slightly greater than the theoretical limit of reduction which is defined as the value to be obtained if all the oxygen is removed as CO. The reason for this is most probably that a small amount of $CO_2$ escaped from the reaction mixture. Since $CO_2$ carries twice as much oxygen per mole of carbon as does CO, the presence of $CO_2$ in the gas raises the apparent fractional reaction. This is also the evidence that reduction took place by way of CO as an intermediate product. The

alternative scheme, the reduction of MnO by graphite at points of contact, produces only CO at temperatures used in the study.

Figures 2.1 - 2.3 show the effect of particle size, temperature, and carbon amount on the reduction rate. The rate of reduction is almost independent of MnO particle size in the size range 63 to 250 $\mu m$.

Terayama (1985) also investigated the effect of temperature, particl. size and amount of carbon on reduction rate of MnO under helium atmosphere at temperature range from 1070°C to 1200°C. He expressed his results with the Figures 2.4-2.6.

He assumed that the reduction proceeds in accordance with the following reactions:

$$7MnO + 13CO = Mn_7C_3 + 10CO_2 \quad \ldots\ldots\ldots\ldots \quad 2.3$$

$$C + CO_2 = 2CO \quad \ldots\ldots\ldots\ldots \quad 2.2$$

$$7MnO + 10C = Mn_7C_3 + 7CO \quad \ldots\ldots\ldots\ldots \quad 2.4$$

and the overall rate is controlled by the rate of oxidation of carbon by carbondioxide as expressed in reaction 2.2. Activation energy of the reaction was calculated as 217 kJ/mol. He stated that reduction reactions between MnO and carbide to yield metallic manganese occurs at the interface of the two solid phases in the later stages of reduction. The reaction is:

$$Mn_7C_3 + 3MnO = 10Mn + 3CO \quad \ldots\ldots\ldots\ldots \quad 2.5$$

The activation energy for this reaction was 259 kJ/mol. The reaction between MnO and $Mn_7C_3$ was not observed when excess carbon was used.

As can be seen Rankin's and Tereyama's study conflict with each other. In spite of using higher experimental temperatures, Rankin found higher activation energy than Terayama for the reduction of MnO by carbon. One of the reasons for this is probably application of different mathematical models to the kinetic data. They differ in reaction products of MnO reduction as well. Rankin's reaction product is the carbide $Mn_5C_2$ while that of Terayama's is $Mn_7C_3$. In both study equimolar amounts of MnO and graphite were used. In such case the same reaction products, particularly in carbide formation, would be expected. Since their experimental temperature were different (Rankin's is 1200°C-1425°C while Terayama's is 1070°C-1200°C), it may be concluded that temperature is important in determination of final reaction products. Furthermore x-ray diffraction peaks of above carbides are close to each other. This may also create difficulties in finding the exact reaction product.

The reduction and mechanism of Mamatwan ore, first time, was studied by W.D. Grimsley and R.P. King (1977) under argon and CO atmospheres using graphite as the reductant at temperatures ranging from 1000°C to 1300°C. They discussed the reduction mechanism in two stages: a) an initial stage during which most of the higher oxides of manganese were reduced to MnO with concurrent formation of $CaMn_2O_4$, and the iron oxide was reduced to metal or carbide. During this stage

diffussion of CO and $CO_2$ influenced the reduction rate; b) a second, slower stage during which MnO and the remaining $MnMn_2O_4$ were reduced to metal or carbide. At temperatures ranging from 1000 to 1300 °C, it was found that as the temperature and amount of carbon increased the rate and degree of the reduction of the ore increased. Their results are represented in Figures 2.7 and 2.8. It was concluded that the percent reduction with time increased markedly as the temperature increased and graphite additions above 10 per cent (by mass) had very little effect on the extent of reduction at 1000 and 1100 °C, but the effect of increased graphite additions became more important at 1200 °C and even more marked at 1300 °C. They carried out several experiments with pura $MnO_2$ and graphite in an argon atmosphere, with pure $MnO_2$ and graphite in a carbon monoxide atmosphere and with $MnO_2$ and carbon monoxide alone at 1000°C and 1200°C to determine the role of carbon monoxide in the reduction of Mamatwan ore with carbon. It was found that almost complete reduction to MnO was achieved within the first 10 minutes when $MnO_2$ was reacted with graphite in a carbon monoxide atmosphere. The reduction of preheated ore by graphite in an atmosphere of carbon monoxide proceeded rapidly until the iron oxide was reduced to metal and the manganese oxide were reduced to MnO. Then the reaction ceased abruptly, indicating that further reduction of MnO to manganese carbide was not feasible in the presence of a pure carbon monoxide atmosphere.

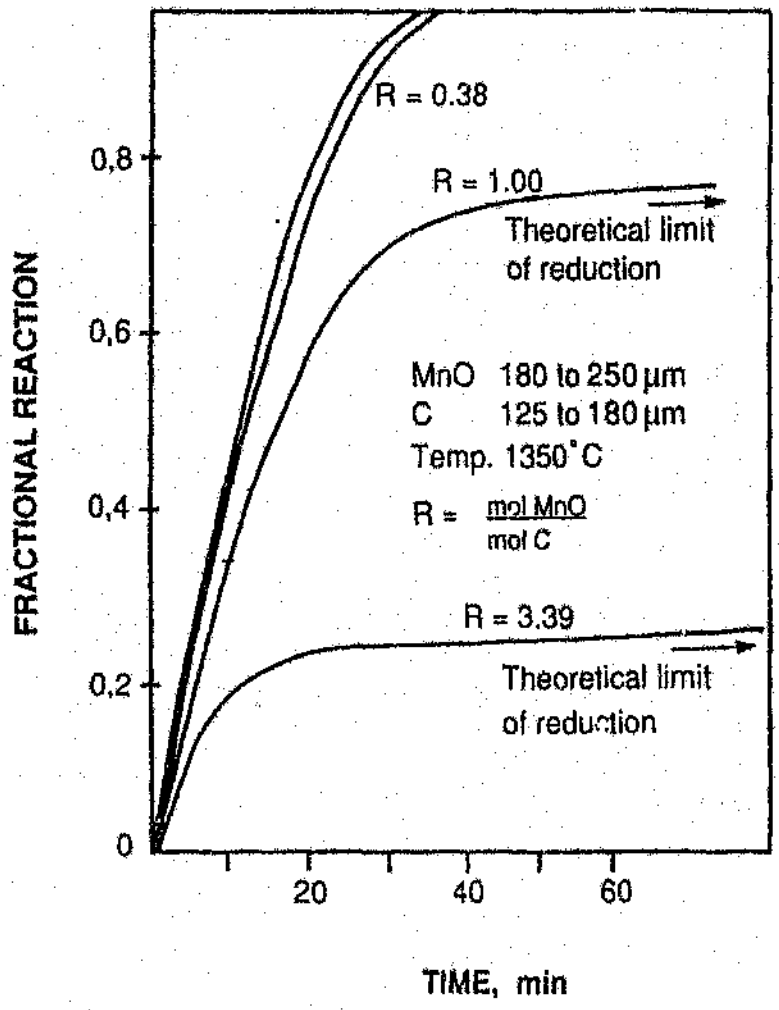


Figure 2.1 The effect of MnO-to-C ratio on the reduction of MnO by c· ·hite (after Rankin, 198·)

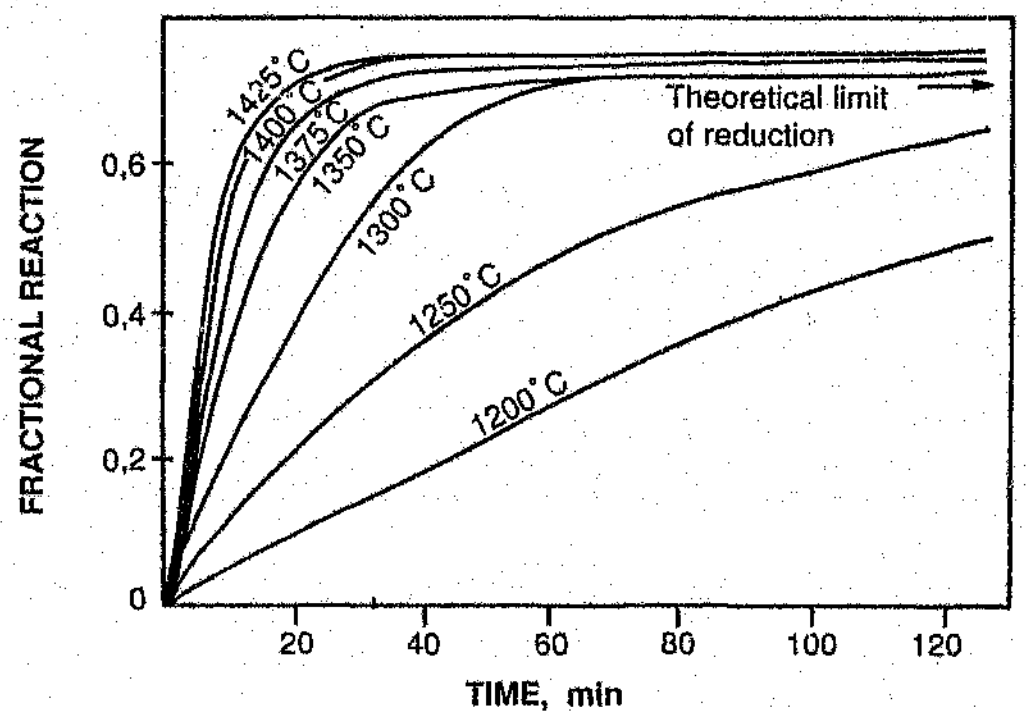


Figure 2.2 The effect of temperature on the reduction of MnO by graphite (after Rankin, 1980).

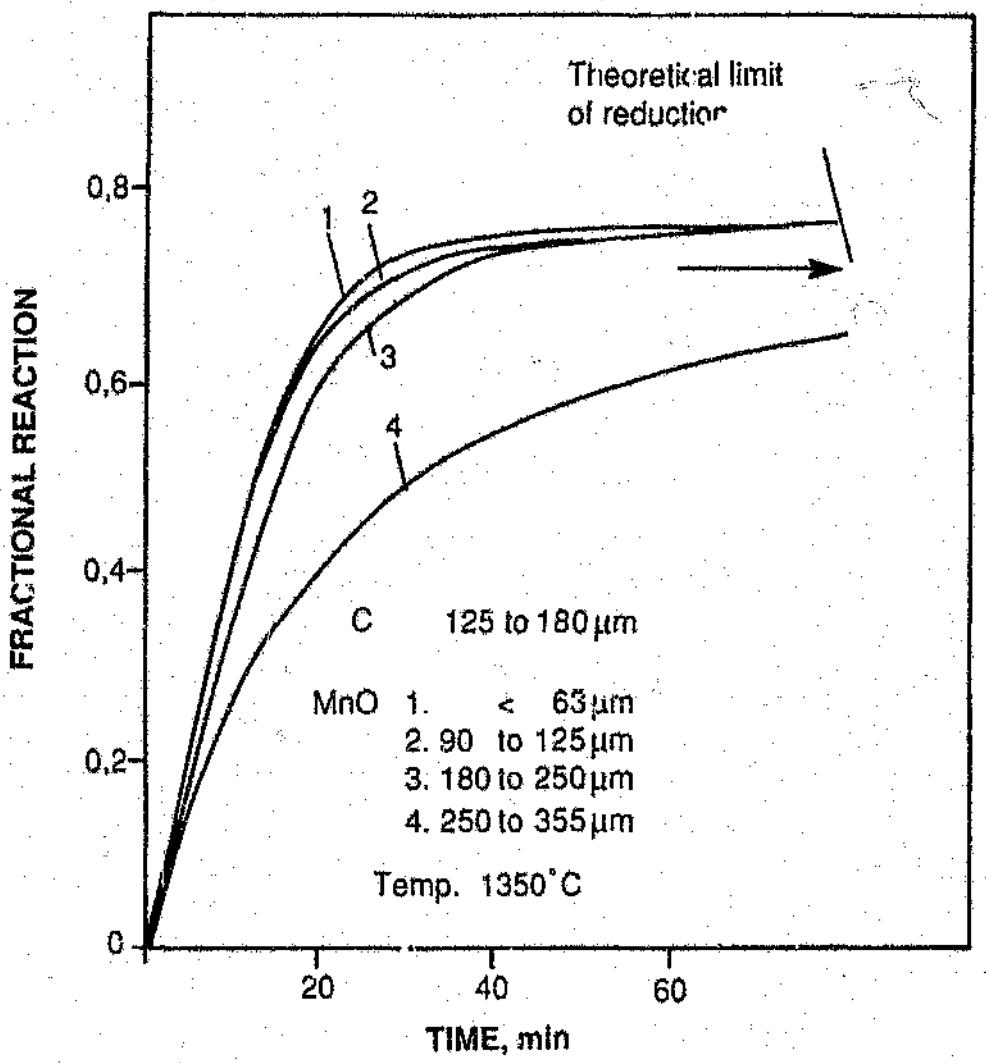


Figure 2.3 The effect of particle size of MnO on the reduction of MnO by graphite (after Rankin, 1980).

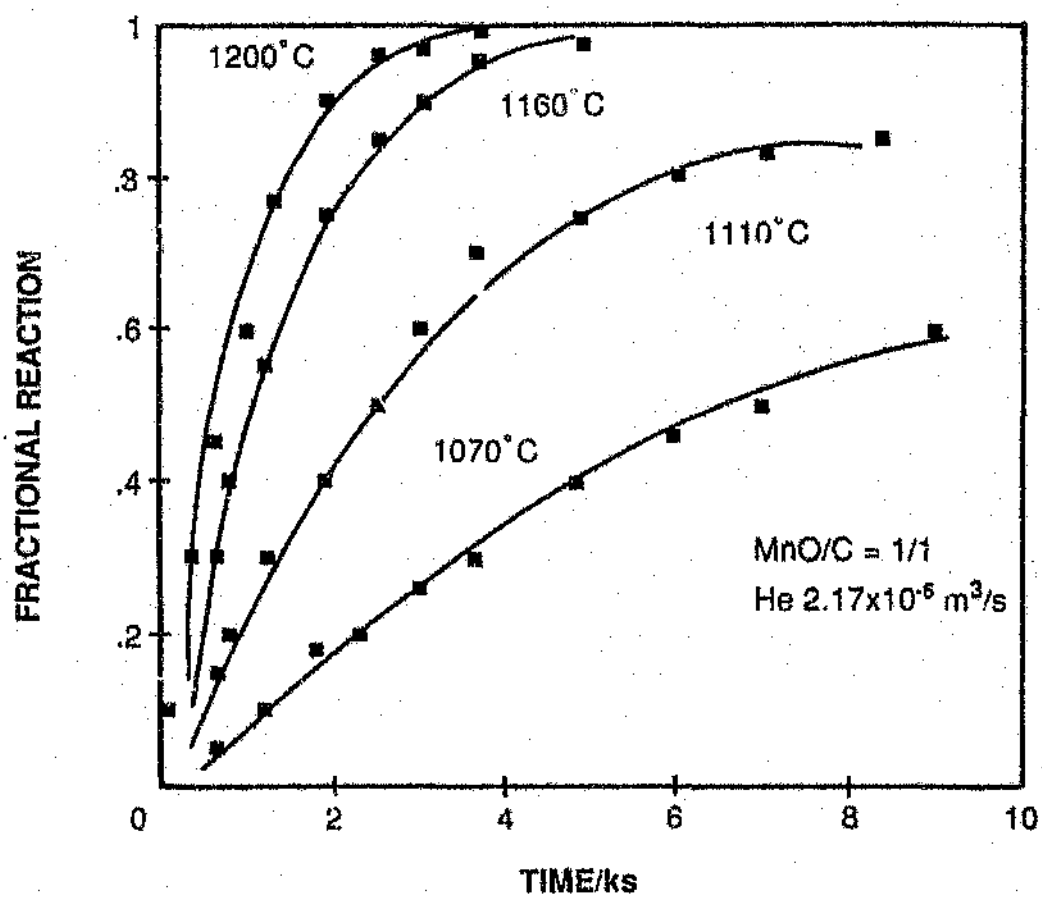


Figure 2.4 The effect of temperature on the reduction of MnO by graphite (after Terayama, 1985).

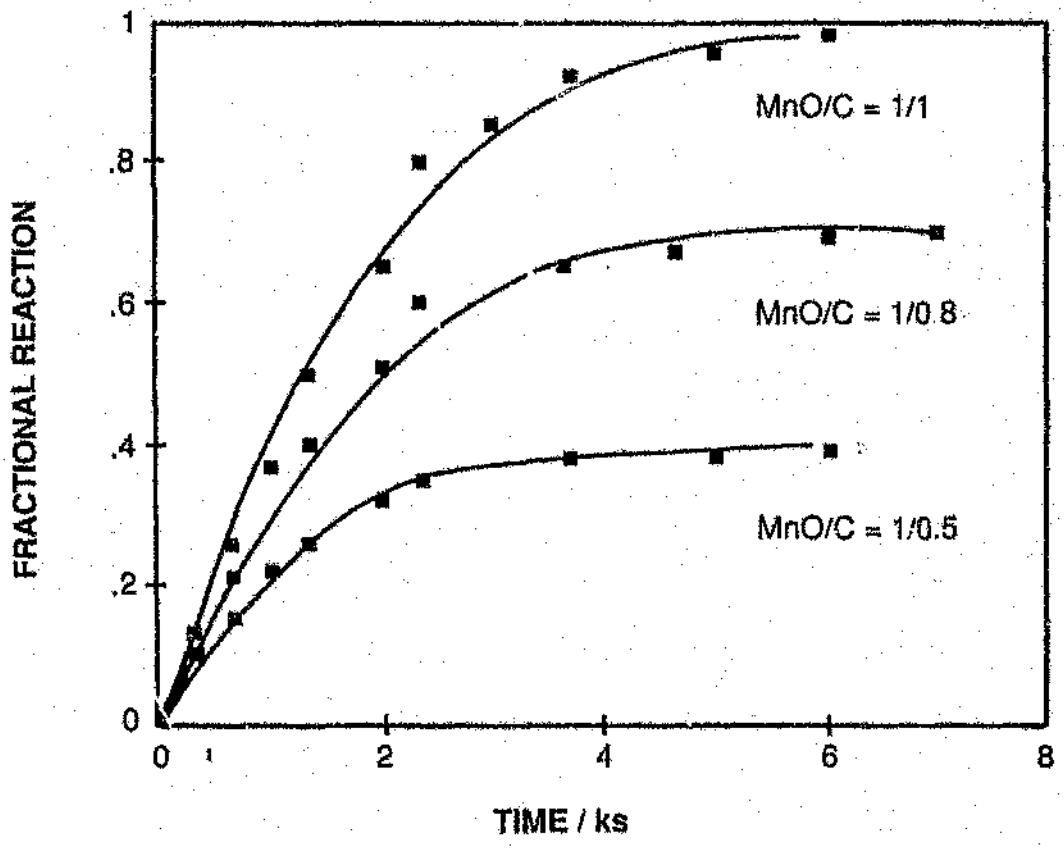


Figure 2.5 The effect of MnO-to-C ratio on the reduction of MnO by graphite (after Terayama, 1985).

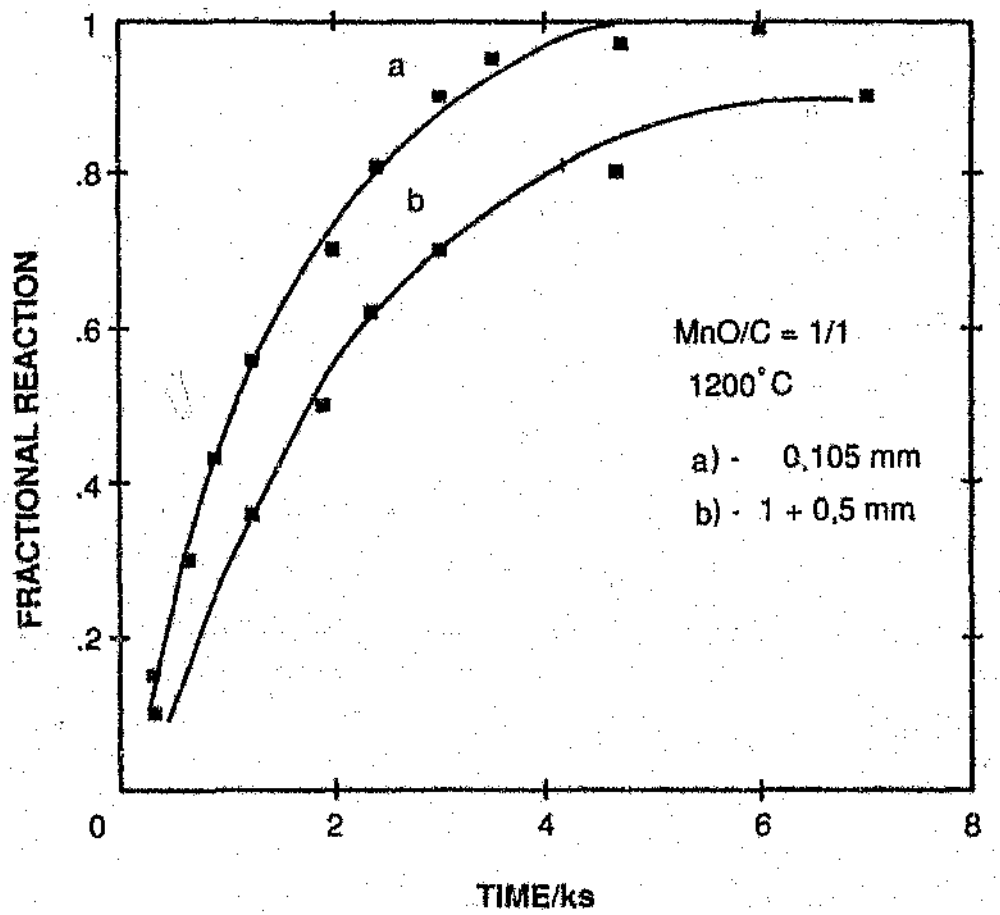


Figure 2.6 The effect of particle size of MnO on the reduction of MnO by graphite (after Tera ma, 1985).

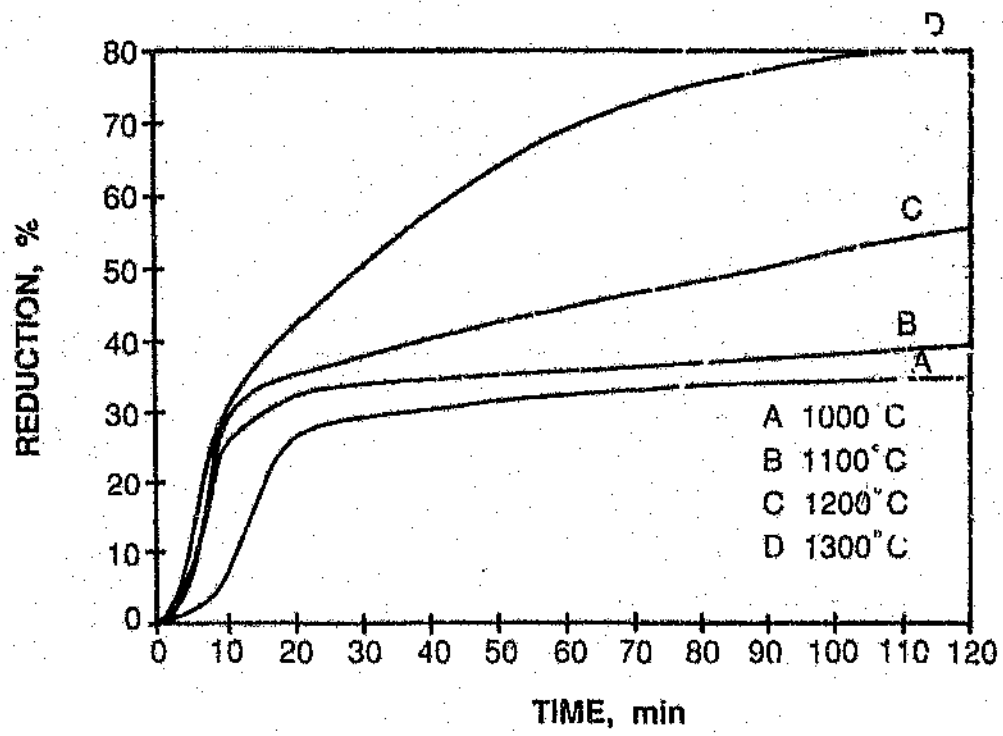


Figure 2.7 The effect of temperature on the reduction of Mamatwan manganese ore by graphite (after Grimsley, 1977).

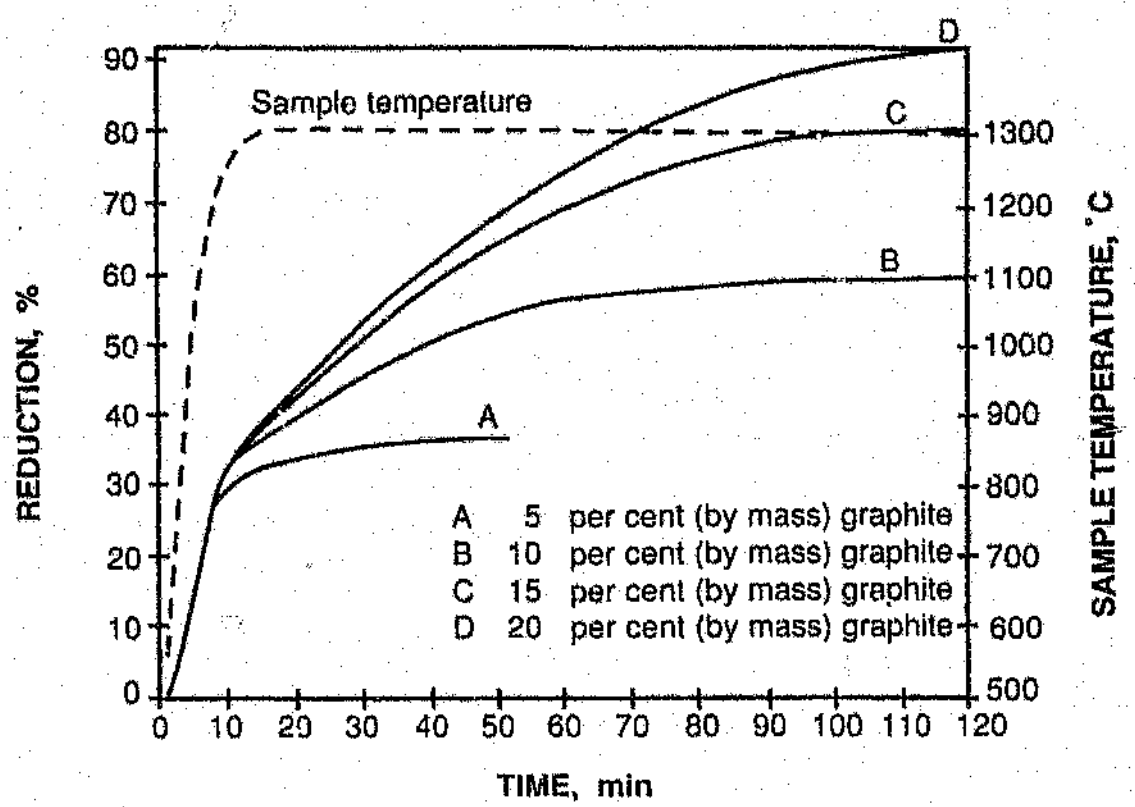


Figure 2.8 The effect of carbon amount on the reduction of Mamatwan manganese ore by graphite (after Grimsley, 1980).

## 2.2 The Studies on Manganese oxides

The four manganese oxides $MnO_2$, $Mn_2O_3$, $Mn_3O_4$ and MnO have been studied by many investigators (De Villiers, 1975; Bystrom and Mason, 1943; Dressel and Kenworthy, 1961; Tobisawa, 1963) and Volkert et al (1972), Dollimore and Tonge (1971) have summarized the findings of all of the above investigators.

Manganese (IV) oxide or manganese dioxide ($MnO_2$) exists in many polymorphic forms. One of these forms is $\beta$-$MnO_2$ or pyrolusite which contains 63.19 mass percent manganese and has the tetragonal tutile structure.

Manganese (III) oxide $Mn_2O_3$ which is also called manganic oxide or manganese sesquioxide, contains 69.9 mass per cent manganese and exits in an alpha and a gamma form. $\gamma$-$Mn_2O_3$ has a similar distorted cubic structure to $Mn_3O_4$ and is a defect spinel with manganese atoms distributed randomly among the available sites. This structure is not very stable and $Mn_2O_3$ usually has the orthorhombic structure known as $\alpha$-$Mn_2O_3$

Manganese tetroxide or mangano-manganic oxide ($Mn_3O_4$) contains 72.03 mass per cent manganese and is a normal spinel ($MnO.Mn_2O_3$) in which $Mn^{+3}$ ions occupy the octahedral sites. In the normal red-brown hausmannite the oxide lattice is tetragonally distorted from the cubic arrangement. In air $Mn_3O_4$ was found to be the stable form of manganese oxide from 1000 $^oC$ up to its melting point. Pentz (1970) and Shantarin et al (1972) have confirmed this result. $Mn_3O_4$ appears to change its

structure during heating in the temperature range from 1000 °C to 1567 °C. Van Hook and Keith (1958) propose that tetragonal $Mn_3O_4$ is stable up to 1160 °C and is converted to the cubic spinel form above this temperature.

Manganese (II) oxide or manganous oxide (MnO) contains 77.4 mass per cent manganese and is green with the sodium chloride lattice structure.

Davies and Richardson (1959) studied the non-stoichiometric behaviour of MnO under various oxygen partial pressures at temperatures in the range 1500 °C to 1600 °C. The oxygen-to-manganese ratio was found to vary from 1 at $P_{O2} = 10^{-9}$ atmospheres to 1.05 at $P_{O2} = 10^{-2}$ atmospheres. The review carried out by Dollimore and Tonge (1971) reveals that non-stoichiometry of MnO persists until the composition reaches $MnO_{1.13}$ before the $Mn_3O_4$ phase appears.

## 2.3 Thermodyanamic data on Manganese oxide reduction

The standard free energy changes for the relevant reactions for manganese oxide reduction were summarized by Grimsley (1977). Table 2.1 and 2.2 show the standard free energy changes of the some manganese oxide reductions by carbon, carbon monoxide and iron carbide. Properties of some manganese carbides are given in Table 2.3. These carbides are the most likely reaction products in the manganese oxide reduction depending on the experimental conditions and the carbon amount used for the reactions.

The stabilities of the different manganese oxides are functions of temperature and oxygen partial pressure (Muan, 1959; Klinsberg, 1960), and Figures 2.9-2.12 show the equilibria between the different manganese oxides expressed in terms of temperature and oxygen partial pressure.

Figures 2.13-2.18 show standard free energy and standard entalphy changes for some manganese oxide dissociation and reduction reactions. Figures 2.13-2.18 were drawn by using values calculated via a computer software called THERMO (Jones and et al, 1980).

The system CaO-manganese oxide in air, shown in Figure 2.19, has been studied by Ribound and Muan (1963) for the temperature range from 1100°C to 1700 °C. The four stable crystalline phases that exist over this temperature range in air are CaO-MnO solid solution, $CaMnO_3$-$CaMn_2O_4$, and $Mn_3O_4$ based spinel. The lime solid solution phase (CaO-MnO) has a sodium chloride structure ranging from pure CaO to a maximum of 14 mass per cent manganese oxide as $Mn_2O_3$.

The $CaMnO_3$ phase contains between 42 to 62 mass per cent of manganese oxide as $Mn_2O_3$. The proportion of manganese in the tetravalent state decreases as the manganese oxide content of the phase increases. The ratio of $Mn^{4+}$ to $Mn^{3+}$ changes from 0.54 at the lime-rich end to 0.33 at the stoichiometric (Ca/Mn = 1) compound. The $CaMn_2O_4$ phase is a solid solution containing 74 to 78 mass per cent manganese oxide as $Mn_2O_3$ whilst the spinel phase is a solid solution with the approximate composition $Mn_3O_4$-$CaMn_2O_4$ which contains a maximum of 16 mass per cent $CaMn_2O_4$. The

transformation temperature of tetragonal $Mn_3O_4$ was found to increase slightly with CaO additions to a maximum of about 1200 $^{o}C$.

The system CaO-MnO-$SiO_2$ was investigated by Glosser (1962). He constructed the phase diagrams illustrated in Figures 2.20 to 2.22. Figures 2.20 and 2.21 represent vertical sections through $Ca_2SiO_4$ and $Ca_2SiO_4$ compositions whereas Figure 2.22 shows the actual ternary system with liquidus projections.

Table 2.1

Standard free energy changes for the reactions of manganese oxides reduction by carbon and carbon monoxide.

| Reaction | $\Delta G^\circ = A + BT\,(kJ)$ A | B | Range (°C) |
|---|---|---|---|
| $2MnO_2 + CO = Mn_2O_3 + CO_2$ | -202.09 | 0.02 | 25-550 |
| $3Mn_2O_3 + CO = 2Mn_3O_4 + CO_2$ | -170.71 | 0.004 | 25-1100 |
| $Mn_3O_4 + CO = 3MnO + CO_2$ | -59.50 | 0.04 | 25-1244 |
| $Mn_3O_4 + CO = 3MnO + CO_2$ | -86.11 | 0.02 | 1244-1700 |
| $MnO + CO = Mn + CO_2$ | 104.56 | -0.01 | 25-1244 |
| $MnO + CO = Mn + CO_2$ | 124.93 | -0.002 | 1244-1700 |
| $MnO_2 + C = Mn_2O_3 + CO$ | -31.63 | 0.19 | 25-550 |
| $3Mn_2O_3 + C = 2Mn_3O_4 + CO$ | -0.25 | 0.17 | 25-1100 |
| $Mn_3O_4 + C = 3MnO + CO$ | 110.96 | 0.21 | 25-1244 |
| $Mn_3O_4 + C = 3MnO + CO$ | -84.35 | 0.20 | 1244-1700 |
| $MnO + C = Mn + CO$ | 275.01 | 0.16 | 25-1244 |
| $MnO + C = Mn + CO$ | 295.39 | 0.18 | 1244-1700 |
| $MnO + 4/3C = 1/3Mn_3C + CO$ | 269.62 | 0.16 | 740-1227 |
| $MnO + 10/7C = 1/3Mn_7C_3 + CO$ | 284.22 | 0.18 | 717-1087 |
| $MnO + 10/7C = 1/3Mn_7C_3 + CO$ | 282.01 | 0.18 | 1087-1137 |
| $MnO + 10/7C = 1/3Mn_7C_3 + CO$ | 280.22 | 0.18 | 1137-1244 |
| $MnO + 10/7C = 1/3Mn_7C_3 + CO$ | 285.95 | 0.18 | 1244-1700 |
| $CO_2 + C = 2CO$ | 170.46 | 0.17 | 25-2000 |

Table 2.2

Standard free energy changes for the reactions of manganese oxides reduction by iron carbide.

| Reaction | $\Delta G^\circ = A + BT(kJ)$ A | B | Range (°C) |
|---|---|---|---|
| $3Mn_2O_3 + Fe_3C = 2Mn_3O_4 + 3Fe + CO$ | -10.61 | 0.16 | 840-1100 |
| $Mn_3O_4 + Fe_3C = 3MnO + 3Fe + CO$ | 100.60 | 0.20 | 840-1244 |
| $Mn_3O_4 + Fe_3C = 3MnO + 3Fe + CO$ | 73.9 | 0.19 | 1244-1537 |
| $MnO + Fe_3C = Mn + 3Fe + CO$ | 264.66 | 0.15 | 840-1244 |
| $MnO + Fe_3C = Mn + 3Fe + CO$ | 285.04 | 0.17 | 1244-1537 |
| $MnO + 4/3Fe_3C = 1/3Mn_3C + 4Fe + CO$ | 255.81 | 0.14 | 840-1087 |
| $MnO + 10/7Fe_3C = 1/7Mn_7C_3 + 30/7Fe + CO$ | 246.09 | 0.17 | 717-840 |
| $MnO + 10/7Fe_3C = 1/7Mn_7C_3 + 30/7Fe + CO$ | 269.42 | 0.17 | 840-1087 |
| $MnO + 10/7Fe_3C = 1/7Mn_7C_3 + 30/7Fe + CO$ | 267.21 | 0.17 | 1087-1137 |
| $MnO + 10/7Fe_3C = 1/7Mn_7C_3 + 30/7Fe + CO$ | 265.42 | 0.17 | 1137-1244 |
| $MnO + 10/7Fe_3C = 1/7Mn_7C_3 + 30/7Fe + CO$ | 271.15 | 0.17 | 1244-1537 |

Table 2.3

Properties of Manganese Carbides

| Carbide | Symmetry | Carbon content (by mass %) | Stability Range °C | Remarks |
|---|---|---|---|---|
| $Mn_{23}C_6$ | Cubic | 5.40 | 25-1020 | Isomorphous with $Cr_{23}C_6$ |
| $Mn_{15}C_4$ | hexagonal | 5.48 | 850-1000 | Originally designated $Mn_7C_2$ |
| $Mn_3C$ | Rhombic | 6.79 | 950-1050 | Isomorhous with $Fe_3C$ |
| $Mn_5C_2$ | Monoclinic | 8.03 | 25-1050 | Isomorphous with $(Fe,Mn)_5C_2$ |
| $Mn_7C_3$ | Hexagonal | 8.56 | 25-1100 | Isomorphous with $Cr_7C_3$ |

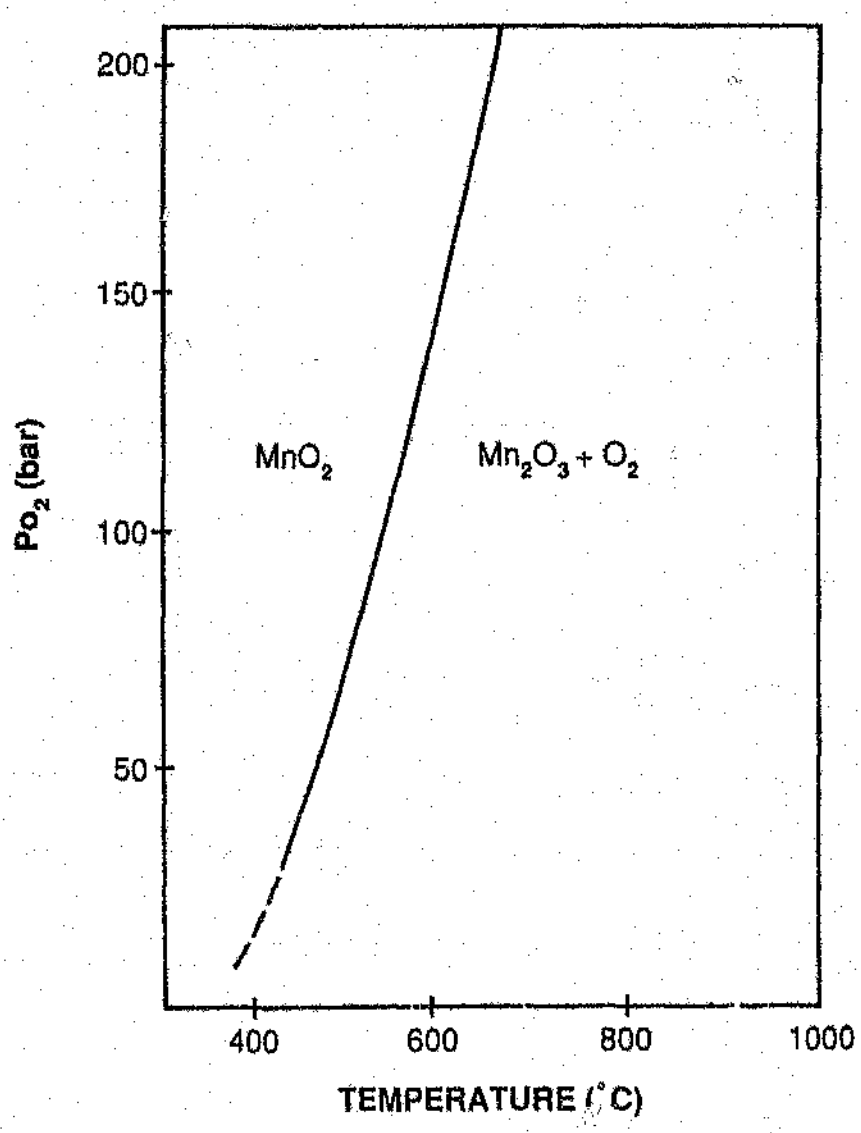


Figure 2.9 System Mn-O; univariant equilibrium curve between $MnO_2$ and $Mn_2O_3$ (after Klingsberg, 1960).

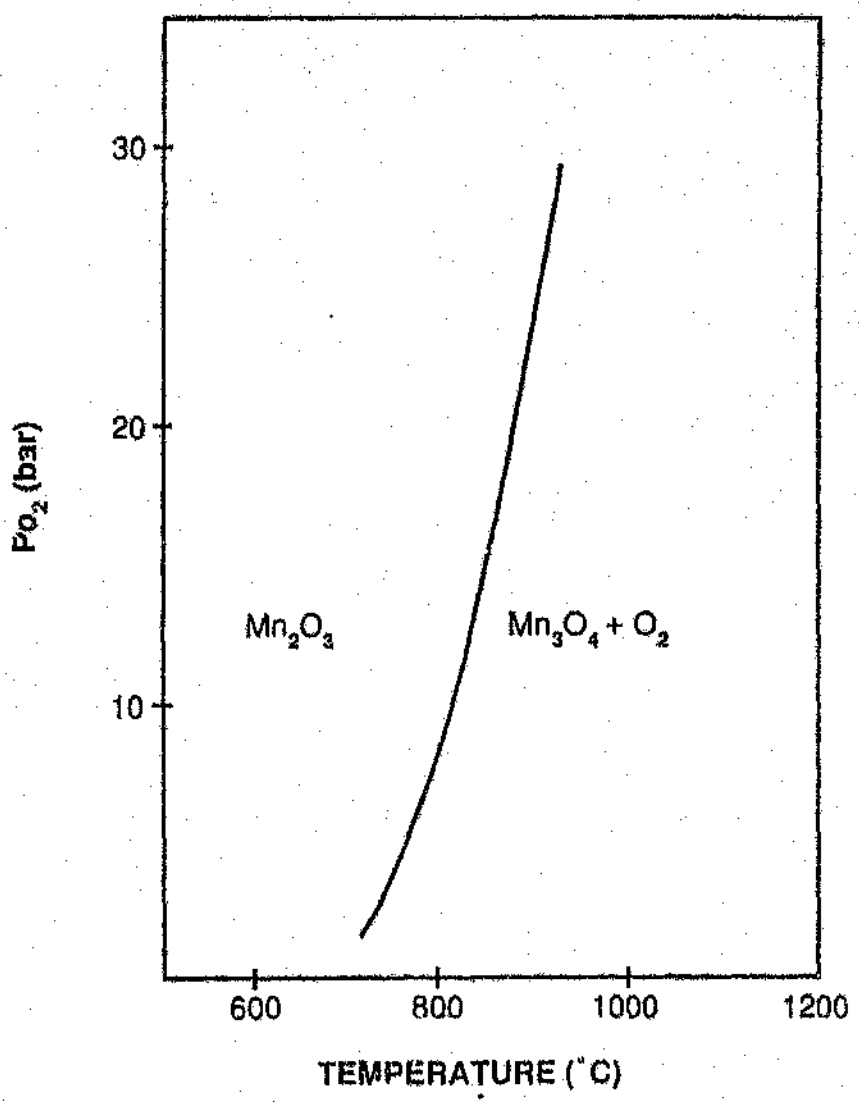


Figure 2.10 System Mn-O; univariant equilibrium curve between $Mn_2O_3$ and $Mn_3O_4$ (after Klingsberg, 1960).

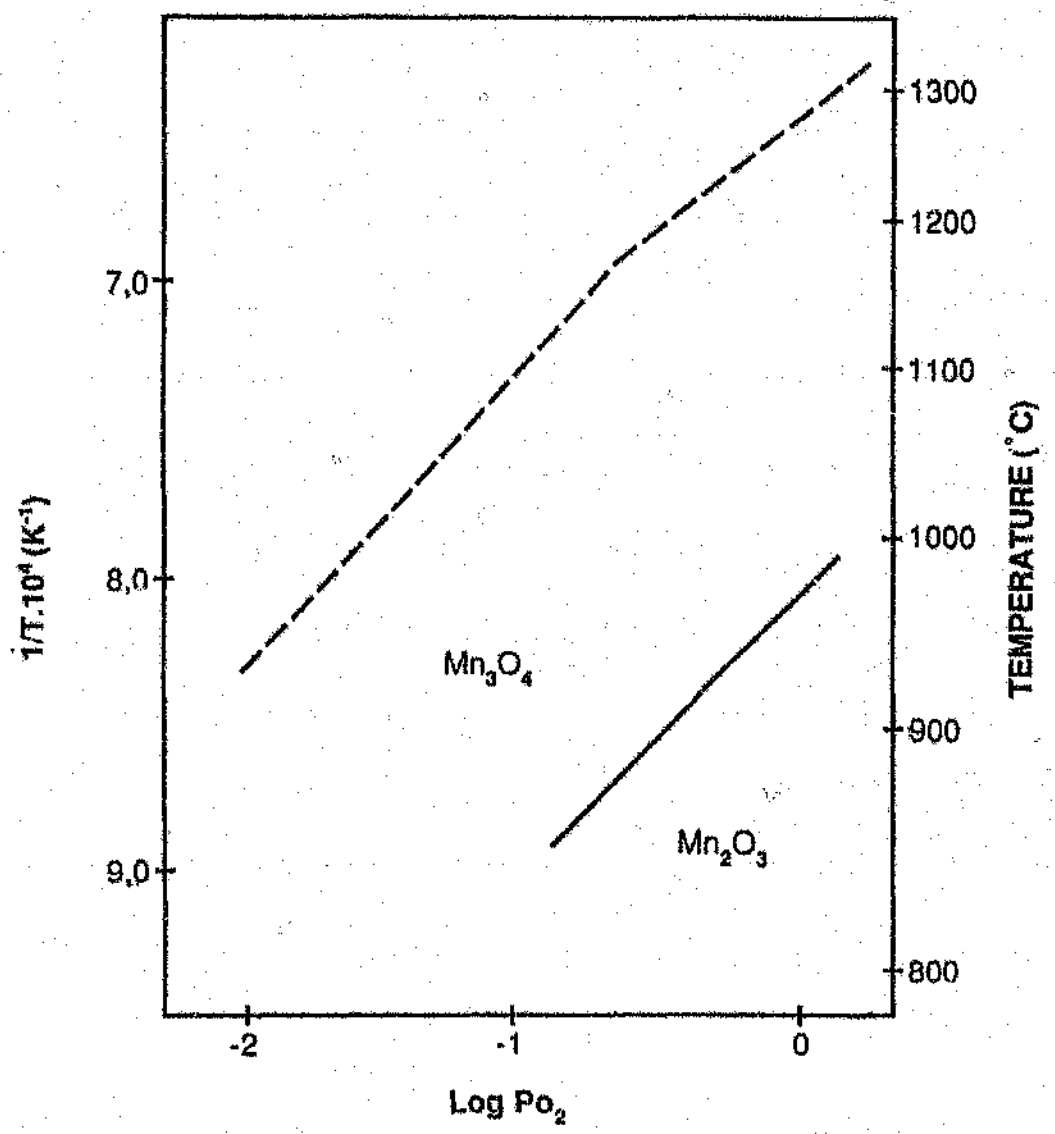


Figure 2.11 System $Mn_2O_3$-$Mn_3O_4$ as a function of oxygen pressure and temperature (after Hahn and et al, 1960).

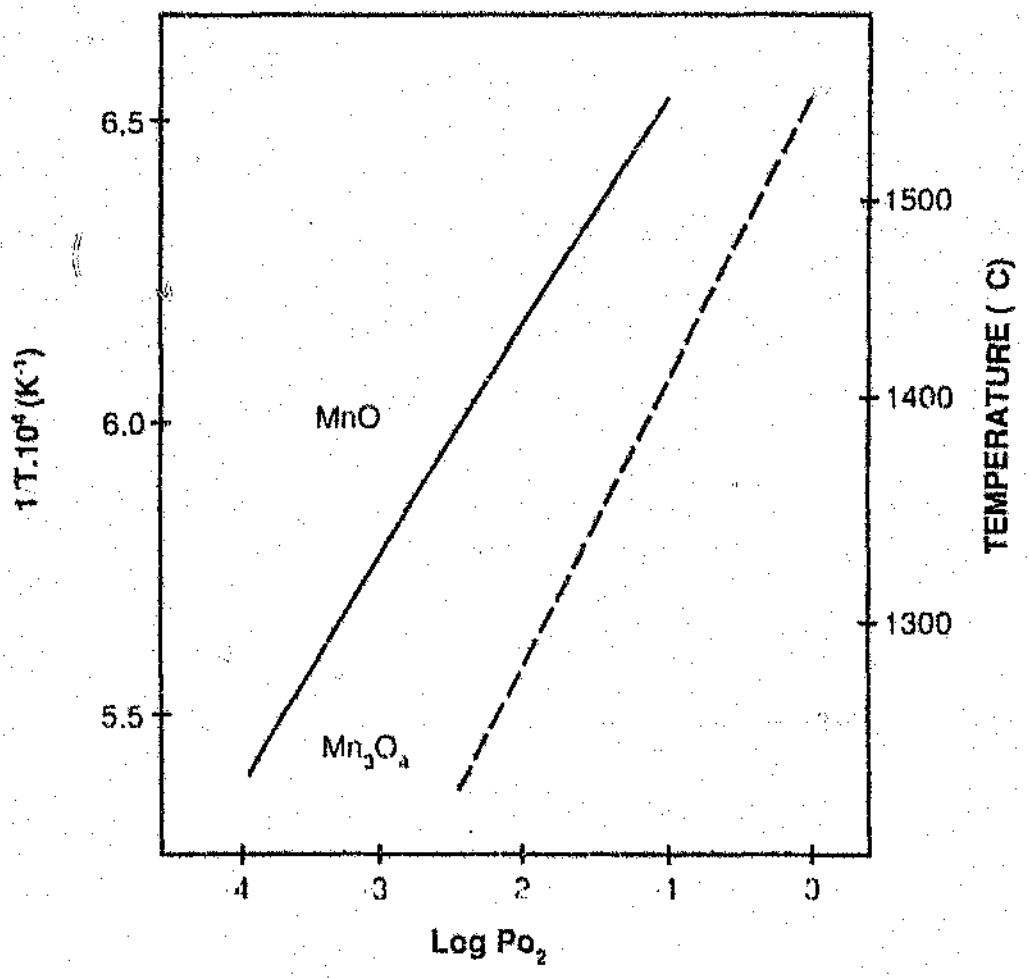


Figure 2.12 System MnO-$Mn_3O_4$ as a function of oxygen pressure and temperature (after Hahn and et al, 1960).

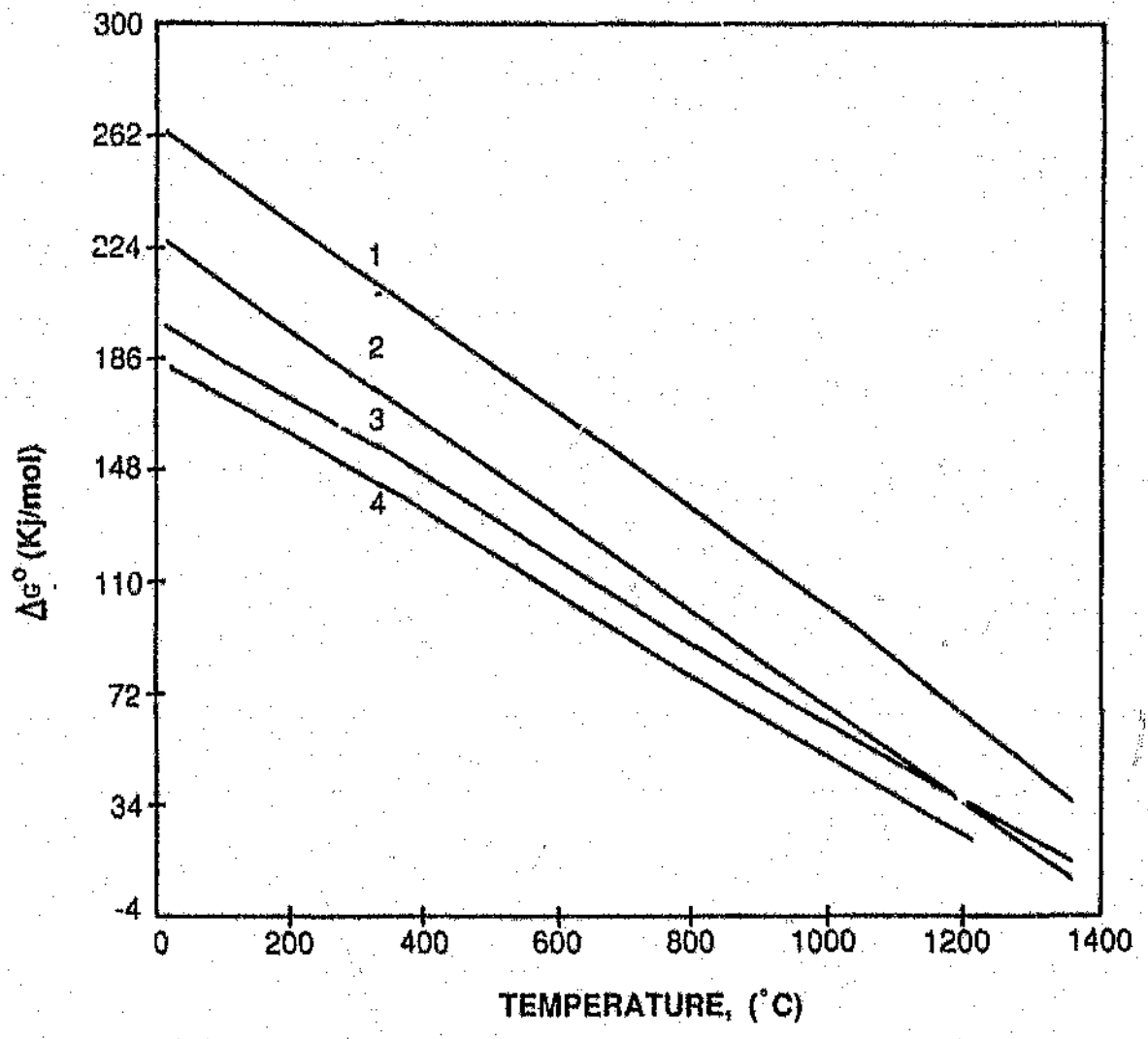


Figure 2.13 Free energy change as a function temperature for some MnO reduction reactions.

1) $MnO + 1/3\ Mn_7C_3 = 10/3\ Mn + CO$
2) $MnO + C = Mn + CO$
3) $MnO + 4/3\ Fe_3C = 1/3\ Mn_3C + 4Fe + CO$
4) $MnO + 10/7\ Fe_3C = 1/7\ Mn_7C_3 + 30/7Fe + CO$

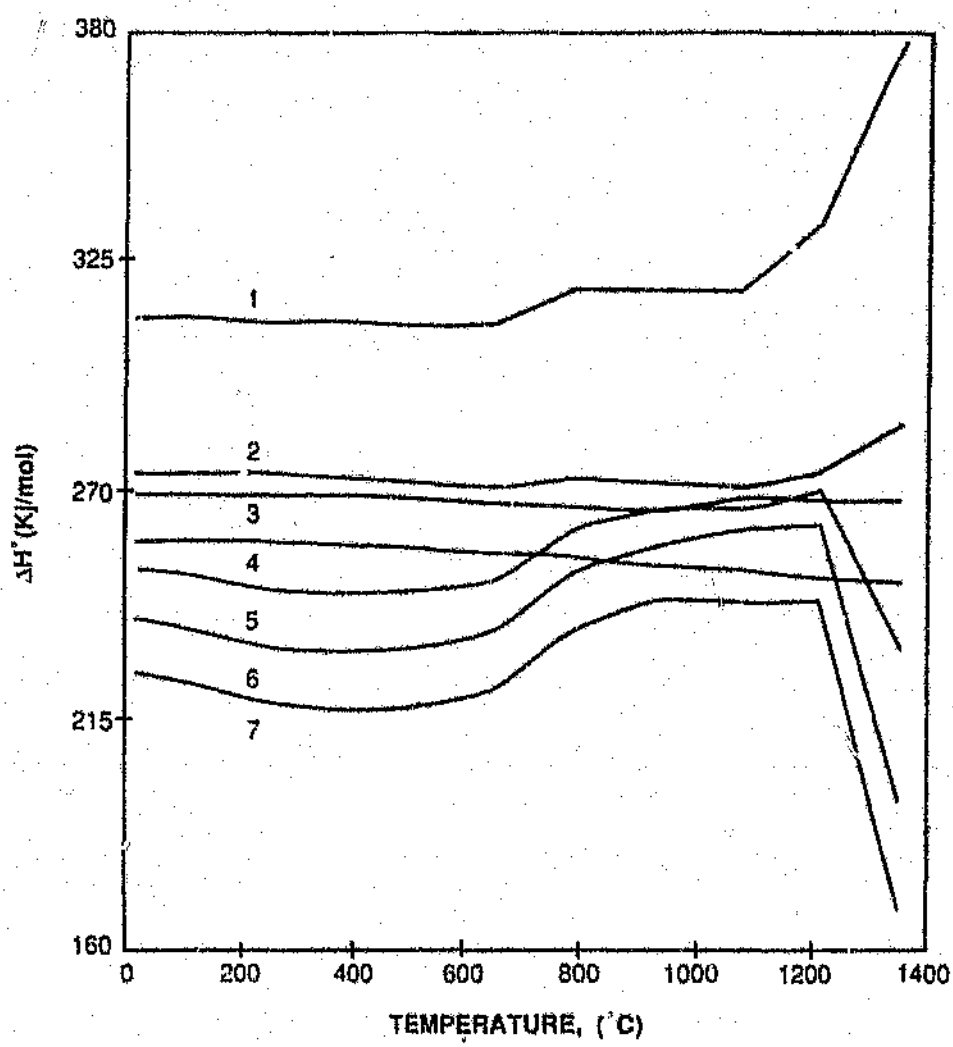


Figure 2.14 Entalphy change as a function temperature for some MnO reduction reactions.

1) $MnO + 1/3\ Mn_7C_3 = 10/3\ Mn + CO$
2) $MnO + C = Mn + CO$
3) $MnO + 4/3 = 1/3\ Mn_3C + CO$
4) $MnO + 10/7\ C = 1/7\ Mn_7C_3 + CO$
5) $MnO + Fe_3C = Mn + 3Fe + CO$
6) $MnO + 4/3\ Fe_3C = 1/3\ Mn_3C + 4Fe + CO$
7) $MnO + 10/7\ Fe\ C = 1/7\ Mn_7C_3 + 30/7Fe + CO$

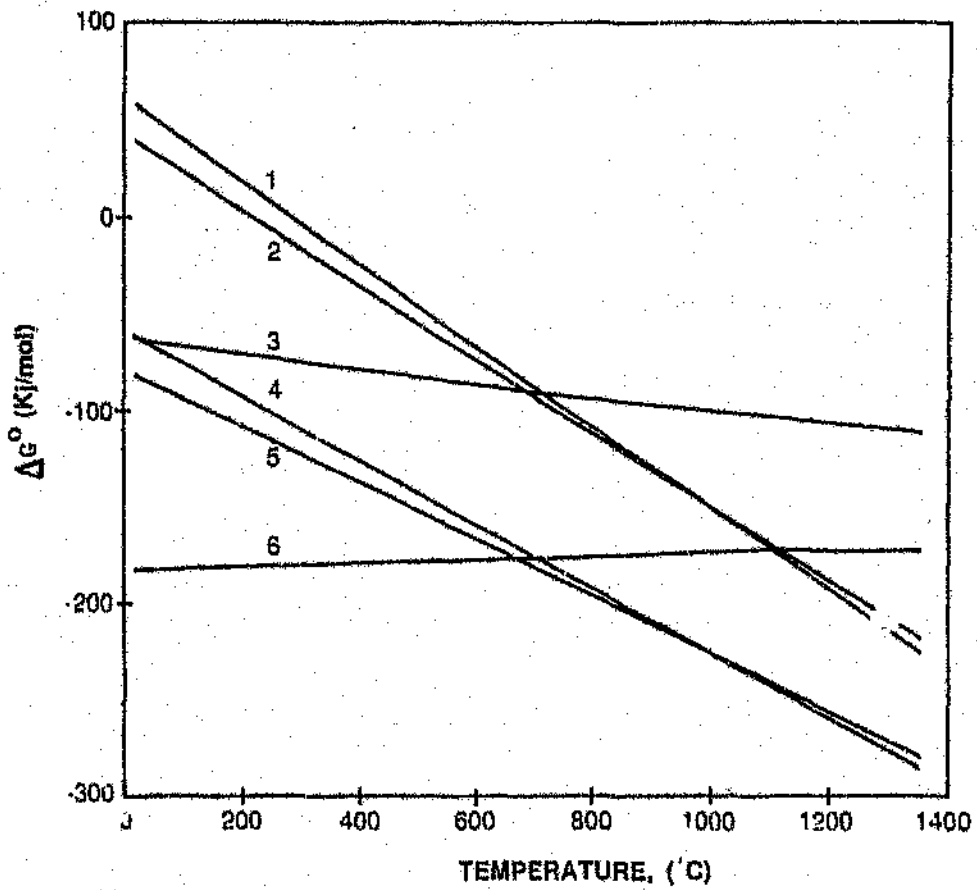


Figure 2.15 Free energy change as a function temperature for some $Mn_2O_3$ and $Mn_3O_4$ reduction reactions.

1) $Mn_3O_4 + C = 3MnO + CO$
2) $Mn_3O_4 + Fe_3C = 3MnO + 3Fe + CO$
3) $Mn_3O_4 + CO = 3MnO + CO_2$
4) $3Mn_2O_3 + C = 2Mn_3O_4 + CO_2$
5) $3Mn_2O_3 + Fe_3C = 2Mn_3O_4 + 3Fe + CO$
6) $3Mn_2O_3 + CO = 2Mn_3O_4 + CO_2$

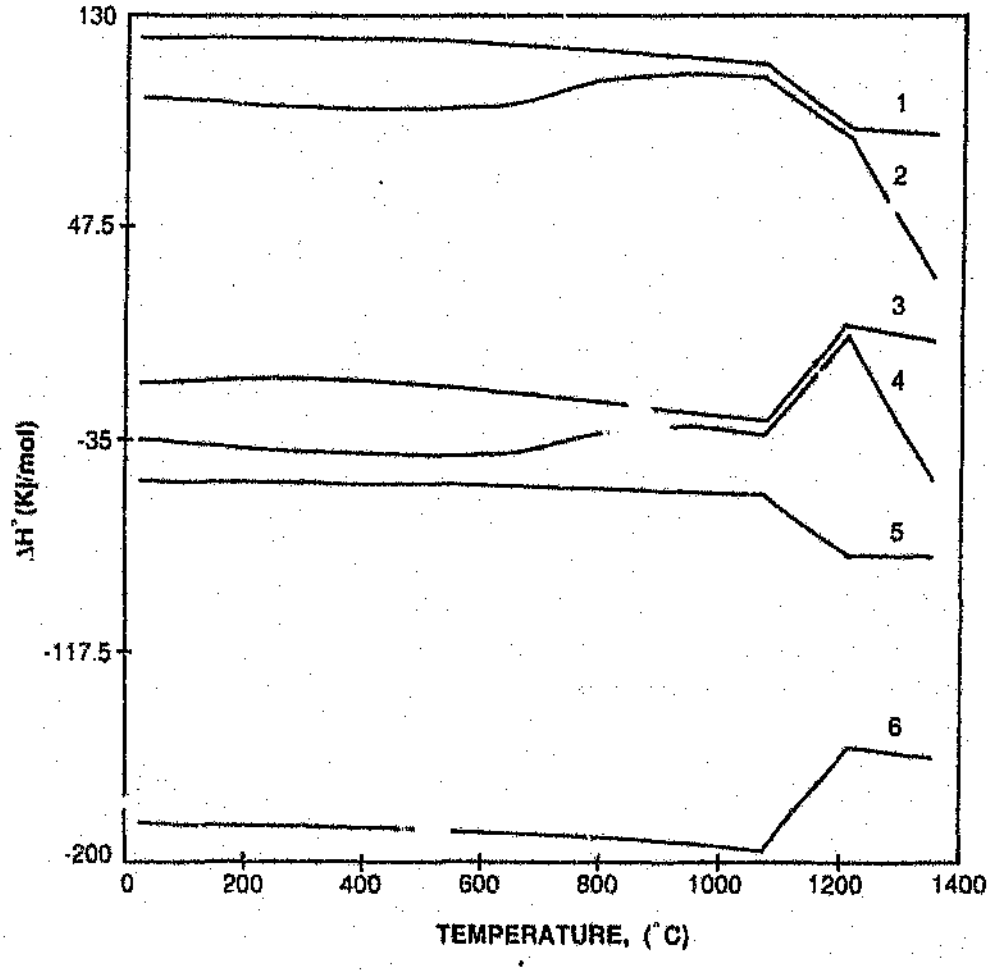


Figure 2.16 Entalphy change as a function temperature for some $Mn_2O_3$ and $Mn_3O_4$ reduction reactions.

1) $Mn_3O_4 + C = 3MnO + CO$
2) $Mn_3O_4 + Fe_3C = 3MnO + 3Fe + CO$
3) $3Mn_2O_3 + C = 2Mn_3O_4 + CO_2$
4) $3Mn_2O_3 + Fe_3C = 2Mn_3O_4 + 3Fe + CO$
5) $Mn_3O_4 + CO = 3MnO + CO_2$
6) $3Mn_2O_3 + CO = 2Mn_3O_4 + CO_2$

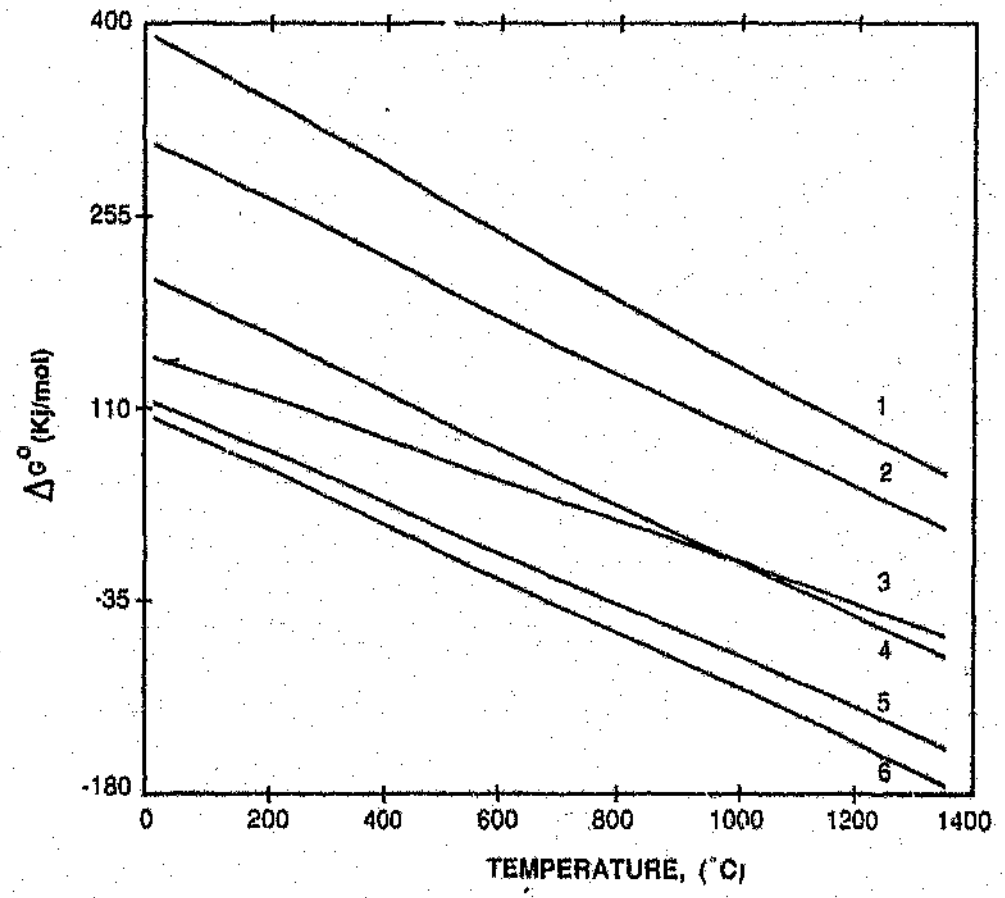


Figure 2.17 Free energy change as a function temperature for some manganese oxides dissociation reactions.

1) $2Mn_3O_4 = 6MnO + O_2$
2) $2Mn_2O_3 = 4MnO + O_2$
3) $6Mn_2O_3 = 4Mn_3O_4 + O_2$
4) $2MnO_2 = 2MnO + O_2$
5) $3MnO_2 = Mn_3O_4 + O_2$
6) $4MnO_2 = 2Mn_2O_3 + O_2$

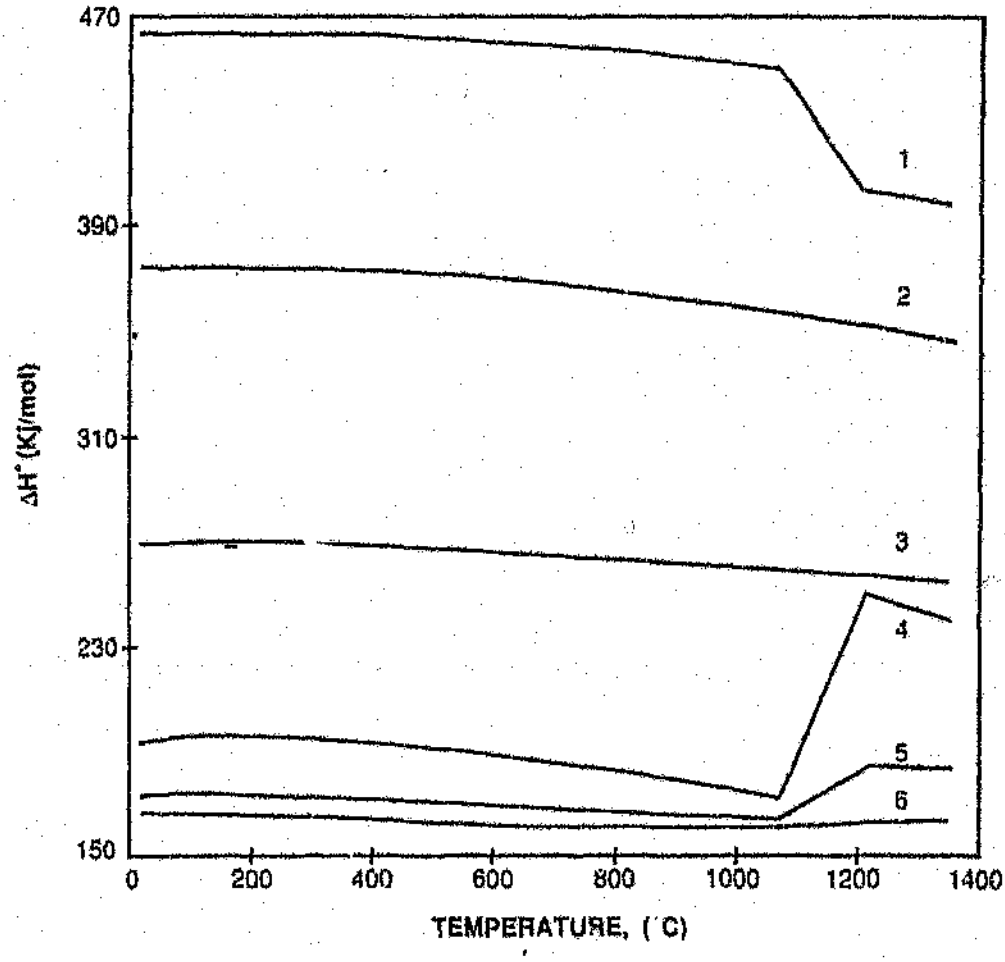


Figure 2.18 Entalphy change as a function temperature for some manganese oxides dissociation reactions.

1) $2Mn_3O_4 = 6MnO + O_2$
2) $2Mn_2O_3 = 4MnO + O_2$
3) $2MnO_2 = 2MnO + O_2$
4) $6Mn_2O_3 = 4Mn_3O_4 + O_2$
5) $3MnO_2 = Mn_3O_4 + O_2$
6) $4MnO_2 = 2Mn_3O_4 + O_2$

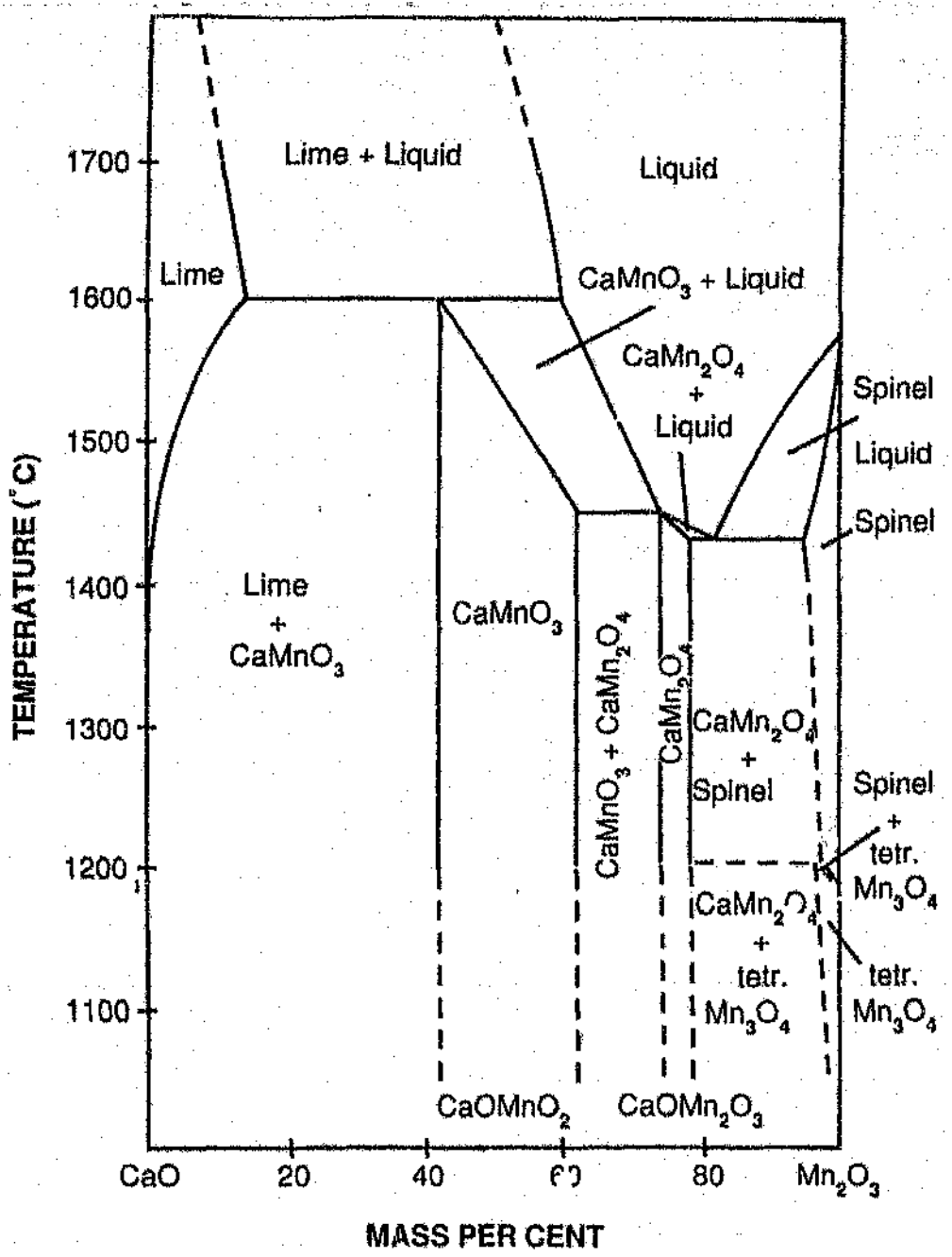


Figure 2.19 Phase relations in the system CaO-manganese oxide above 1100°C. (after Ribound and et al, 1963).

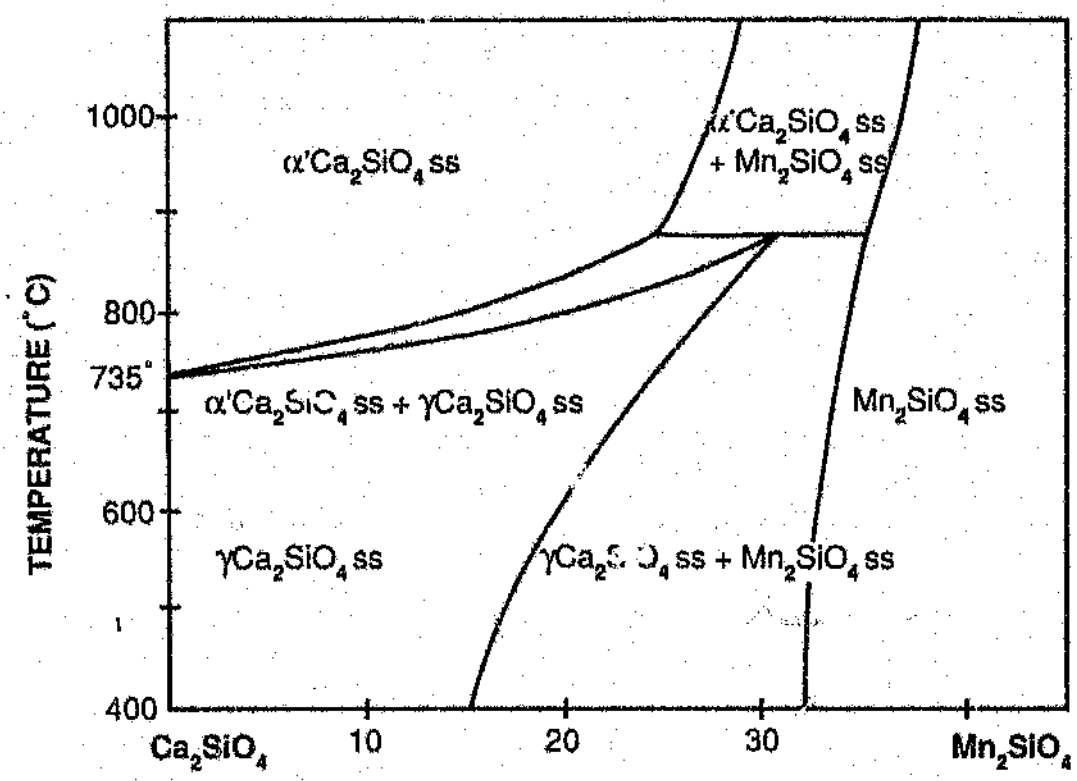


Figure 2.20 Phase relations in the system $CaO-MnO-SiO_2$ below 1000°C. (after Glosser, 1962).

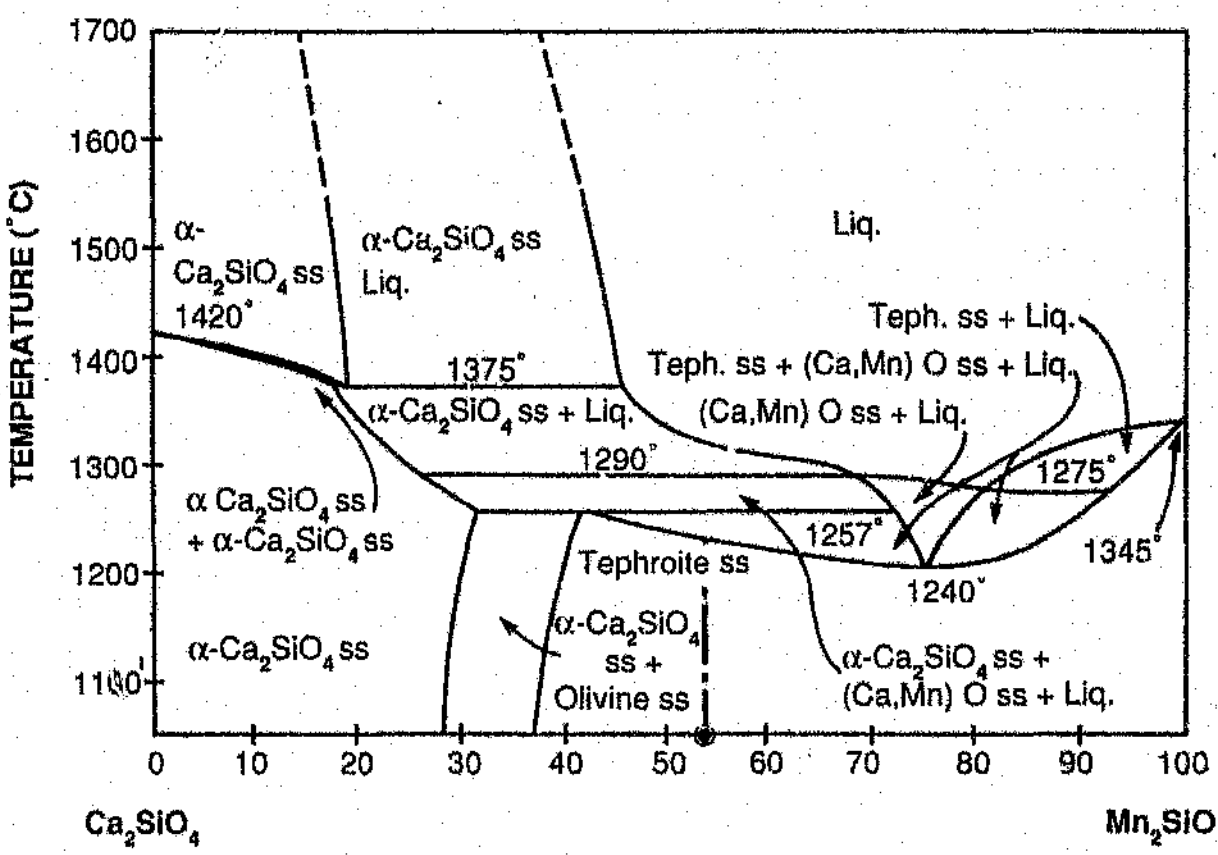


Figure 2.21 Phase relations in the system $CaO-MnO-SiO_2$ above 1000°C. (after Glosser, 1962).

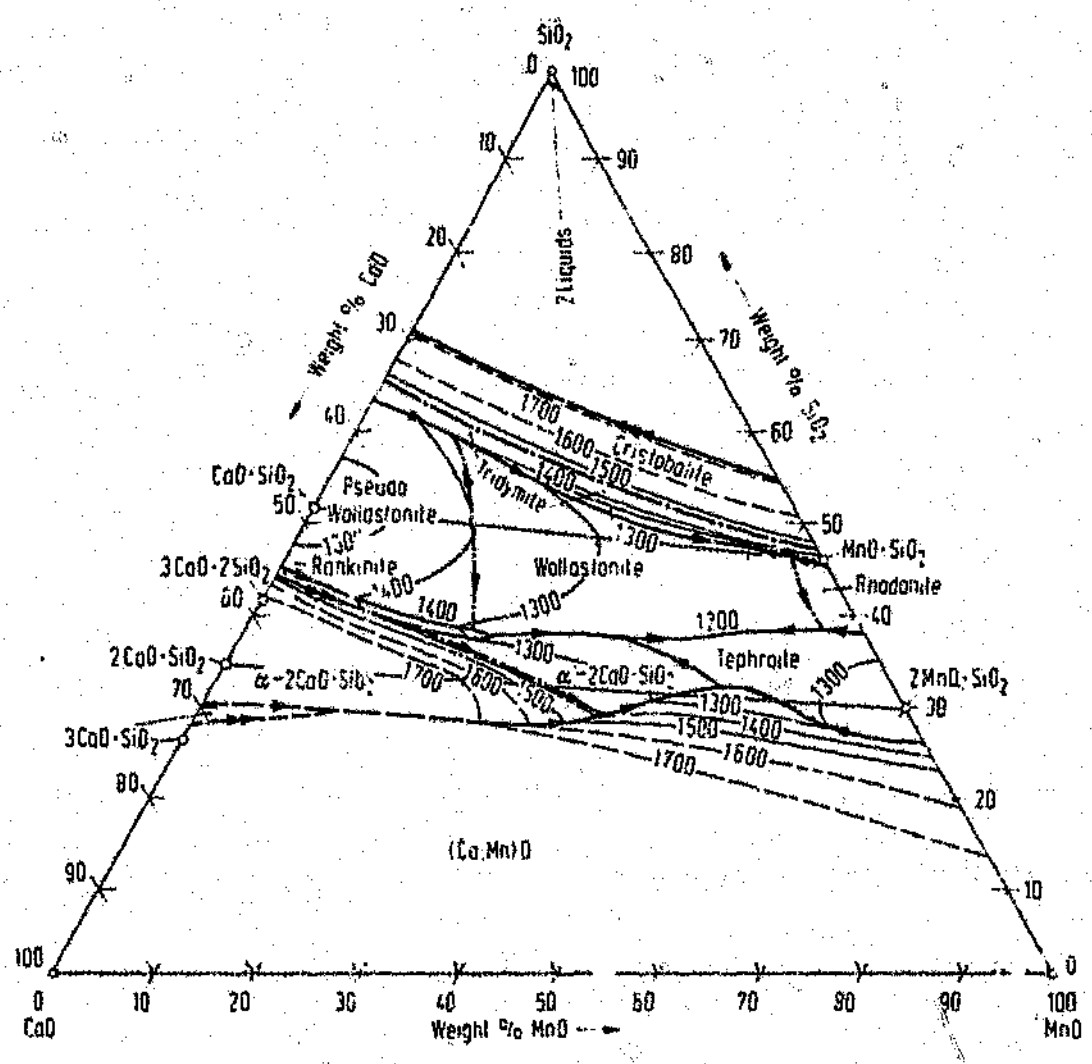


Figure 2.22 The system CaO-MnO-$SiO_2$.
(after Glosser, 1962).

## 2.4 The System C-Mn and C-Fe-Mn

The manganese-carbon phase diagram is shown in Figure 2.23. It is apparent that four solid solutions of carbon in manganese ($\alpha$,$\beta$,$\delta$ and $\gamma$) and five carbides are stable at various compositional and temperature ranges. $Mn_{23}C_6$, $Mn_5C_2$ and $Mn_7C_3$ are the most important carbide phases depending on the carbon content. For carbon contents of between 0 and 1.5 weight per cent, only $\alpha$-*manganase* metal should be present at room temperature. From 1.5 to 5.40 weight per cent carbon $\alpha$-*manganase* and $Mn_{23}C_6$ are stable at room temperature. A further increase in the carbon content to between 5.40 and 8.03 weight per cent results in manganese metal no longer being stable, and $Mn_{23}C_6$ and $Mn_5C_2$ are the stable carbides at room temperature. Between 8.03 and 8.56 weight per cent carbon $Mn_5C_2$ and $Mn_7C_3$ are present, and if the carbon content exceeds 8.56 weight per cent, $Mn_7C_3$ and graphite are formed.

In the presence of iron the above carbide phases probably become $\alpha$-*FeMn* + $(Fe,Mn)_{23}C_6$, $(Fe,Mn)_{23}C_6$ + $(Fe,Mn)_5C_2$, $(Fe,Mn)_5C_2$ + $(Fe,Mn)_7C_3$, $(Fe,Mn)_7C_3$ + graphite, as the iron manganese carbides have similar carbon contents to their manganese carbide counterparts.

The system C-Fe-Mn has been studied by numerous investigators (Vogel and Doring, 1935; Isobe, 1951; Schurmann and et al, 1977). The resulting liquidus projection of the ternary Fe-Mn-C system is illustrated in Figure 2.24.

The primary crystallization areas shown in the Figure 2.24 are for $\delta Mn$,$\delta Fe$,$\gamma Fe$ (continuous solid solution with $\gamma Mn$)$M_3C$, $\epsilon$ which is solid solution of Fe, Mn and C appearing above 60 wt % Mn, $Mn_5C_2$, $Mn_7C_3$ and graphite. Schurman and Geissler established that between 0 and 3% Mn graphite separates as the stable phase. This observation contradicts the assumption generally made in the earlier literature that the $M_3C$ phase extents to the binary C-Fe axis, but agrees with solid-state studies in which equilibrium between $\gamma Fe$ and graphite at Mn contents up to 1% and from temperatures of 1100°C down was established. In general agreement between sources is very reasonable. Difficulties arise considerably at the higher manganese contents.

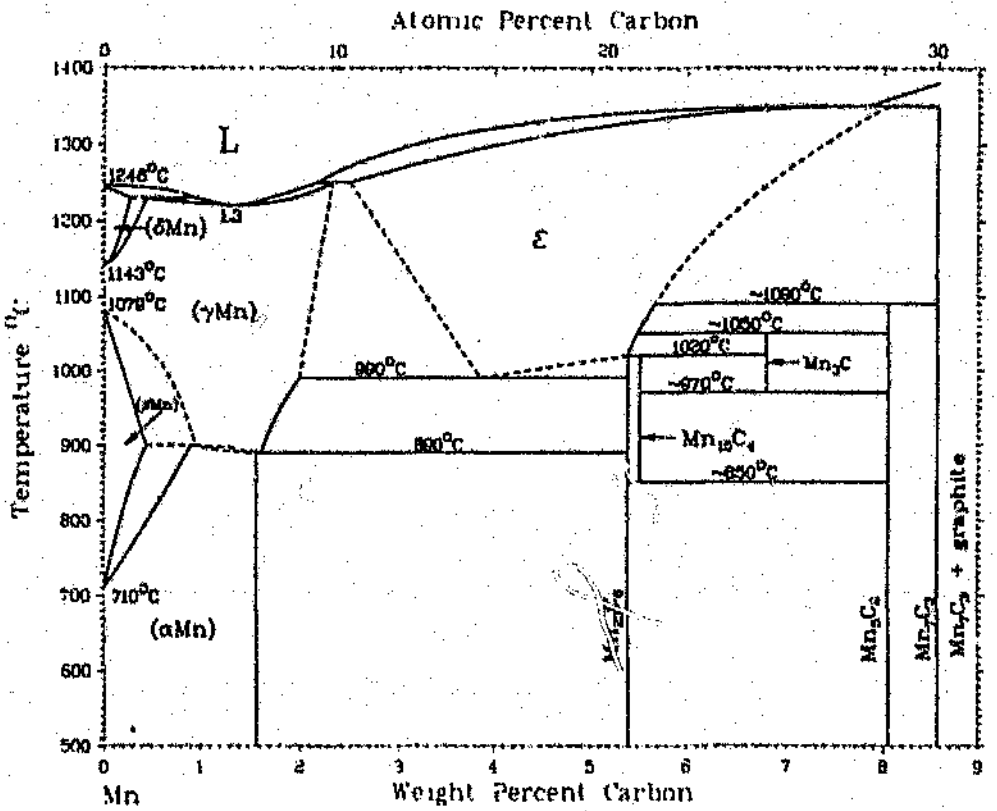


Figure 2.23 Binary Mn-C phase diagram.
(after Benz and et al, 1973).

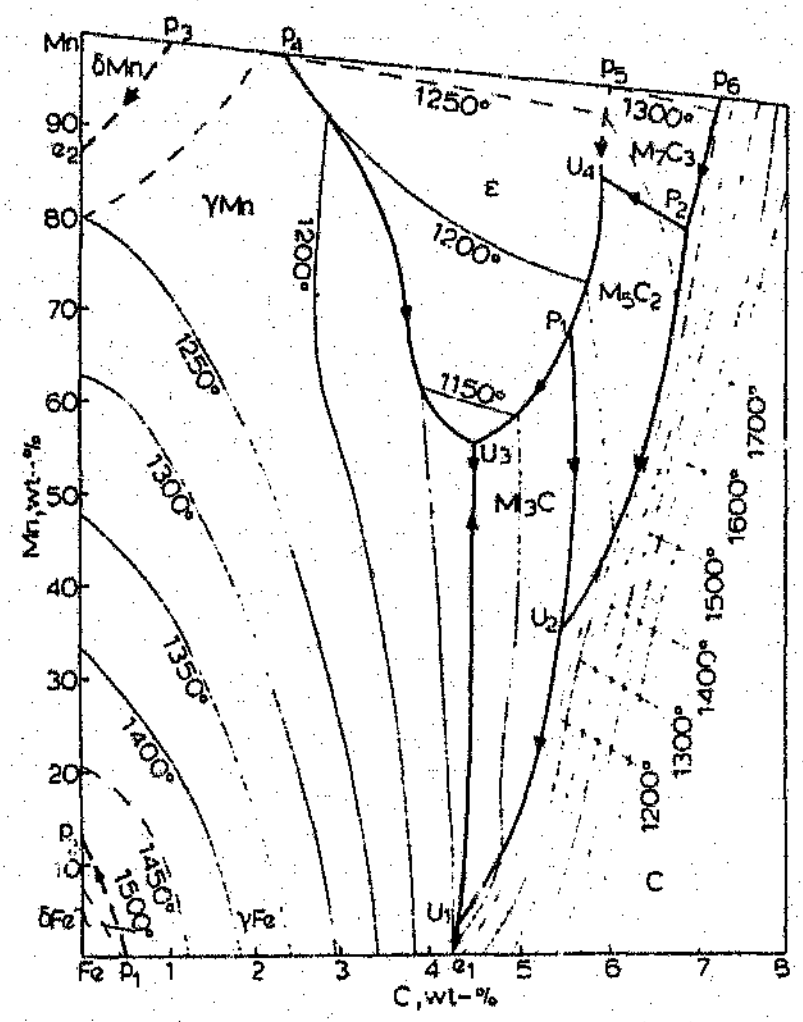


Figure 2.24 Liquidus projection of C-Fe-Mn system. (after Schurmann, 1977: Schenck and et al, 1963: Chipman, 1952).

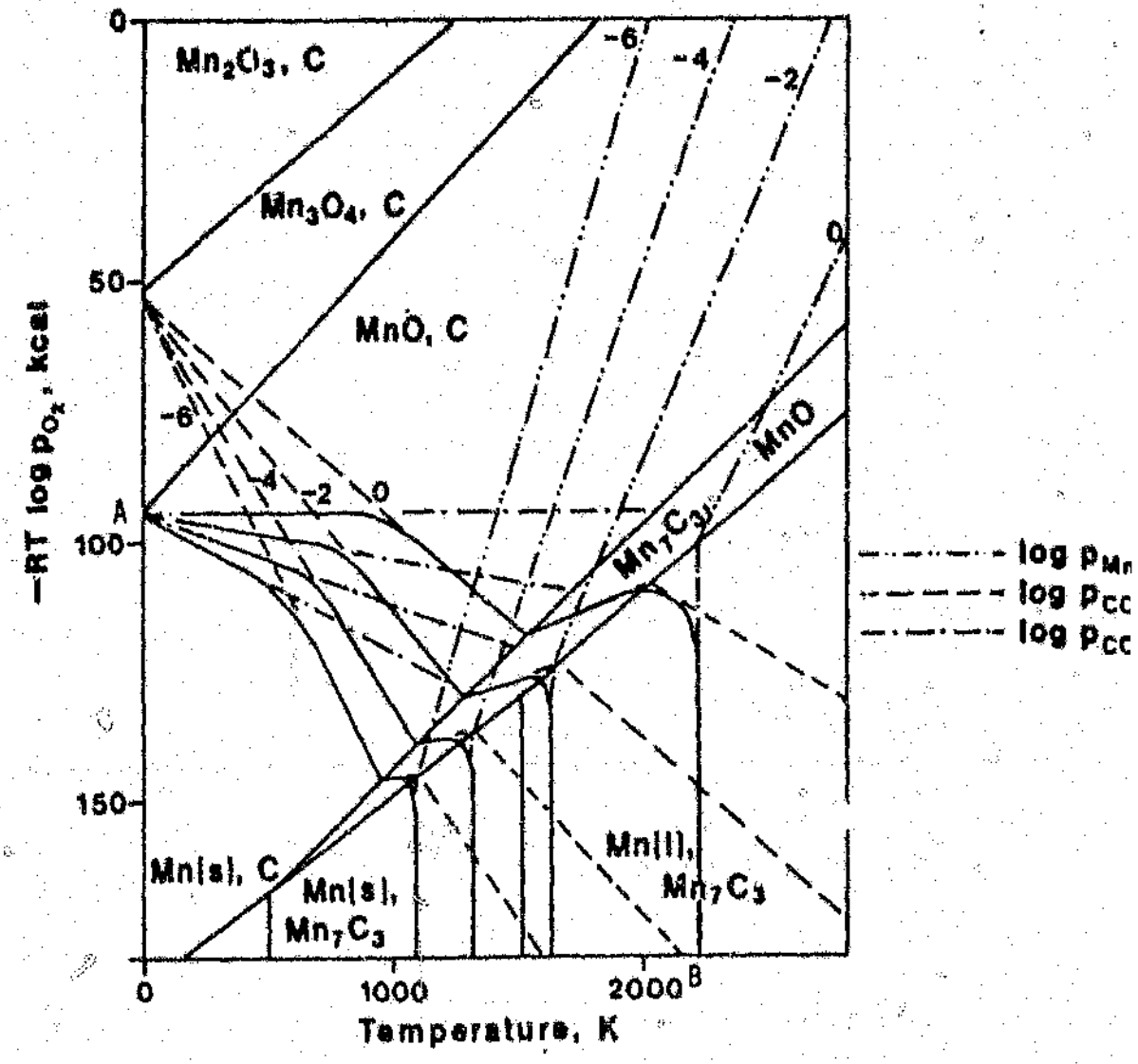


Figure 2.25 Pourbaix diagram for the Mn-O-C system. (after Downing, 1963).

# 3 EXPERIMENTAL PROCEDURE

## 3.1 Raw Materials

Manganese ore from the Mamatwan mine was supplied by Samancor. This was a bore hole sample which represented three zones namely M, C, N with a depth from 216'5", to 260'3", from 260'3" to 281'1" and from 281'1" to 289'0" respectively. The sample was crushed and milled to under 420 $\mu m$. As it was planned to examine the manganese particles after various stages of reduction, it was decided to use particles in as narrow a size range as could be conveniently obtained by screening. In principle this would permit all particles to undergo the same degree of reduction in a given time. For this purpose, samples were wet-ground in a rod mill and wet-screened to yield a number of closely sized particles from a representative sample weighing 500 g using the Tyler screen set of 420, 297, 210, 149, 105, 74, 61 $\mu m$. The samples for the experiments were separated from the mixture by the laboratory scale rotary arc-path sampler. This machine allowed splitting of a given amount of the sample into the representative smaller portions by a rotating and distributing mechanism. Table-3.1 and Table-3.2 show the screen analysis and chemical analysis of the ore respectively.

Chemical analyses of the unreduced manganese ore, determined for every alternate particle size range, gave almost identical results, i.e. the composition of the ore was found to be quite uniform over the entire size range. Fine powdered ,- 43 $\mu m$, spectroscopic graphite was the reducing agent.

## 3.2 Description of Equipment

In order to perform a detailed experimental investigation of manganese ore reduction, a technique was required for continuously monitoring the changes occurring within the sample while it was maintained under closely controlled conditions in terms of atmosphere and temperature. Barnes (1981) has reviewed the techniques that have been used to examine reduction behaviour. He stated that thermogravimetric analysis (TGA), i.e. measurement of mass change as a function of time (with the charge material at a constant temperature under the selected atmosphere), gave a complete picture of the rate of reduction of the sample at that temperature. Kucukkaragoz et al (1983) and Soykan and Eric (1988) used the same technique to determine the reduction behaviour of the BC chromites. They stated that, by TGA, runs could easily be duplicated and provision could be made easily for controlling the atmosphere. In view of the above, it was decided to examine the reduction of mixtures of manganese ore and graphite by thermogravimetric analysis (TGA).

A molybdenum wound resistance furnace with a recrystallized alumina work tube which has an inside diameter of 50 mm was used. Figure 3.1 illustrates the schematic drawing of the furnace. Furnace windings were protected from oxidation by an atmosphere of cracked anhydrous amonia. The temperature was measured and controlled by two (Pt-6% RH - Pt-30% RH) thermocouples placed next to each other suspended to just above the sample from the top of the furnace. Temperature was

controlled by a Euroterm type 020 temperature controller coupled to a 25 amper type 031 thyristor unit. This combination is reported to have a calibrated accuracy of +/- 2°C at 1200°C - 1400°C according to the user manual of the temperature controller.

A digital electronic balance was placed in an airtight perspex box and the pan of the balance was replaced with an alumina rod and pedestal. The balance case was connected to the furnace work tube by gas tight flexible bellows from the bottom of the furnace so that gas tightness was maintained during experiments.

Data gathering was performed using a computerised data gathering and display system comprising a mettler PE400 electronic balance coupled to an computer for data logging. The analogue output from the Mettler balance was received by a CL241 analogue to digital interface. The computer programme processed 100 data points per minute from the balance. The average of these points was taken as the weight loss. By this way weight loss values were continuously stored on the 5 1/4 inch floppy disc. The weight loss data were then converted to percent reduction and TGA curves was obtained from a HP 7470A plotter with data points at one minute intervals.

The complete experimental set-up, including the furnace and its ancillary equipment, gas train, TGA and data logging computer is illustrated in Figure 3.2.

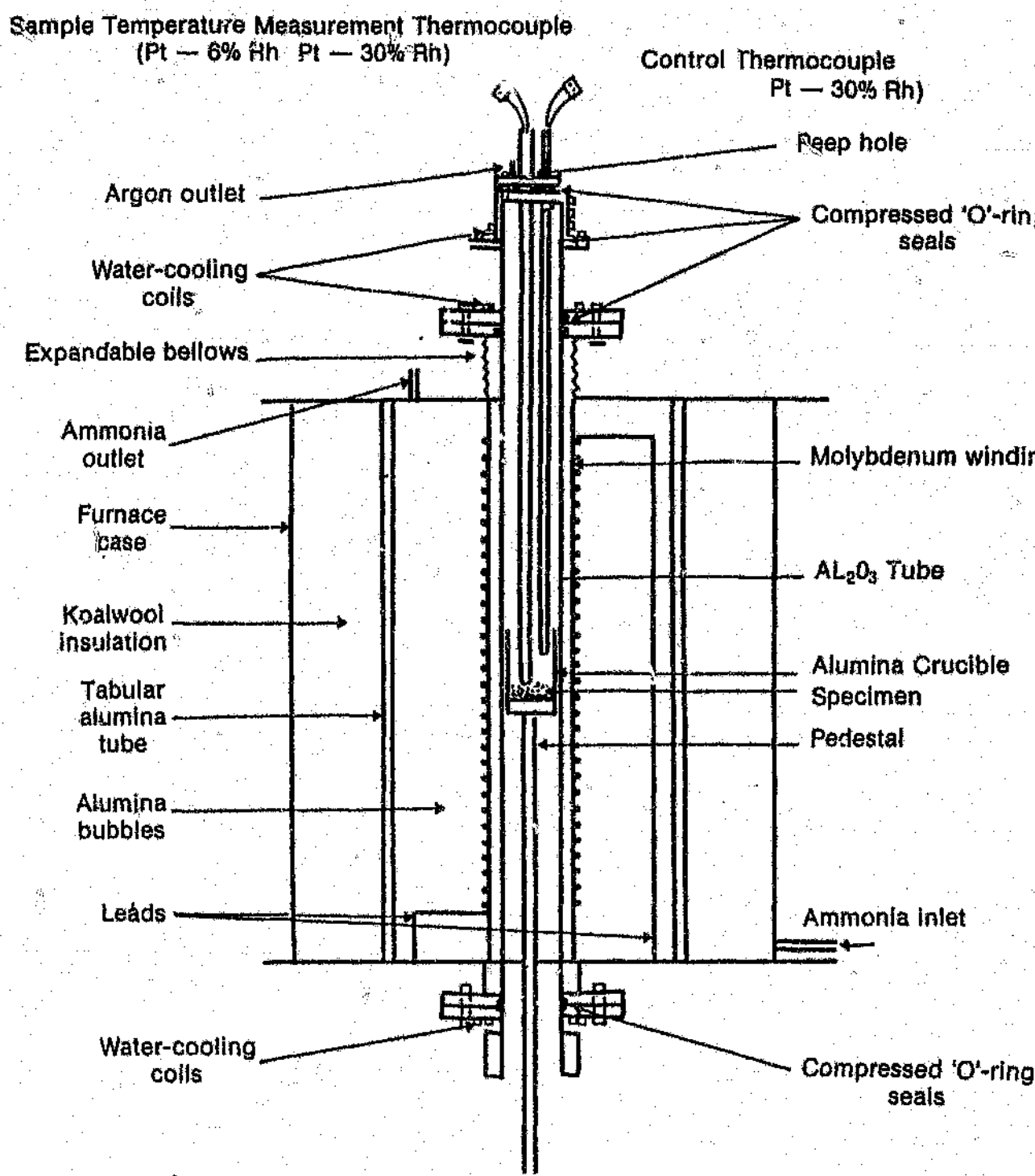


Figure 3.1 The vertical molybdenum-wound resistance furnace.

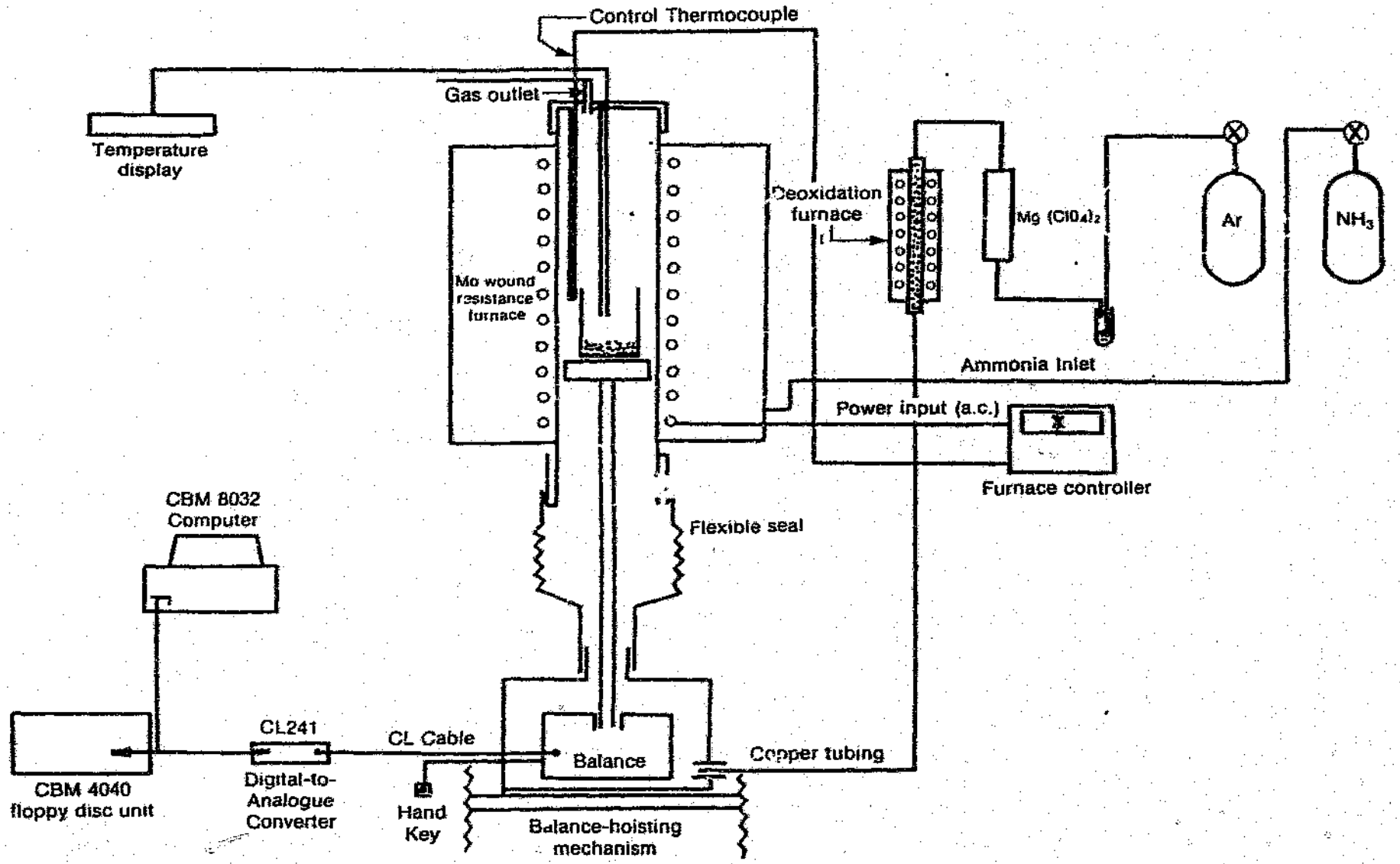


Figure 3.2 Schematic representation of experimental apparatus

### 3.3 Reduction Runs

Reduction experiments were conducted by making use of the TGA apparatus, the details of which were explained above.

All The manganese ore samples were calcined prior to reduction to remove the crystalline water and $CO_2$ at 1000°C in the reduction furnace. The charges were prepared by mixing calcined manganese ore and graphite under acetone in an agate mortar. Since pelletizing of the same size range particles is difficult and kinetics of the reaction is affected by the pressure used in briquetting (McRae, 1977) loosely packed powder charges of 5-7 g were used, contained in an Alsint sintered alumina crucible which had a diameter of 35 mm, height of 60 mm and wall thickness of 2 mm. The wet mixture was charged to the cru ible and was dried in a drying oven at 100 °C. The crucible was weighed with and without its contents prior to experiments and after the completion of reduction runs. The crucible and its contents were placed on the pedestal of the TGA system and the rubber bellows was connected to the furnace and the experimental system was continuously purged with deoxidized argon. The crucible was then raised into the hot zone of the furnace. The hot zone of the furnace was about 3 cms along which no temperature variation was observed. The argon flow was maintained at 1000 $cm^3$/min., measured at 25 °C and atmospheric pressure. Since the spectroscopic argon contains 5 ppmm oxygen and water vapour, before entering the system argon was dried in a drying chamber filled with anhydrous ($Mg(ClO_4)_2$) as a dessicant and deoxidized in a copper

chips furnace at 500 $^{o}$C. This is a vertical Kanthal wound resistance furnace with a work tube filled with copper chips. The copper chips in the tube can react with the oxygen in the argon gas at 500$^{o}$C according to the following reaction.

$$2Cu(s) + 1/2\ O_2(g) = Cu_2O(s) \quad \ldots\ldots\ldots \quad 3.1$$

In certain experiments, the argon atmosphere was replaced by either CO or $CO_2$ gases to reveal the effect of different atmospheres on reduction behaviour. When these gases were employed, the furnace work tube was first flushed with argon gas for 5 minutes before the introduction of CO or $CO_2$ gases. The copper chips furnace was not utilised in these experiments.

Experimental runs were allowed to proceed up to 90 minutes whereupon they were stopped by lowering the balance assembly quickly so that the sample could cool in stream of argon gas to prevent reoxidation at the cold end of the furnace. The checking of the weights of the crucible before and after the reduction on a separate balance proved that the reduction percentage calculated by the computer was correct and the results were reproducible.

Tests were performed at regular intervals to check for possible air leaks in the system. This was done by replacing the experimental sample with a pure carbon charge over periods up to 2 hours in argon atmosphere. The apparatus was never found to have any detectable air leaks as shown by the zero mass loss recorded.

After each reduction test, a representative sample of the reduction products was split off using a riffle and sent for chemical analysis. The remainder was retained for mounting in polished sections for scanning electron microscopy (SEM), optical microscopy and energy dispersive analysis of x-rays (EDAX) as well as diffraction analysis.

### 3.4 Definition of the Degree of Reduction

Reducibility is a measure of the relative ease with which an ore can be reduced to metal and it is defined as the measured weight loss of the ore during the reduction with carbon after a time at a given temperature, expressed as a percentage of the theoretical weight loss for the total reduction of the ore. Therefore the degree of reduction of manganese, R %, can be described as:

$$R\% = \frac{\text{Mass of oxygen removed}}{\text{Mass of Removable oxygen}} \times 100$$

Three major oxide components namely manganese oxide (MnO), Manganese dioxide ($MnO_2$) and iron oxide ($Fe_2O_3$) were considered to be reducible whereas the other oxide components, namely alumina ($Al_2O_3$), silica ($SiO_2$) and magnesia (MgO) were all classed as non-reducible under the condition of solid state reduction of manganese ore with carbon.

It is known that thermodyanamically carbon monoxide is the stable gas above 900 $^{o}C$ according to the Boudouard

reaction:

$$2CO_2 + C = 2CO \quad \ldots\ldots\ldots\ldots\ldots\ldots \quad 2.2$$

The measurement of mass loss by thermogravimetry during reduction indicates the quantity of CO released during the reduction and is directly proportional to the mass of oxygen lost from the oxides and hence to the degree of reduction. The degree of reduction is therefore defined as :

$$R\% = \frac{\text{Mass of CO evolved}}{(28/16) * \text{Mass of Removable oxygen}} \times 100$$

This was the definition used in this investigation.

The stoichiometric amount of carbon was defined as the amount required for complete reduction of the iron and manganese oxides to the metal. For all reduction tests, carbon in excess of that defined by the stoichiometric requirements discussed above was mixed with each sample of manganese ore. In this way errors that would arise from the incomplete reduction was prevented. The percentage of excess carbon is simply expressed as:

$$\text{Excess percent carbon} = \frac{\text{C mass \% (total)} - \text{C mass \% (stoichiometric)}}{\text{C mass \% stoichiometric}} \times 100$$

Table - 3.1

Screen Analysis of Mamatwan Ore

| Sieve Size | | Mass (g) | Mass (%) | Cumulative % |
|---|---|---|---|---|
| Tyler Mesh | $\mu m$ | | | Finer than |
| 35 | 297 | 0.0 | 0.0 | 100.00 |
| 48 | 210 | 103.26 | 20.65 | 79.35 |
| 65 | 149 | 70.65 | 14.13 | 65.22 |
| 100 | 105 | 70.00 | 14.00 | 51.22 |
| 150 | 74 | 54.34 | 10.87 | 40.35 |
| 200 | 61 | 27.17 | 5.43 | 34.92 |
| 250 | 43 | 10.87 | 2.17 | 32.75 |
| -250 | -43 | 163.70 | 32.75 | - |

Table 3-2

Chemical Analysis of Mamatwan Ore

| Mesh | MgO | $Al_2O_3$ | $SiO_2$ | CaO | $Fe_2O_3$* | $H_2O$ | $CO_2$ | $Mn_2O_3$* |
|---|---|---|---|---|---|---|---|---|
| -35 + 48 | 2.49 | 0.30 | 4.66 | 13.16 | 5.99 | 0.20 | 15.90 | 56.69 |
| -48 + 65 | 2.02 | 0.30 | 3.30 | 12.90 | 5.88 | 0.10 | 16.60 | 56.33 |
| -65 + 100 | 2.30 | 0.30 | 3.60 | 13.80 | 5.88 | 0.20 | 15.40 | 55.33 |
| -100 + 150 | 2.27 | 0.30 | 3.26 | 13.36 | 5.90 | 0.20 | 15.40 | 55.55 |
| -150 + 200 | 2.55 | 0.30 | 3.15 | 14.23 | 5.80 | 0.30 | 15.50 | 54.12 |
| -200 + 250 | 2.44 | 0.30 | 2.96 | 14.11 | 5.87 | 0.30 | 15.40 | 55.30 |
| -250 | 2.19 | 0.30 | 2.45 | 14.74 | 5.88 | 0.20 | 16.30 | 53.54 |

* Total Mn and Fe are expressed as $Mn_2O_3$ and $Fe_2O_3$ respectively

### 3.5 X-ray Diffraction Analysis (XRD)

All X-ray diffraction analysis were performed at MINTEK. In order to determine the phase changes occurring in the manganese ore with increasing extent of reduction, a split from the samples was finely ground and analysed by a Philips x-ray diffractometer with a monochrometer using metallic copper as the source of x-rays. The resulting x-ray is the $k-\alpha$ radiation of copper with a wavelength of 1.54 $A^{o}$. Concentrations of less than 3 % could not be detected by XRD techniques.

### 3.6 Optical Examination and Energy Dispersive Analysis of X-rays (EDAX)

Standard metallographic techniques and optical microscopes were used for the preliminary optical examination of product samples. Energy dispersive analysis of x-rays (EDAX) and electron optical examination were carried out by a Jeol 840 scanning electron microscope, which had a link x-ray microanalysis system, type AN10000, attachment by which a particle could be point-scanned for a particular element.

### 3.7 Chemical Analysis

All the chemical and x-ray diffraction analyses of the samples were done at MINTEK with standard procedures. The accuracy of the chemical analyses as given by the Analytical Science Division of Mintek are as follows:

a) Accuracies of more than 1 percent (relative) can be obtained for manganese and iron when the atomic emission method is used

b) Carbon analysis were carried out by use of the standard Leco analyser with an accuracy range of 0.02 to 1 percent. This analyser works as the following: 0.5-2 gm of the sample is mixed with the metal accelerator then put into the combustion furnace through which oxygen is admitted with a furnace temperature 1600°C. The carbon amount is determined by the infrared method using $CO_2$ outlet gas.

# 4 EXPERIMENTAL RESULTS AND DISCUSSIONS

## 4.1 Kinetic Results

All the experimental samples were preheated before reduction experiments to decompose the carbonates and drive off crystalline water. Otherwise the mass loss due to these reactions would mask the mass loss occurring in the initial stage of the reduction. During preheating a total mass loss of about 17.5 percent was observed within 30 minutes at 1000 $^{o}$C in argon atmosphere. The work of Dressel and Kenworthy (1961) on the reduction of various manganese minerals indicates that braunite decomposes to MnO and $Mn_2SiO_4$ when heated to 1000$^{o}$C. Although the ore becomes gravimetrically stable after 10 minutes at 1000$^{o}$C in argon atmosphere, the work of de Villiers (1973) indicates that minor structural changes may continue to occur for periods of up to 3 to 4 hours at this temperature. The X-ray diffraction studies carried out by de Villiers on Mamatwan ore which had been heated to 1000$^{o}$C for up to 4 hours showed small variations in the relative amounts of braunite, hausmannite, $Ca(OH)_2$, $CaMn_2O_4$ and $CaMnO_3$ during this period. Figure 4.1 shows the mass loss on preheating of the ore at 1000$^{o}$C under argon atmosphere.

During the reduction of the manganese ore with carbon various factors were observed to have influenced the rate and degree of the reduction reactions. These factors are reaction temperature, particle sizes of both ore and carbon, amount of reducing agent and the reduction atmosphere.

According to the TGA results obtained, temperature was the most significant factor influencing reduction extent of the Mamatwan manganese ore. A three-fold increase on the reduction extent was observed as the temperature increased from 1100 to 1350 $^{o}$C. This is illustrated in Figure 4.2. This result may be expected since it is known that an increase in reaction temperature increases the rates of all reactions in general. Theoretically the rate of reduction of oxides to their metallic states increases with temperature. All the reduction versus time curves showed a marked decrease in the rate from about 4 minutes of reaction time depending upon temperature. The point of changes in slope of kinetic curves corresponded to approximately 30 percent reduction at temperatures above 1250 $^{o}$C. The change in slope and thus change in the rate is probably due to a change in mechanism rather than a temperature effect. The reduction-time curves at all temperatures indicated the possibility of three distinct stages in the reduction process. The initial stage where rates are very high, is followed by the second stage which is characterized by a drop in rate and a possible change in mechanism. This step is followed by a third one which is very slow compared to the first two. At the end of the reduction the ore has shown a mass loss which is almost one-third of its original weight as it is seen in Figure 4.3.

Up to approximately 30 percent reduction, the effect of particle size on the reduction extent and rate was not very pronounced. Thereafter it was found that reduction rate is also a function of particle size, i.e. it is decreasing with increasing particle size. This effect can be explained as follows: decreased particle sizes

of both the manganese ore and carbon result in
1) higher total surface areas of both manganese and carbon particles exposed to the reducing atmosphere.
2) larger number of the contact points between the manganese and carbon particles
3) Shorter diffusion paths in the manganese ore particles.

Higher reactant surface area, larger number of contact points and shorter diffusion paths all give rise to increased reaction rates. However, at particle size finer than 149 $\mu m$ the trend is very indistinct and particles of different sizes react at similar rates at 1350 $^{o}$C. The effect of particle size on reduction rate and degree at 1100$^{o}$C, 1200$^{o}$C, 1300$^{o}$C and 1350$^{o}$C are shown in Figures 4.4-4.7. The strong influence of particle size at 1300 $^{o}$C is more noticeable as shown in Figure 4.6. This result was supported by other investigations which have been carried out on the reduction of manganese oxide (Rankin, 1980; Terayama, 1985). For further analysis of effect of particle size on reduction, kinetic data were replotted as reduction percentage versus particle size at 20, 50, 70 minutes retention times at 1300$^{o}$C and 50 minutes retention time at 1350$^{o}$C in Figure 4.8. This figure shows that it is possible to achieve different degrees of reduction from the same ore by altering the particle size in a given time at a given temperature. The linear relationship of reduction with particle size at a given time and temperature was confirmed by the regression analysis of the data and the equations are listed in Table 4.1, where R is reduction percent and X is the particle size.

Table 4.1

Regression analysis of reduction vs particle size data

| Temperature | Time (min) | Equation | correlation coefficient |
|---|---|---|---|
| a) 1350°C | 50 | R = 98.16 - 43.01 X | 0.990 |
| b) 1300°C | 70 | R = 94.54 - 91.10 X | 0.996 |
| c) 1300°C | 50 | R = 81.94 - 75.42 X | 0.993 |
| d) 1300°C | 20 | R = 52.73 - 39.60 X | 0.990 |

The quantity of reductant which is over stoichiometric requirement was found to have slight effect on the rate and degree of reduction. Degree of the reduction was found to increase 10 percent in changing the amount of carbon from 30 percent excess to 200 percent excess. The increase in degree of the reduction was about 12 percent when the carbon particle size was decreased from 105 $\mu m$ to 43 $\mu m$. The results of these experiments are shown in Figures 4.9 and 4.10.

A set of experiments with pure $Mn_3O_4$ and $Fe_2O_3$ were carried out using graphite at 1300°C and 1350°C under an argon atmosphere to assist in the interpretation of the results for Mamatwan ore. The course of the reduction reaction between Mamatwan ore and carbon is difficult to follow due to the presence of iron oxide and gangue minerals in the ore, and so the reduction of pure manganese oxide by carbon was compared with the reduction of Mamatwan ore by carbon. The results are shown in Figure 4.11. It is noticed that rate and degree of reduction of Mamatwan ore is higher than of

the pure $Mn_3O_4$ up to 68 percent and 64 percent reduction at 1350°C and 1300°C respectively. This is probably due to the presence of $Fe_2O_3$ in the Mamatwan ore. The decrease in the rate and degree of the reduction of Mamatwan ore in the later stage may be caused by the formation of silicate phase which covers the oxide phase.

In order to shed some light on some reactions occurring during the reduction process and to see the effect of the reaction atmosphere on reduction, the neutral reaction atmosphere was replaced with carbon monoxide and carbondioxide atmospheres separately. Figure 4.12 summarizes the experimental results carried out under these atmospheres.

The reduction of manganese oxide to metal probably occurs through the following reactions.

$$MnO + CO = Mn + CO_2 \quad \ldots\ldots\ldots\ldots \quad 4.1$$

$$C + CO_2 = 2CO \quad \ldots\ldots\ldots\ldots \quad 2.2$$

$$MnO + C = Mn + CO \quad \ldots\ldots\ldots\ldots \quad 4.2$$

Under Argon atmosphere, the rate and extent of the reduction reaction was higher than the ones obtained under CO and $CO_2$ atmospheres all in the presence of carbon. This is illustrated in Figure 4.12. It can be expected that carbon dioxide and carbon monoxide atmosphere would effect the above reactions. The first reaction (4.1) will have a tendency to reverse in $CO_2$ rich conditions which prevents further MnO reduction. The second reaction (2.2) which is the gasification of

carbon will quickly consume most of the carbon in the reaction mixture. This is due to the thermodynamically favourable conditions for the formation of CO at such high temperatures. On the other hand under pure CO atmosphere, reaction (2.2) will be suppressed resulting in low reduction rate and extent. Therefore, it can be concluded in the lights of above experiments that reduction of MnO should be considered as a gas/solid type reaction in the presence of carbon. Grimsley (1977) also reported that complete reduction of higher manganese oxide to MnO is possible under CO atmosphere at 1000 $^{o}$C and 1200 $^{o}$C , This conversion could easily be achieved in the experiments done at 1300 $^{o}$C under CO atmosphere in the present work. This is also a proof that higher manganese oxides can be reduced to MnO by the following reaction.

$$Mn_2O_3 + CO = 2MnO + CO_2 \quad \ldots\ldots\ldots \quad 4.3$$

The abrupt termination of the reaction between the ore and carbon in an atmosphere of carbon monoxide after the conversion of the higher manganese oxides to MnO indicates that the overall reaction 4.2 can not proceed. The standard free energy change for reaction 4.1 is positive over the temperature range 25$^{o}$C to 2000$^{o}$C and it is generally accepted that gaseous reduction of MnO does not take place in the absence of carbon (Pilter, 1967; Yagihashi et al, 1963; Pentz, 1975).

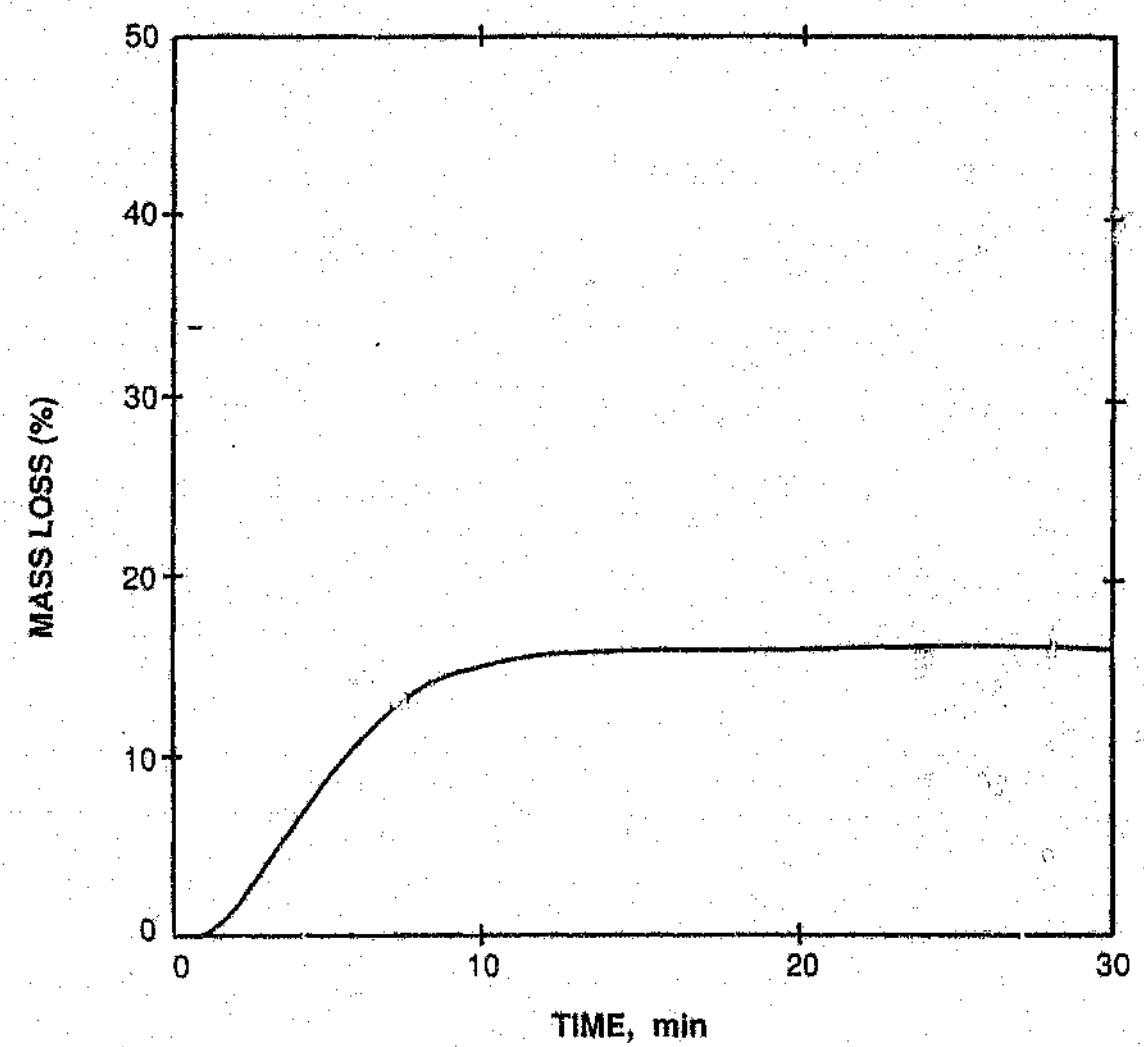


Figure 4.1 The effect of preheating on the Mamatwan manganese ore at 1000 $^{o}$C.

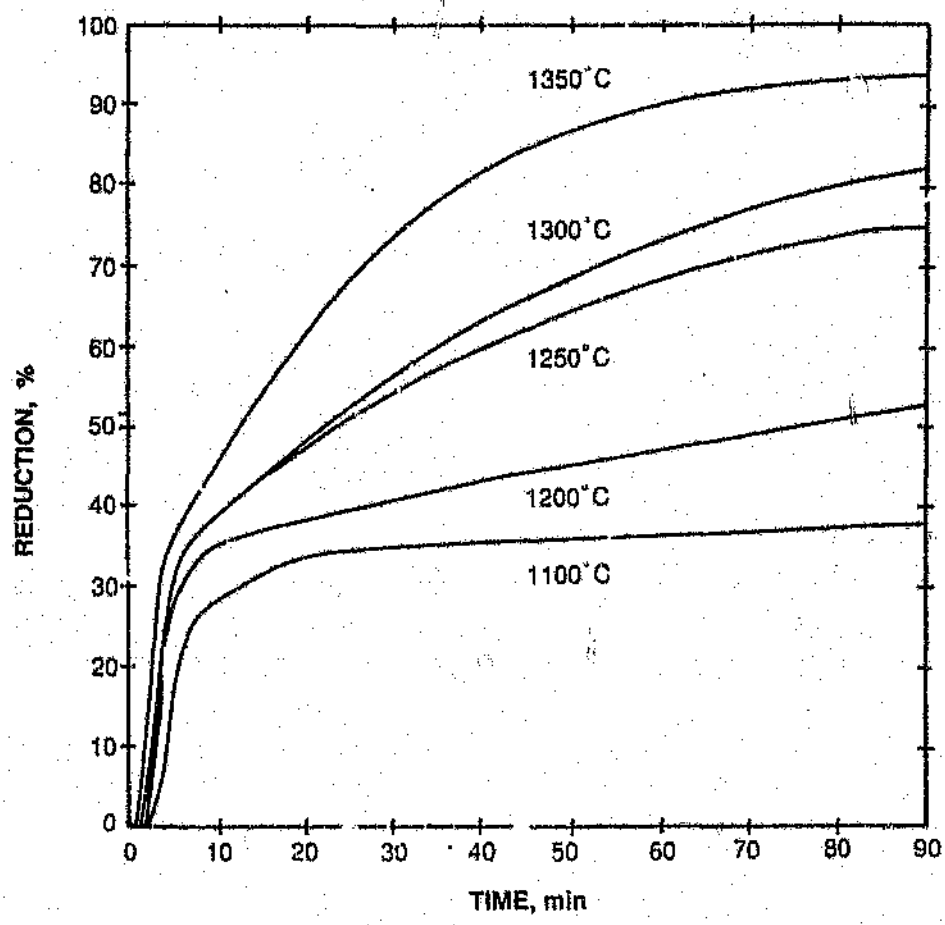


Figure 4.2 The effect of temperature on the reduction of the Mamatwan manganese ore. (The ore is -0.42 mm).

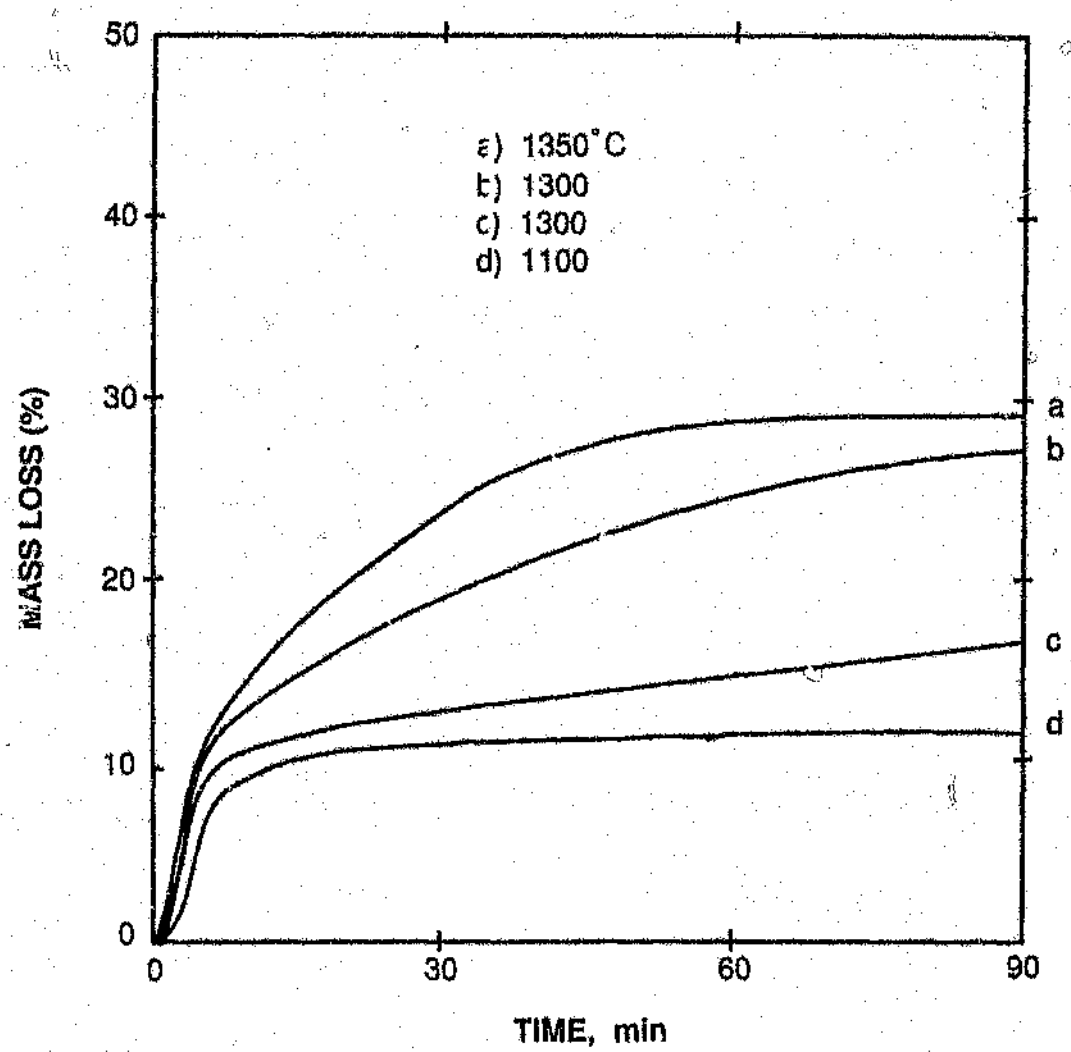


Figure 4.3 The effect of temperature on the mass loss of the Mamatwan manganese ore.

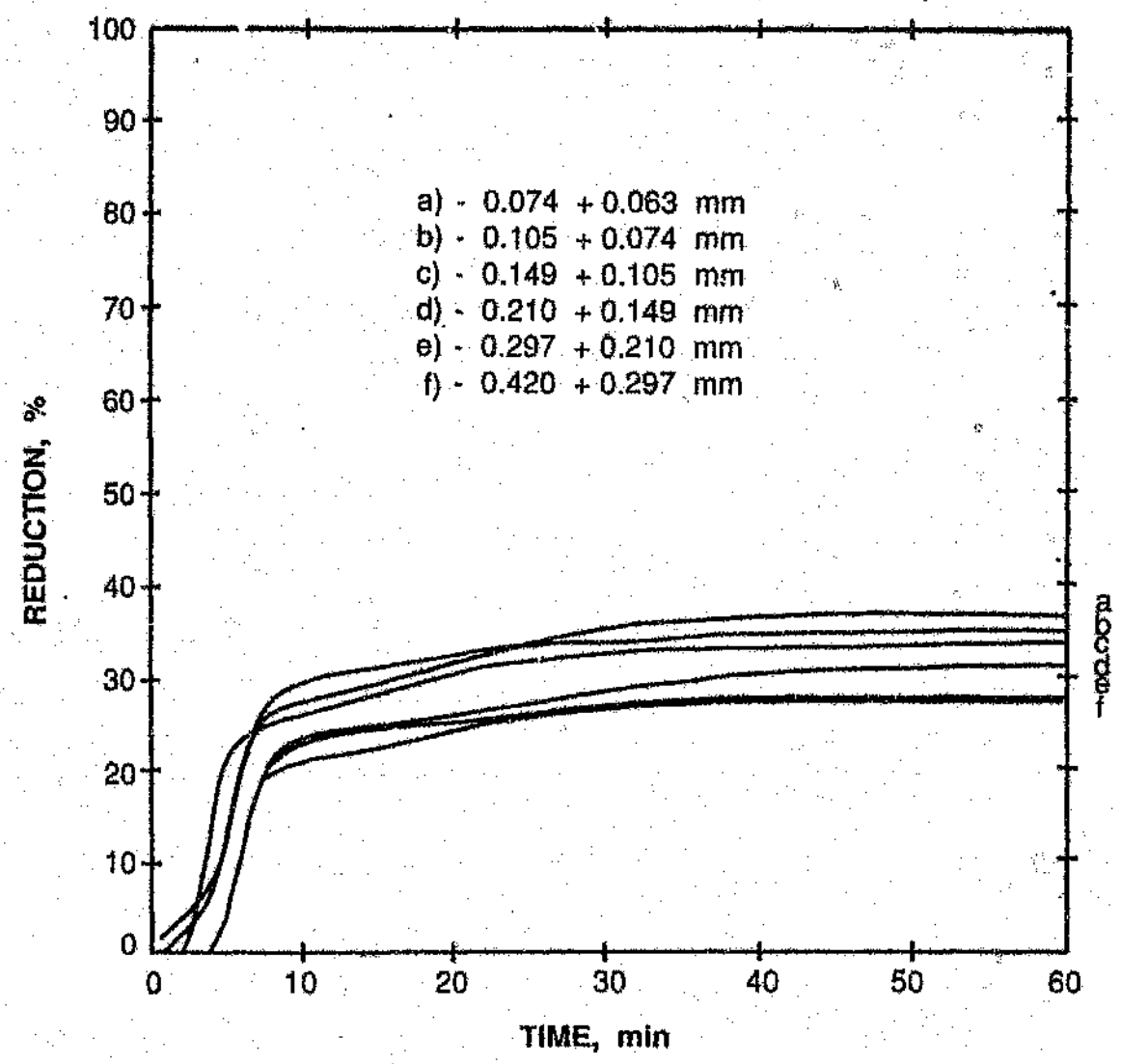


Figure 4.4 The effect of particle size on the reduction of the Mamatwan manganese ore at 1100 $^{o}$C.

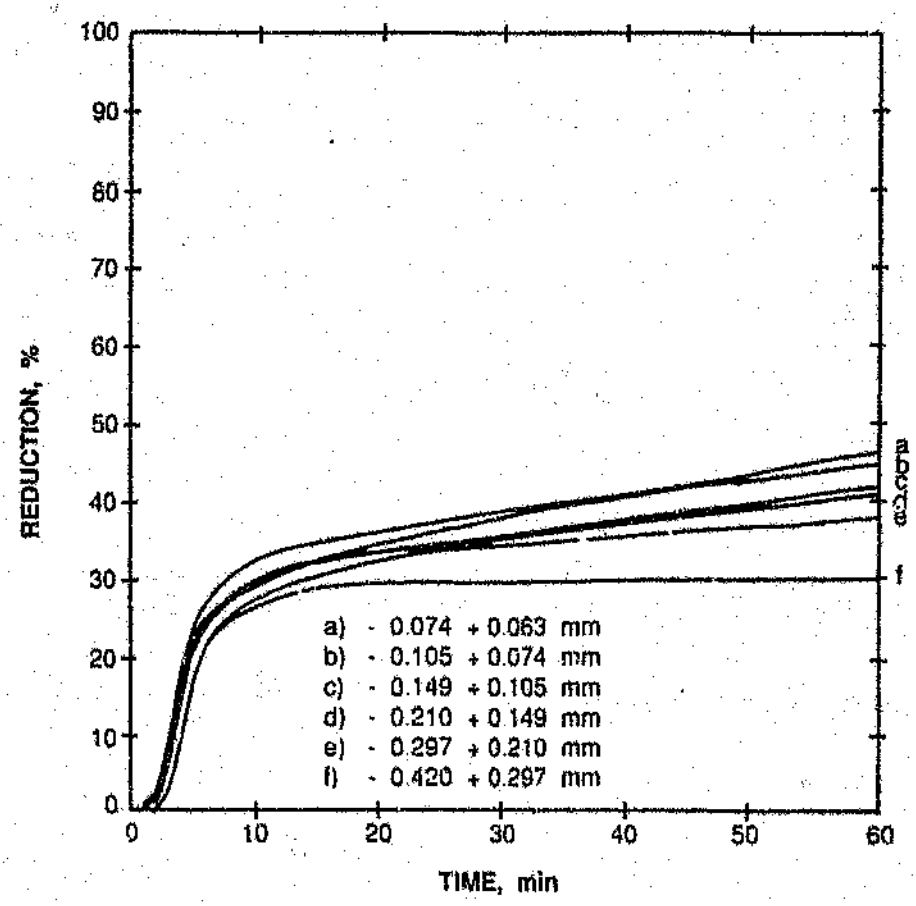


Figure 4.5 The effect of particle size on the reduction of the Mamatwan manganese ore at 1200 °C.

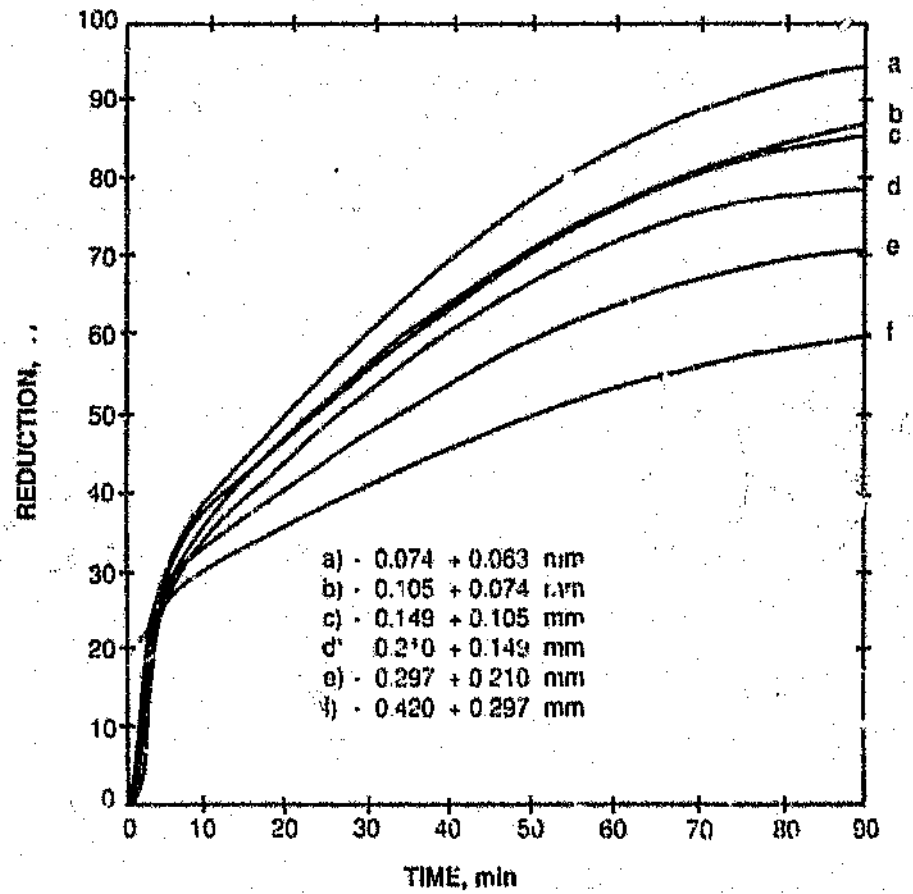


Figure 4.6 The effect of particle size on the reduction of the Mamatwan manganese ore at 1300 °C.

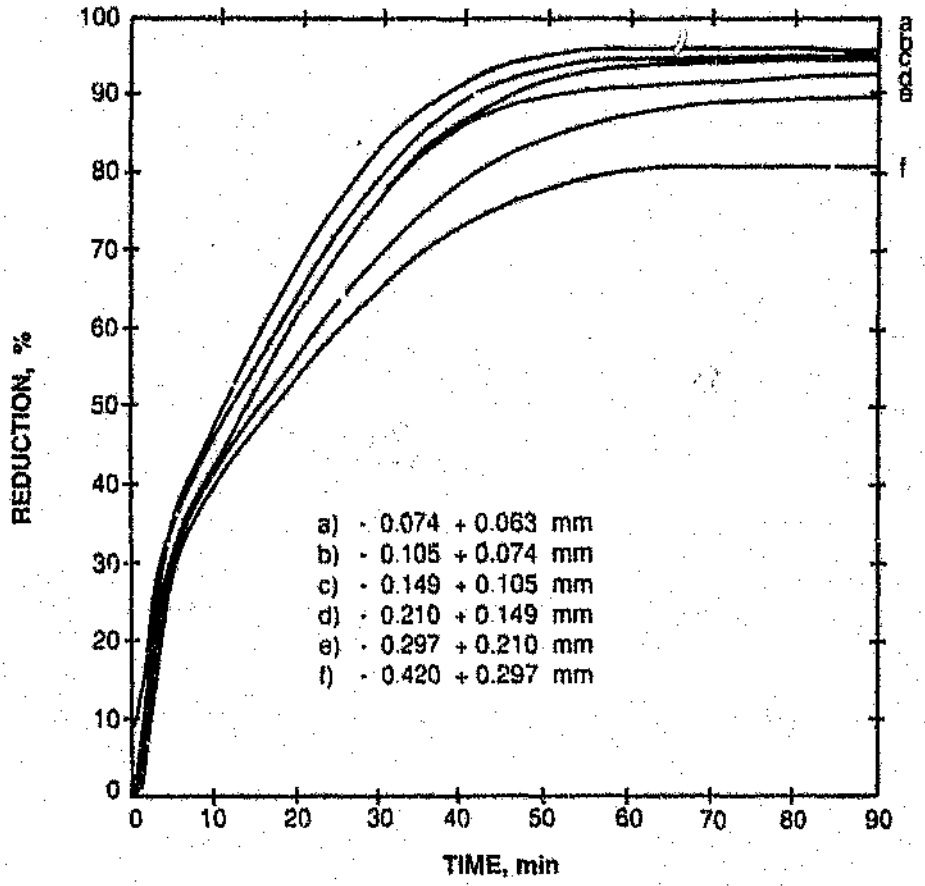


Figure 4.7 The effect of particle size on the reduction of the Mamatwan manganese ore at 1350 °C.

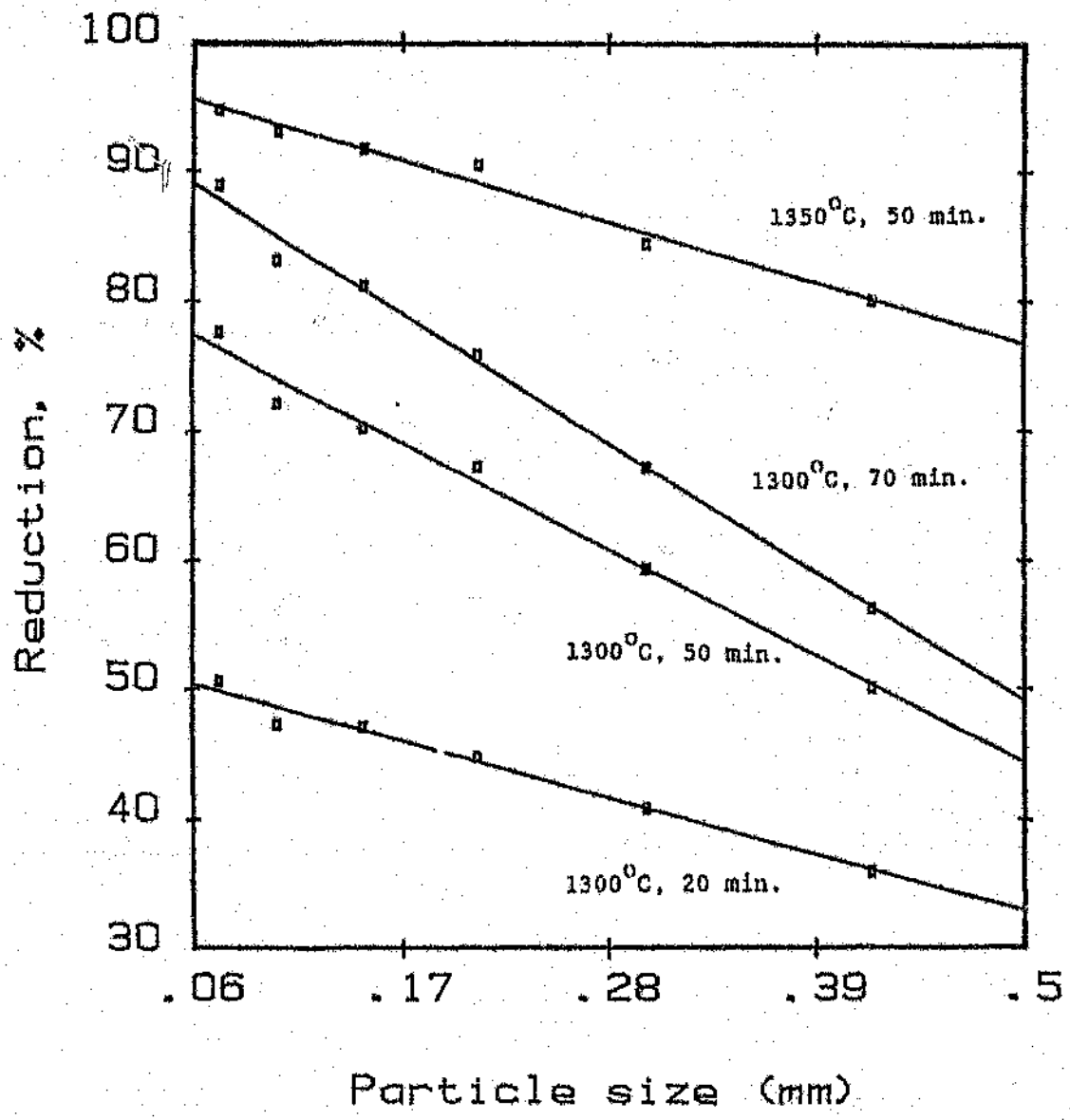


Figure 4.8 The effect of particle size on the reduction of the Mamatwan manganese ore after 20, 50, 70 minutes retention times at 1300°C and 1350°C.

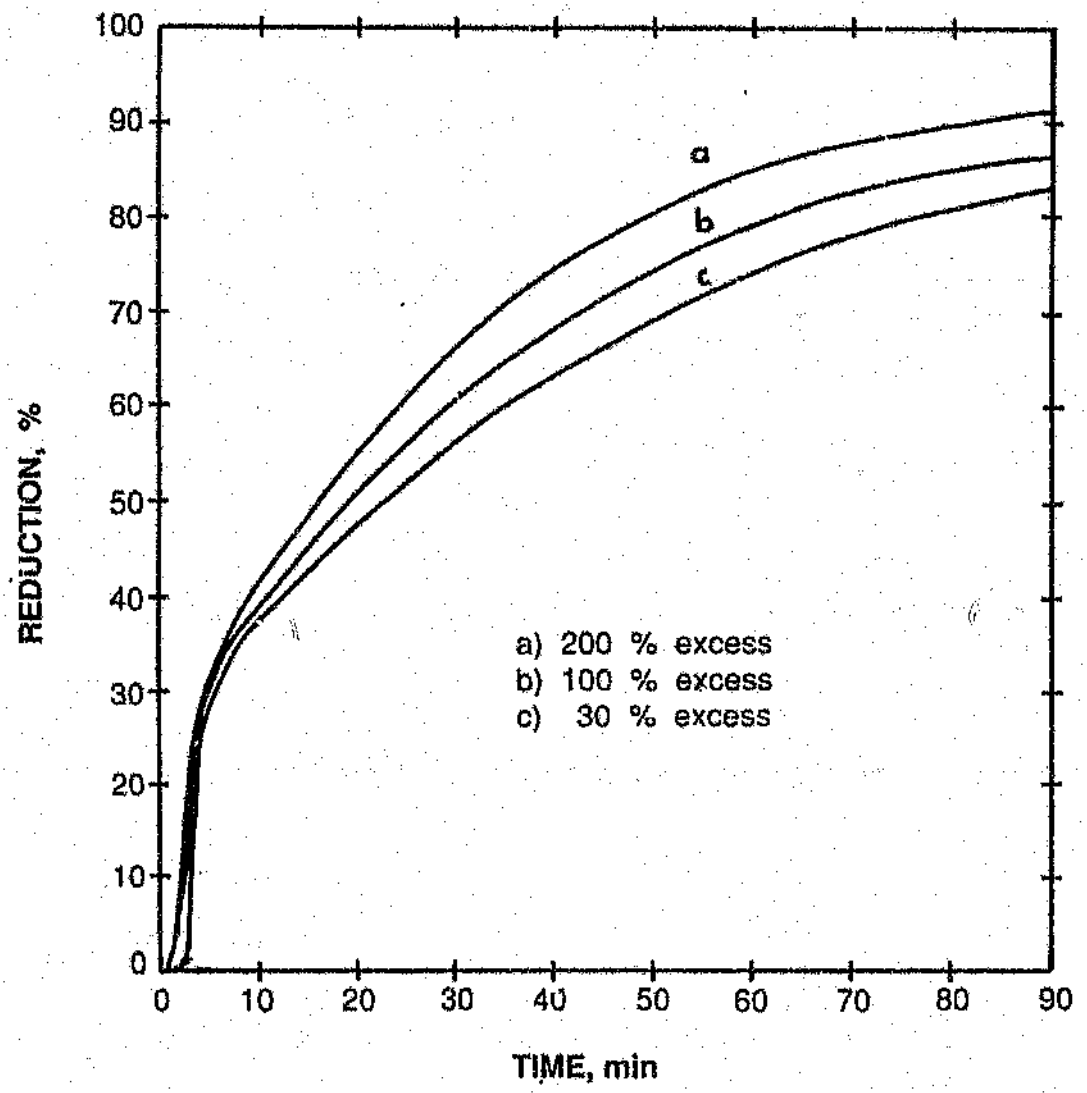


Figure 4.9 The effect of carbon amount on the reduction of the Mamatwan manganese ore at 1300 °C.

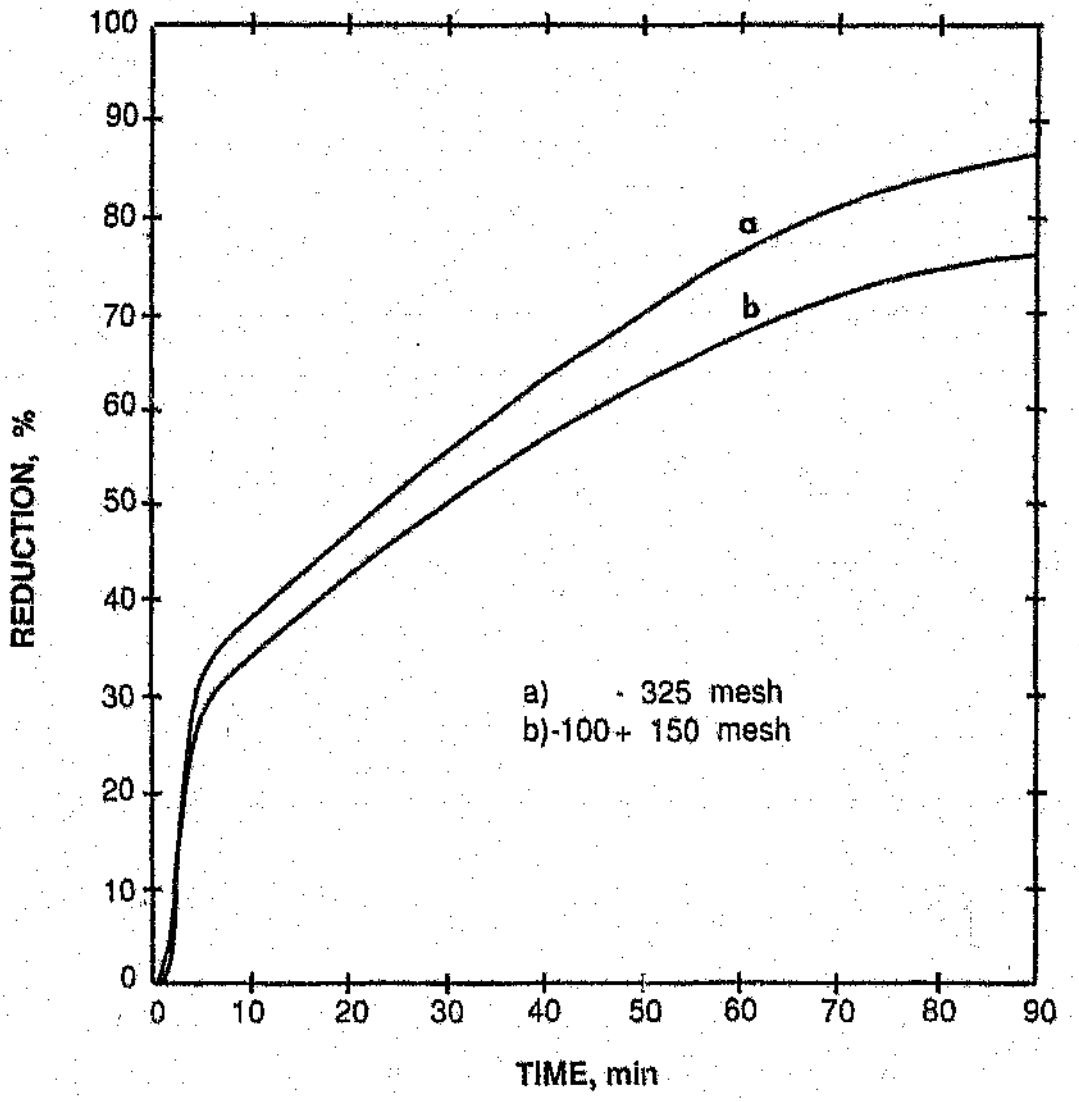


Figure 4.10 The effect of carbon particle size on the reduction of the Mamatwan manganese ore at 1300 °C.

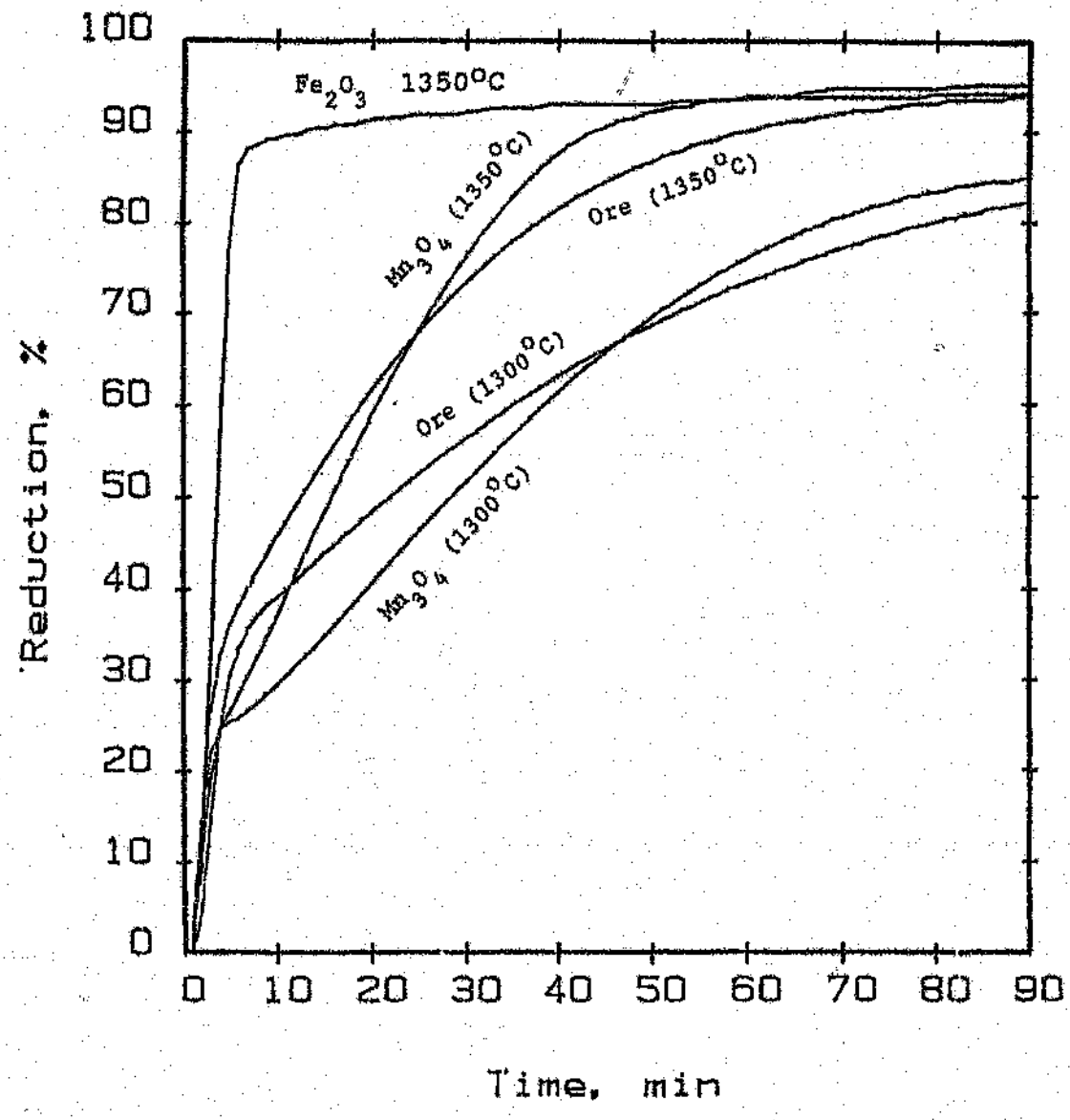


Figure 4.11 The effect of temperature on the reduction of pure $Mn_3O_4$ and $Fe_2O_3$.

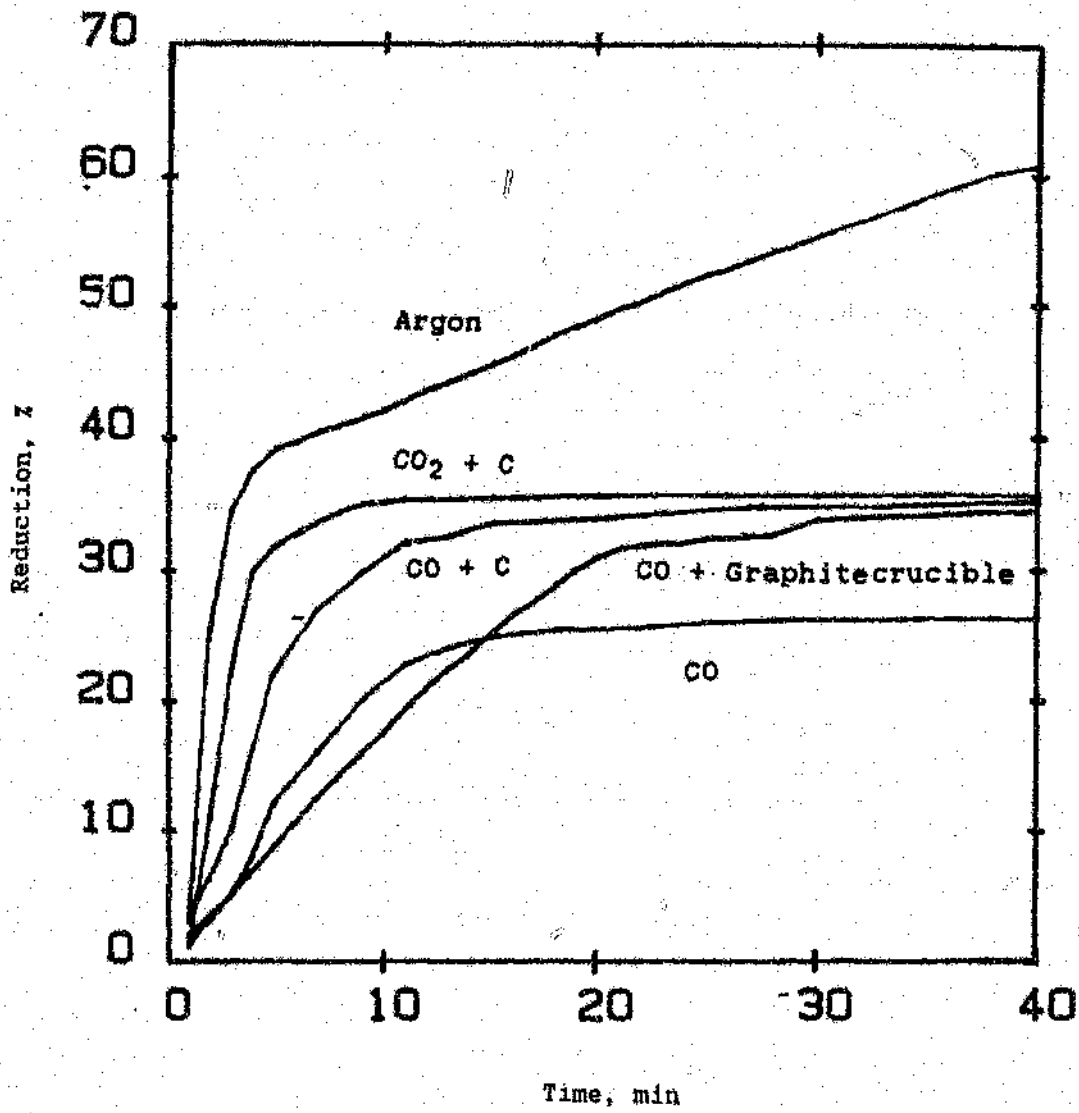


Figure 4.12 Reduction of the Mamatwan manganese ore under CO and $CO_2$ atmospheres at 1300 °C.

## 4.2 Investigation of Reaction Products

In the forgoing section it was apparent that TGA and chemical analysis alone could not facilitate the development of the reduction mechanism, as the reduction reaction could not be explicitly understood. For this reason, determination of the phases present in reduced samples was carried out by the use of optical, x-ray diffractometric and SEM-EDAX techniques.

X-ray diffraction analysis (XRD) analysis of the samples showed that Braunite ( $Mn^{+2}(Mn,Fe)^{+3}{}_6SiO_{12}$ ) was present in both the ore and the preheated ore. The phases detected from the diffraction patterns of the original Mamatwan ore are shown in Table 4.2. The compositional changes taking place during the reaction at 1300 $^oC$ and 1350 $^oC$ are summarised in Table 4.3. It is evident that a high degree of metallization and formation of silicate phase are achieved at 1300 $^oC$ and 1350 $^oC$. Rankin (1980) also found $Mn_5C_2$ as the reaction product in his study of reduction of MnO by carbon at 1350$^oC$.

The microphotographs and EDAX analysis of the intermediate phases in the reduction of preheated Mamatwan ore by carbon at 1350$^oC$, 1300$^oC$, 1200$^oC$, and 1100$^oC$ are shown in Figures 4.13 to 4.28.

$CaMn_2O_4$ formation was detected in the very early minutes of reduction together with MnO by EDAX analysis although this was not detected in x-ray analysis. This is probably due to the relatively small amount of this phase. Light areas in Figure 4.13 are MnO and $CaMn_2O_4$.

These phases were more or less of the same colour under microscope but they were distinguished by EDAX analysis. The microphotograph in Figure 4.14 indicates the random nucleation of metal throughout the ore particle. Small white nuclei on the edge of grey MnO areas are the iron rich manganese carbides. At this stage grains are largely unreduced.

Growth of these metal nuclei and start of formation of silicate phase are shown in Figure 4.15 to 4.17. Until 50 minutes retention time, silicate phase contains substantial amount of MnO. Figures 4.18 to 4.20 reveal that there is drastic increase in metallization and formation of silicate phase as the reduction proceeded. Metal phase gradually covers the grain while some parts of the grain are in the silicate form. Only metal (carbide, $(Mn,Fe)_5C_2$ ) and silicate phases were detected in the late part of the reduction.

The same reaction products namely $(Mn,Fe)_5C_2$ and silicate phase ($Ca_2SiO_4$) were also found at 1300°C. It was noticed that silicate phase still contains some MnO even after 90 minutes of reaction time. Figure 4.21 and 4.22 show the microphotographs of grains reduced at 1300°C. The reaction product $CaMn_2O_4$ reported by the previous investigator Grimsley (1977) at 1300°C could not be observed in present study.

The kinetic curves of reactions reveal that incomplete reduction was obtained at 1100°C and 1200°C. Microphotographs Figures 4.23 and 4.24 show a large percentage of unreduced oxides in the grains reduced at

these temperatures. Reduction reactions ceased after formation of iron-rich metal nuclei. $CaMnO_3$ was also detected in the products of 1100°C reduction.

In microscopic examination of reaction products, it was common to observe highly cracked, porous grains in different stages of reduction. Some of the selected microphotographs are shown in Figures 4.25 and 4.28. Figure 4.25 and 4.26 show the microphotographs of grains reduced for 50 and 10 minutes at 1350°C respectively while Figures 4.27 shows a grain subjected to 25 minutes retention time at 1300°C. As reduction progresses, cracks (possibly along certain crystallographic planes) appear in ore particles. These cracks are inaccessible by solid carbon and therefore reduction by CO gas may cause metallization to occur within these cracks which are points where the nucleation of new metal would be easiest, because of low surface energy (Lida, 1962).

Table 4.4 gives the Mn and Fe percentages of the metal phase determined by EDAX with increasing extent of reduction at 1350 °C. The first value in the table gives 61.94 % Fe and 25.3 % Mn for the metal phase adjoining a MnO area inside the particle which was reduced about 34 percent.

Therefore it can be concluded that metallization starts with nucleation of iron which is immediately followed by the nucleation of manganese. Table 4.4 also shows a significant increase in the manganese concentration of the metal phase as reduction proceeds. The iron content

of the metal phase decreases with reduction to a value of 6.52 % at about 95 % reduction. During this stage, the manganese content of the metal phase increases drastically. The manganese content is 76.89 % at this reduction stage.

Chemical analysis results of reaction products shown in Table 4.5 were plotted against reduction time in Figures 4.29-4.32 to follow carbon, oxygen, manganese, iron changes during the reduction process. As expected carbon content of the reaction sample decreased drastically as the reduction proceeded. It is understood from the Figure 4.29 that carbon consumption of the reaction sample is very low after about 50 minutes of retention time which corresponds about 85 percent reduction at 1350°C. Figure 4.30 shows that oxygen removal of the reaction sample carried on until about 70 minutes of retention time. Decrease in carbon consumption and oxygen removal rate may also indicates that later minutes of reduction process involves a different mechanism. Figure 4.31 and 4.32 show that of manganese and iron contents of the reaction mixture is increased by about 13 percent (from 38 percent to about 51 percent) and by 1.6 percent (from 4.70 p rcent to 6.30 percent) respectively during the reduction process. Of course this is mainly due to the relative decrease of the weight of the reaction mixture when oxygen is removed together with some carbon.

On samples reacted at 1350 °C, very small amount of MgO was found deposited as a white powder covering the surface and as feathers at the top of the crucible. The

appearance strongly suggested the involvement of a vaporous transport mechanism in the formation of this product (Kucukkaraǧoz and et al, 1983)

Table - 4.2

Mineralogical Analysis of Mamatwan ore

| Mineral | Composition |
|---|---|
| Braunite | $Mn^{2+}(Mn,Fe)^{3+}_6SiO_{12}$ |
| Calcite | $CaCO_3$ |
| Kutnahorite | $Ca_{0.97}Mn_{0.5}Mg_{0.5}Fe_{0.03}(CO_3)_2$ |
| Hausmannite | $Mn_3O_4$ |
| Manganite | $\gamma$-$MnOOH$ |
| Hematite | $Fe_2O_3$ |

Mineralogical Analysis of Preheated Ore

| Mineral | Composition |
|---|---|
| Braunite | $Mn^{2+}(Mn,Fe)^{3+}_6SiO_{12}$ |
| Hausmannite | $Mn_3O_4$ |
| Manganosite | MnO |
| Jacopsite | $MnFe_2O_4$ |
| Lime | CaO |

Table - 4.3

The Phases detected by X-ray in the Samples of 1300 °C and 1350 °C reaction products.

| Reaction Time (min) | Reduction percent 1300°C | 1350°C | Phases |
|---|---|---|---|
| 3 | 14.19 | 26.64 | Graphite<br>MnO<br>$MnFe_2O_4$ |
| 9 | 38.20 | 43.72 | Graphite<br>MnO<br>$(Mn,Fe)_5C_2$ |
| 25 | 52.61 | 68.09 | Graphite<br>MnO<br>$(Mn,Fe)_5C_2$<br>$Ca_2SiO_4$ |
| 50 | 68.75 | 86.83 | Graphite<br>$(Mn,Fe)_5C_2$<br>MnO<br>$Ca_2SiO_4$ |
| 90 | 82.45 | 94.45 | Graphite<br>$(Mn,Fe)_5C_2$<br>$Ca_2SiO_4$<br>MnO |

Phases are in decreasing order of abundance.

Table - 4.4

EDAX Analysis of Metal Phases in Reaction Products at 1350 $^{o}$C

| Reaction Time (minute) | Reduction percent | Mn (%) | Fe (%) |
|---|---|---|---|
| 6 | 38.14 | 25.30 | 61.94 |
| 10 | 45.54 | 48.18 | 37.88 |
| 25 | 68.09 | 51.49 | 29.44 |
| 35 | 78.03 | 65.66 | 24.56 |
| 50 | 86.83 | 73.17 | 11.29 |
| 70 | 92.15 | 73.93 | 9.10 |
| 90 | 94.45 | 76.89 | 6.52 |

Table 4.5

Total manganese, iron, carbon and oxygen contents of the reaction mixture at 1350°C.

| Reduction Time (min) | Reduction per cent | Mn % | Fe % | C % | O % |
|---|---|---|---|---|---|
| 2 | 14.39 | 38.05 | 4.70 | 16.35 | 22.60 |
| 4 | 32.76 | 41.00 | 5.10 | 14.35 | 22.40 |
| 6 | 38.14 | 41.20 | 5.20 | 13.45 | 21.70 |
| 9 | 43.72 | 41.70 | 5.30 | 13.20 | 21.20 |
| 16 | 55.69 | 45.60 | 5.50 | 11.85 | 19.90 |
| 28 | 71.45 | 47.20 | 5.70 | 9.75 | 17.90 |
| 42 | 82.96 | 50.60 | 6.00 | 6.90 | 16.45 |
| 76 | 92.88 | 51.00 | 6.30 | 6.85 | 13.30 |
| 120 | 95.11 | 51.20 | 6.30 | 6.50 | 12.90 |
| The ore | - | 38.90 | 4.90 | 4.55 | 23.90 |

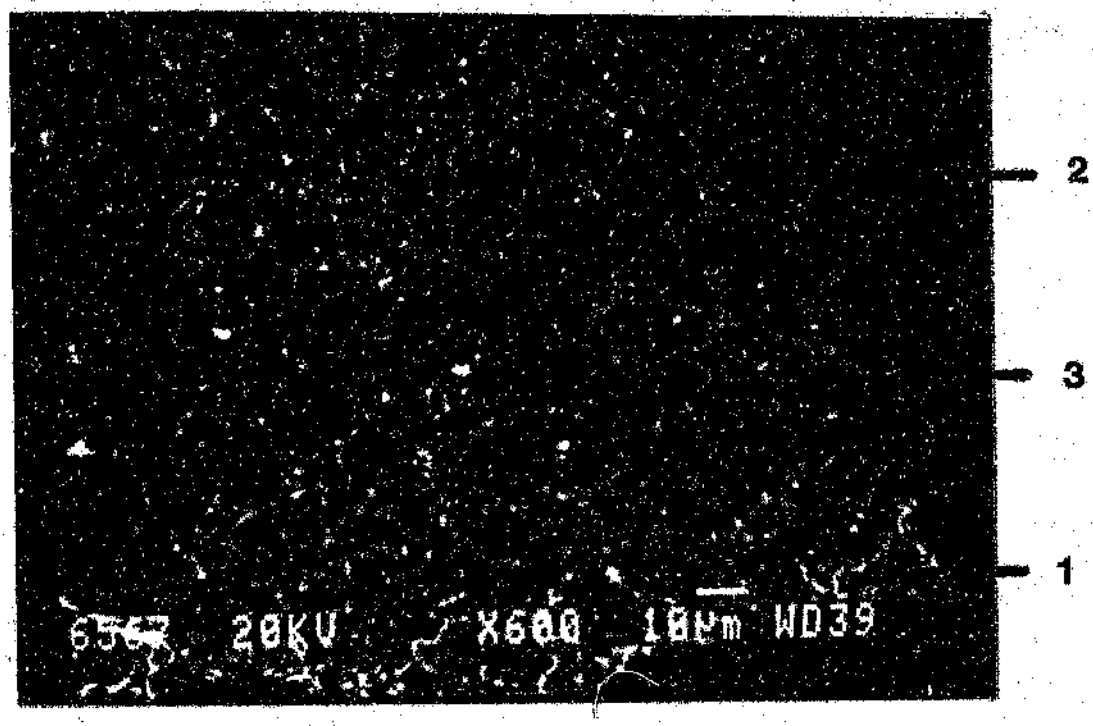


Figure 4.13 A Mamatwan manganese ore grain subjected to 26.64 percent reduction for 3 minutes at 1350 °C. Mag. 600X

Element concentrations determined by EDAX

| | 1 | 2 | 3 |
|---|---|---|---|
| Mn | 44.84 | 64.30 | 18.90 |
| Ca | 12.74 | 2.72 | 19.43 |
| Fe | 4.31 | 4.50 | 0.32 |
| Mg | 2.58 | 0.72 | 12.41 |
| Si | 4.11 | 1.10 | 0.63 |
| possible phase | $CaMn_2O_4$ | MnO | unreduced part |




Figure 4.14 A Mamatwan manganese ore grain subjected to 38.14 percent reduction for 6 minutes at 1350 °C. Mag. 2000X

Element concentrations determined by EDAX

| | 1 | 2 | 3 |
|---|---|---|---|
| Mn | 72.80 | 25.30 | 24.41 |
| Ca | 0.62 | 1.02 | 20.66 |
| Fe | 1.78 | 61.94 | 0.62 |
| Mg | 0.33 | 0.57 | 12.54 |
| Si | 0.71 | 1.50 | 0.47 |
| possible phas | MnO | Carbide | unreduced part |

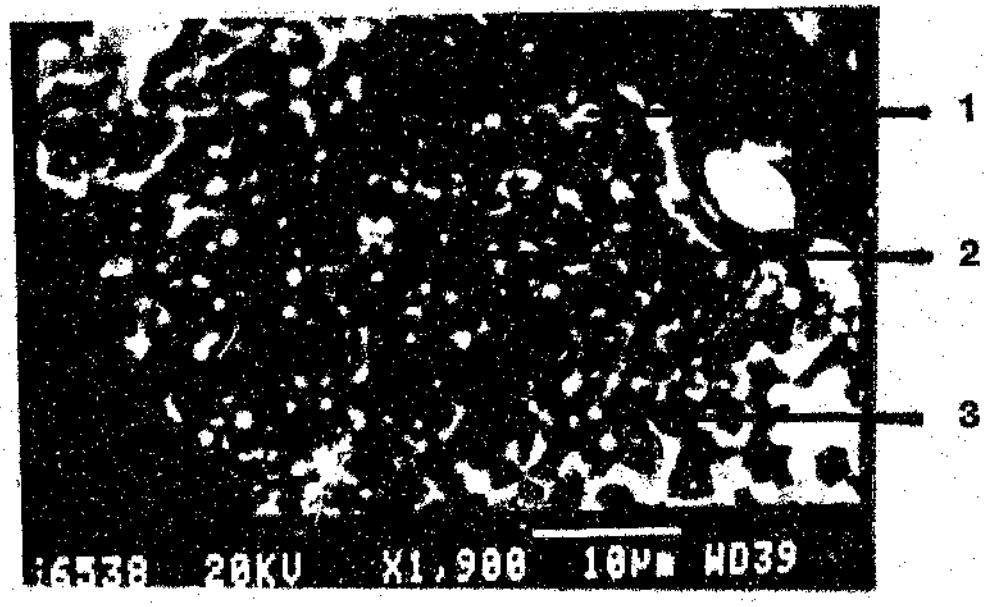


Figure 4.15 A Mamatwan manganese ore grain subjected to 45.54 percent reduction for 10 minutes at 1350 °C. Mag. 1900X

Element concentrations determined by EDAX

| | 1 | 2 | 3 |
|---|---|---|---|
| Mn | 48.18 | 69.60 | 25.70 |
| Ca | 1.50 | 1.70 | 24.30 |
| Fe | 37.88 | 0.82 | 1.51 |
| Mg | 0.43 | 4.80 | 1.82 |
| Si | 0.55 | 0.31 | 9.70 |
| possible phase | carbide | MnO | MnO dissolved $Ca_2SiO_4$ |

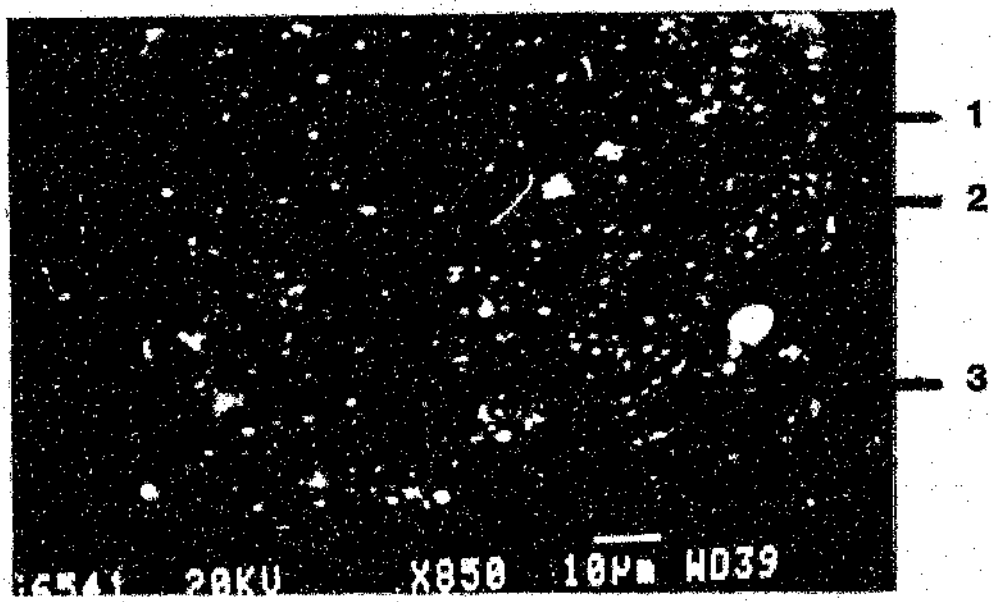


Figure 4.16 A Mamatwan manganese ore grain subjected to 68.09 percent reduction for 25 minutes at 1350 °C. Mag. 850X

Element concentrations determined by EDAX

| | 1 | 2 | 3 |
|---|---|---|---|
| Mn | 51.49 | 66.90 | 24.43 |
| Ca | 1.40 | 0.71 | 20.12 |
| Fe | 29.44 | 0.32 | 0.62 |
| Mg | 0.82 | 5.60 | 3.00 |
| Si | 0.46 | 0.67 | 13.11 |
| possible phase | carbide | MnO | MnO dissolved $Ca_2SiO_4$ |

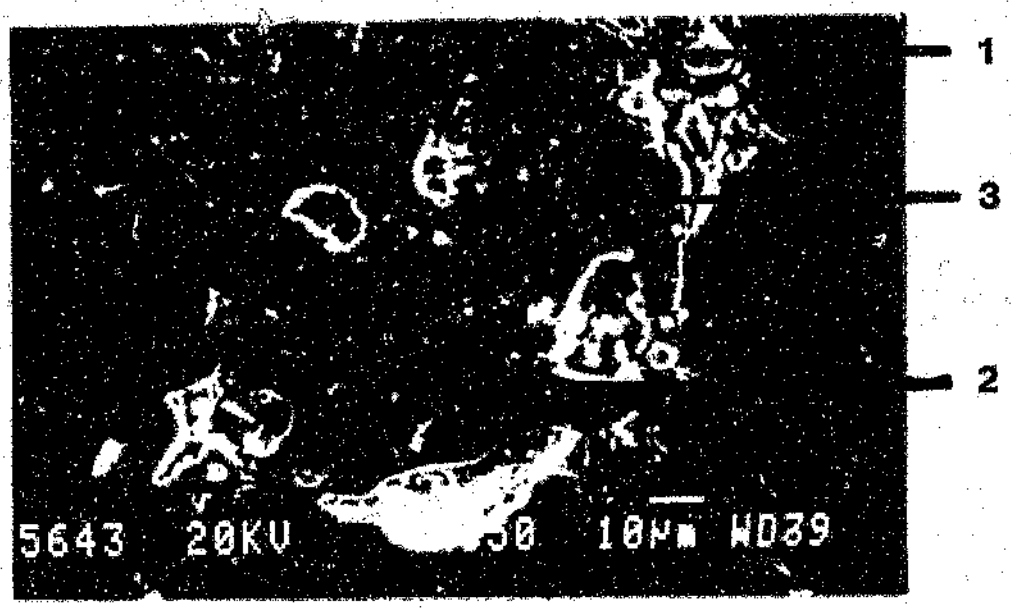


Figure 4.17 A Maratwan manganese ore grain subjected to 78.03 percent reduction for 35 minutes at 1350 °C. Mag. 650X

Element concentrations determined by EDAX

| | 1 | 2 | 3 |
|---|---|---|---|
| Mn | 65.66 | 16.95 | 52.54 |
| Ca | 1.20 | 34.35 | 17.61 |
| Fe | 24.56 | 0.52 | 0.52 |
| Mg | 0.32 | 0.61 | 4.60 |
| Si | 0.21 | 11.27 | 0.33 |
| possible phase | carbide | $Ca_2SiO_4$ | $CaMn_2O_4$ |

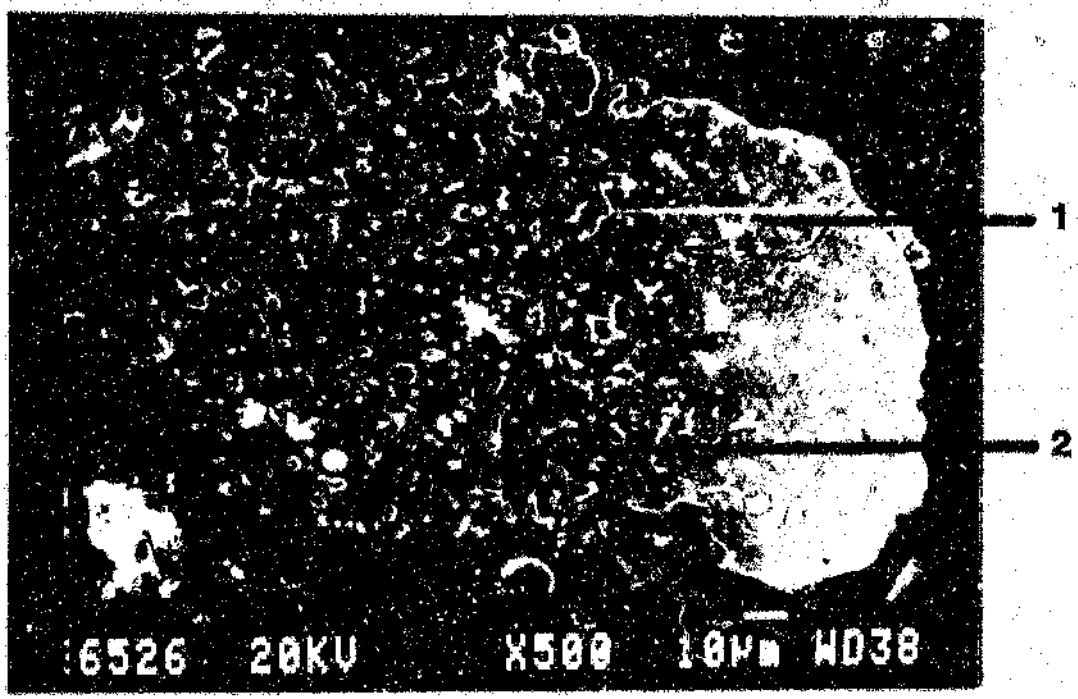


Figure 4.18 A Mamatwan manganese ore grain subjected to 86.83 percent reduction for 50 minutes at 1350 °C. Mag. 500X

Element concentrations determined by EDAX

| | 1 | 2 |
|---|---|---|
| Mn | 73.17 | 10.84 |
| Ca | 0.31 | 44.07 |
| Fe | 11.29 | 0.25 |
| Mg | 0.15 | 0.22 |
| Si | 0.21 | 13.27 |
| possible phase | carbide | $Ca_2SiO_4$ |

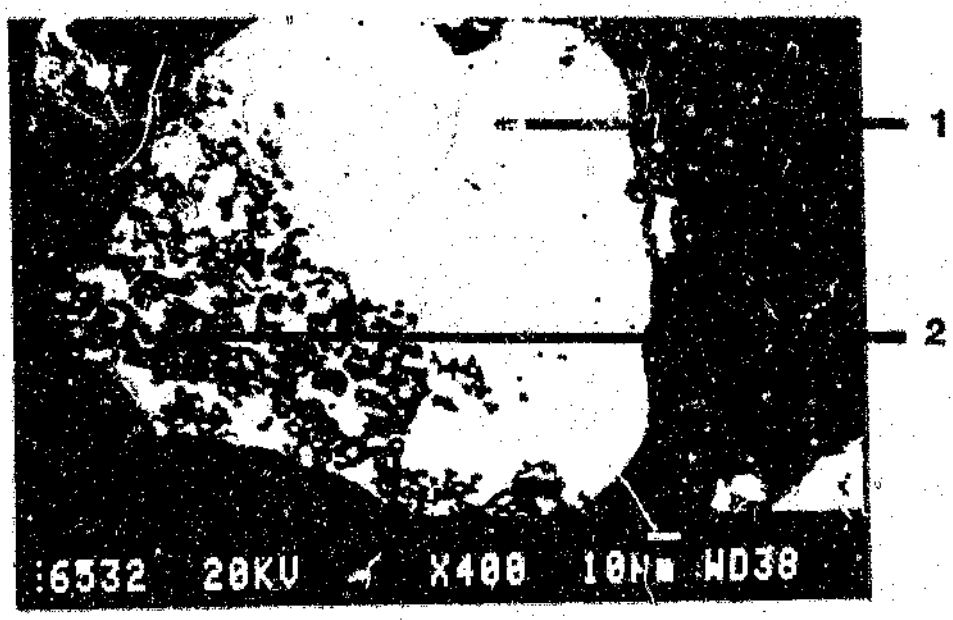


Figure 4.19 A Mamatwan manganese ore grain subjected to 92.15 percent reduction for 70 minutes at 1350 °C. Mag. 400X

Element concentrations determined by EDAX

| | 1 | 2 |
|---|---|---|
| Mn | 73.93 | 8.56 |
| Ca | 0.31 | 43.11 |
| Fe | 9.10 | 0.62 |
| Mg | 0.44 | 0.43 |
| Si | 0.11 | 13.20 |
| possible phase | carbide | $Ca_2SiO_4$ |

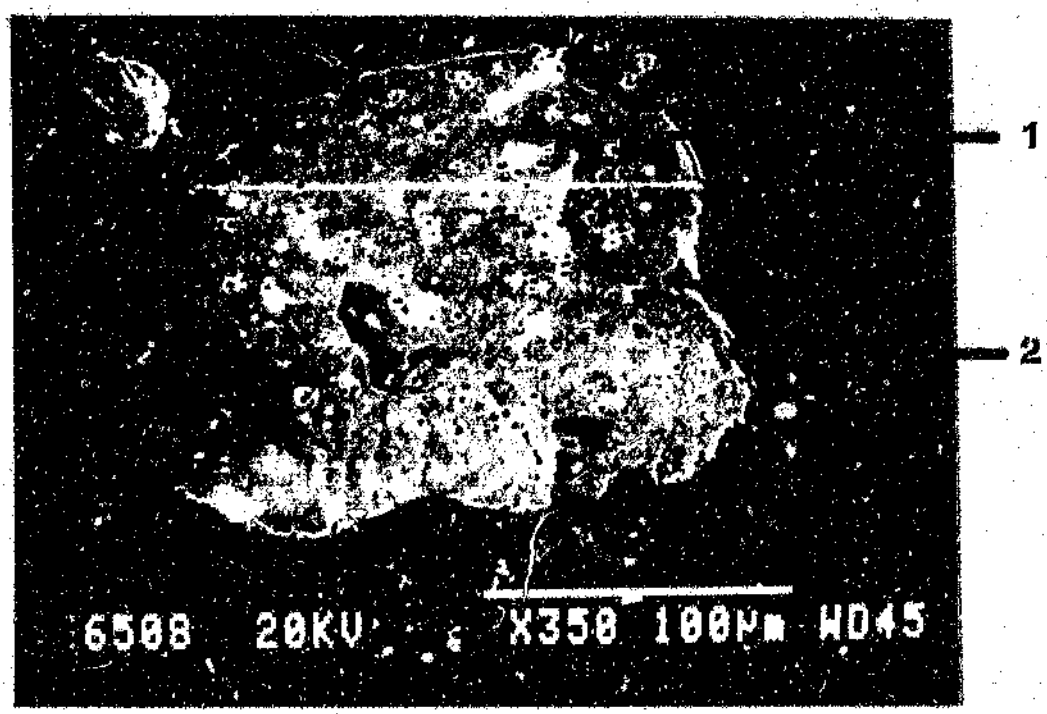


Figure 4.20 A Mamatwan manganese ore grain subjected to 94.01 percent reduction for 90 minutes at 1350 °C. Mag. 350X.

Element concentrations determined by EDAX

| | 1 | 2 |
|---|---|---|
| Mn | 76.89 | 6.22 |
| Ca | 0.22 | 43.45 |
| Fe | 6.52 | 0.34 |
| Mg | 0.11 | 0.50 |
| Si | 0.65 | 13.80 |
| possible phase | carbide | $Ca_2SiO_4$ |

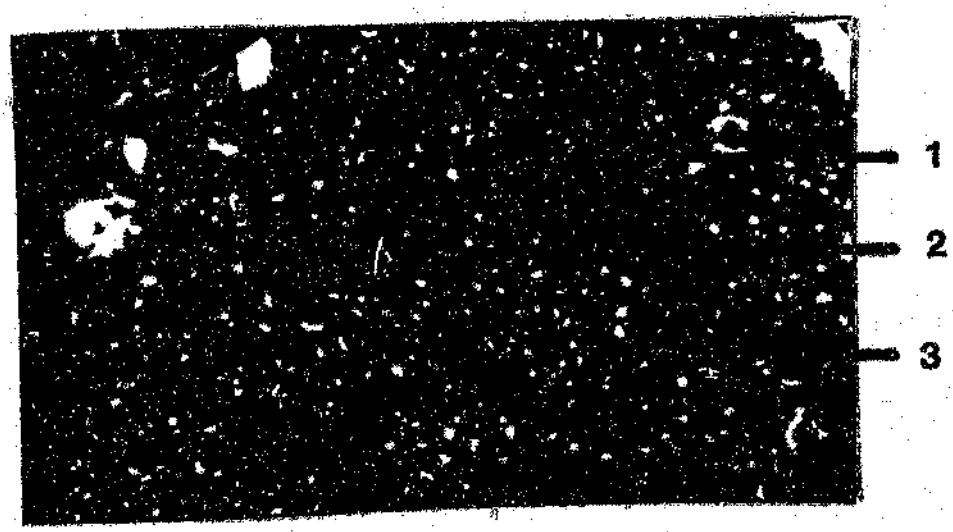


Figure 4.21 A Mamatwan manganese ore grain subjected to 52.61 percent reduction for 25 minutes at 1300 °C. Mag. 1000X

Element concentrations determined by EDAX

| | 1 | 2 | 3 |
|---|---|---|---|
| Mn | 50.77 | 16.10 | 73.31 |
| Ca | 0.24 | 43.20 | 2.20 |
| Fe | 36.61 | 0.71 | 0.41 |
| Mg | 0.61 | 0.34 | 5.86 |
| Si | 0.56 | 15.21 | 0.37 |
| possible phase | carbide | $Ca_2SiO_4$ | MnO |

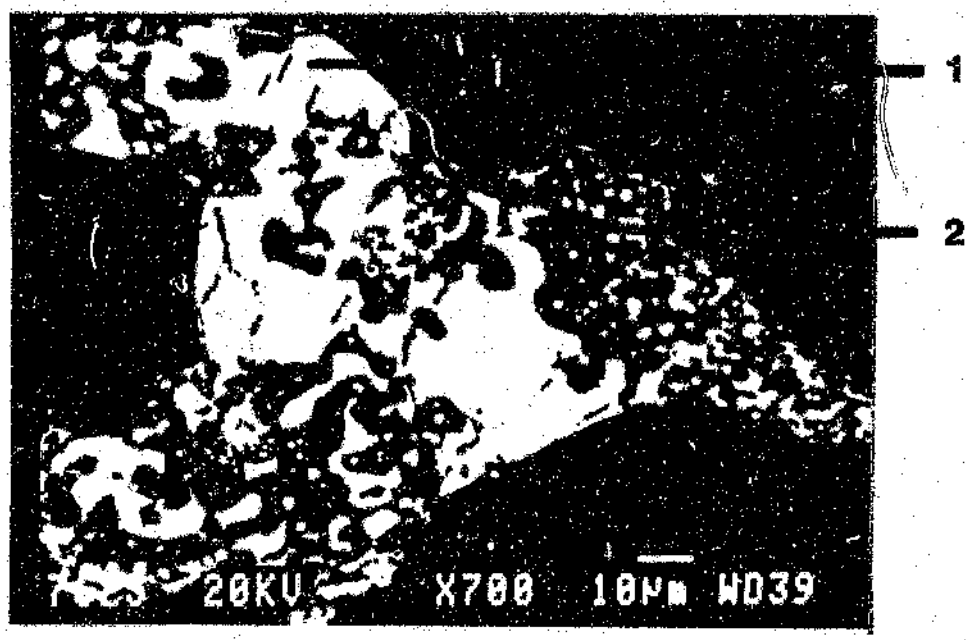


Figure 4.22 A Mamatwan manganese ore grain subjected to 82.45 percent reduction for 90 minutes at 1300 °C. Mag. 700X

Element concentrations determined by EDAX

| | 1 | 2 |
|---|---|---|
| Mn | 78.30 | 4.71 |
| Ca | 0.43 | 46.32 |
| Fe | 8.00 | 0.33 |
| Mg | 0.11 | 0.51 |
| Si | 0.72 | 13.10 |
| possible phase | carbide | $Ca_2SiO_4$ |

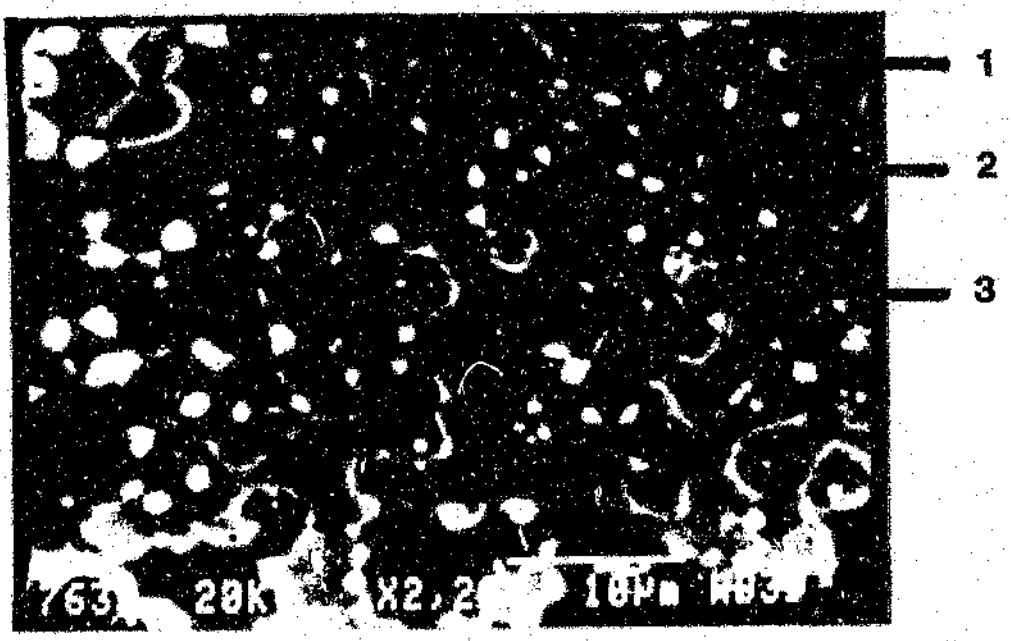


Figure 4.23 A Mamatwan manganese ore grain subjected to 53.09 percent reduction for 90 minutes at 1200 °C. Mag. 2200X

Element concentrations determined by EDAX

| | 1 | 2 | 3 |
|---|---|---|---|
| Mn | 58.49 | 70.53 | 35.52 |
| Ca | 3.04 | 1.83 | 16.80 |
| Fe | 23.53 | 1.73 | 1.82 |
| Mg | 0.56 | 4.00 | 1.55 |
| Si | 0.54 | 0.00 | 13.65 |
| possible phase | carbide | MnO | unreduced part |

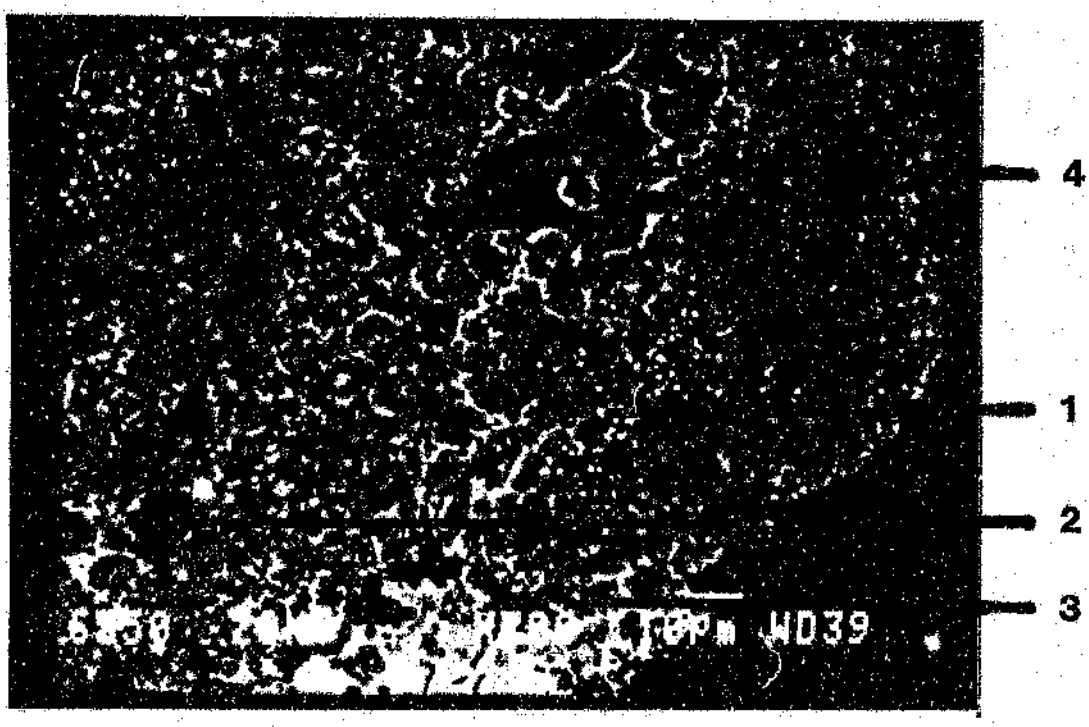


Figure 4.24 A Mamatwan manganese ore grain subjected to 37.81 percent reduction for 90 minutes at 1100 °C. Mag. 700X

Element concentrations determined by EDAX

| | 1 | 2 | 3 | 4 |
|---|---|---|---|---|
| Mn | 35.00 | 33.99 | 32.80 | 68.57 |
| Ca | 3.81 | 30.27 | 15.50 | 2.70 |
| Fe | 41.70 | 0.74 | 0.21 | 0.41 |
| Mg | 5.41 | 3.53 | 14.40 | 1.40 |
| Si | 0.12 | 2.26 | 0.66 | 1.80 |
| possible phase | carbide | $CaMnO_3$ | unreduced part | MnO |



Figure 4.25 Selected microphotograph of partially reduced Mamatwan manganese ore grain (1350°C, 50 minutes retention time). Mag. 550X.

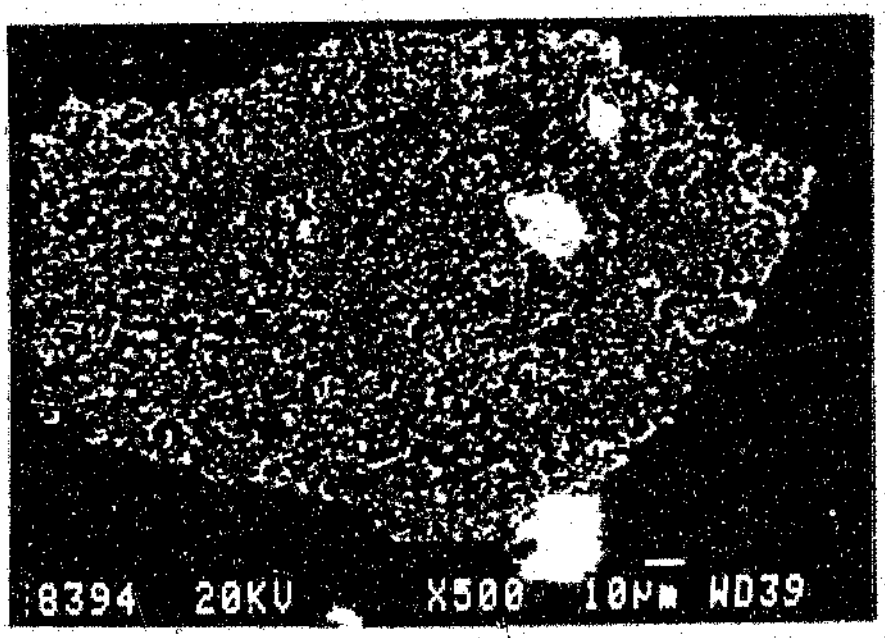


Figure 4.26 Selected microphotograph of partially reduced Mamatwan manganese ore grain (1350°C, 10 minutes retention time). Mag. 500X.

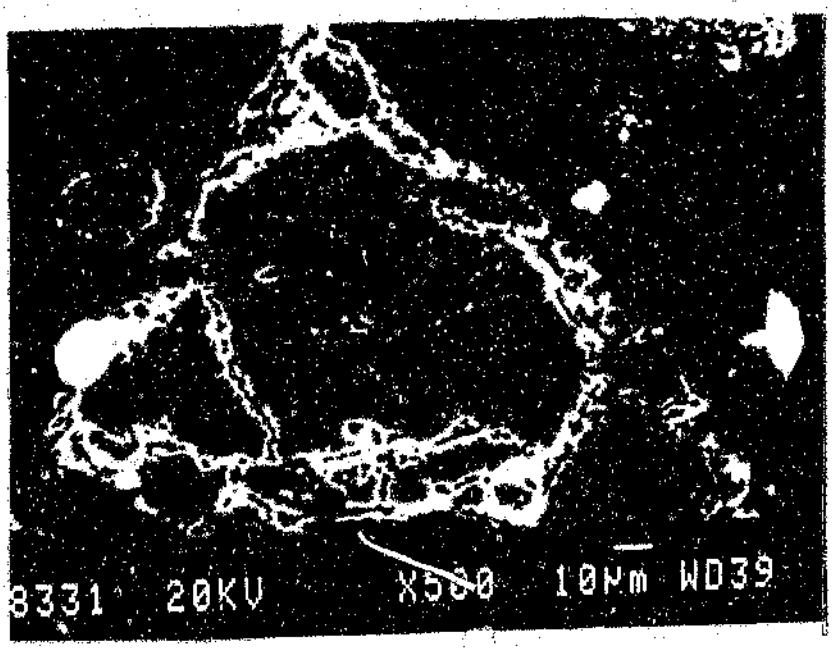


Figure 4.27 Selected microphotograph of a partially reduced Mamatwan manganese ore grain (1300°C, 25 minutes retention time) Mag. 500X.

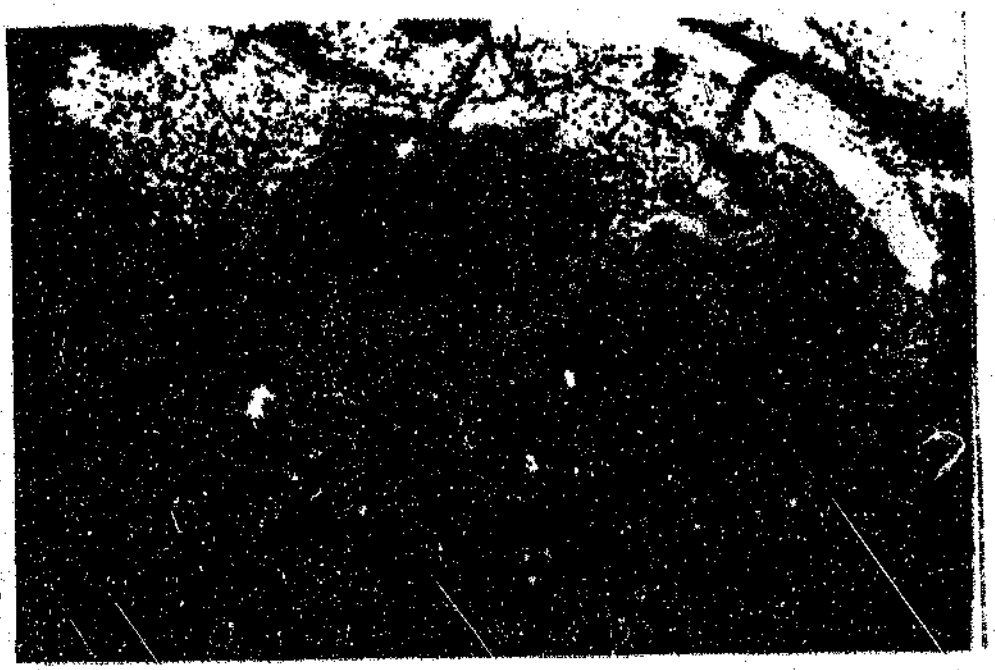

Figure 4.28 Microphotograph of a partially reduced Mamatwan manganese ore grain (1350°C, 2 minutes retention time). Note that formation of porous oxide product layer around ore grain. Light area is mostly MnO. Mag. 740X

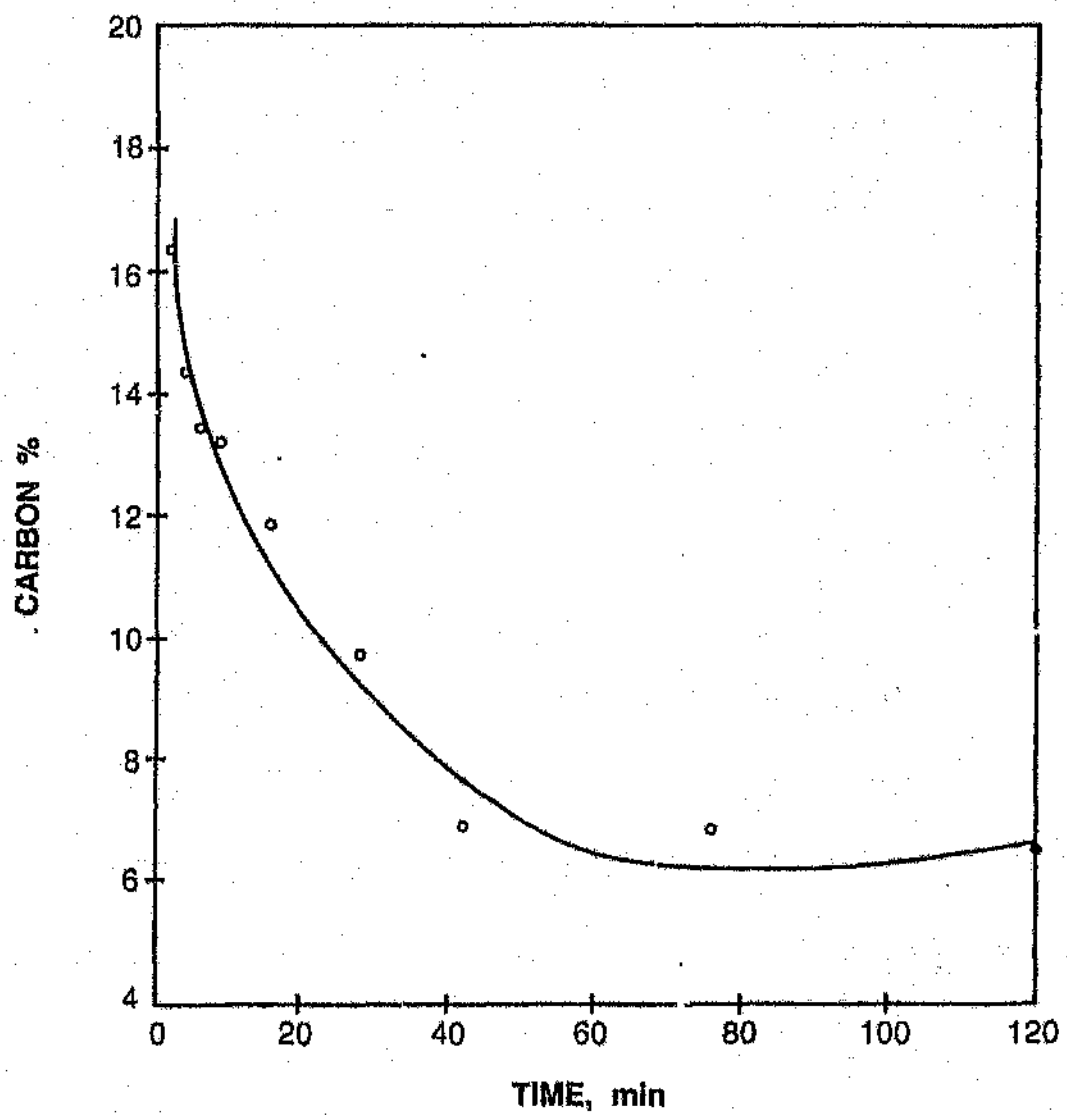


Figure 4.29 Carbon content variation of the reaction mixture during the reduction at 1350 °C.

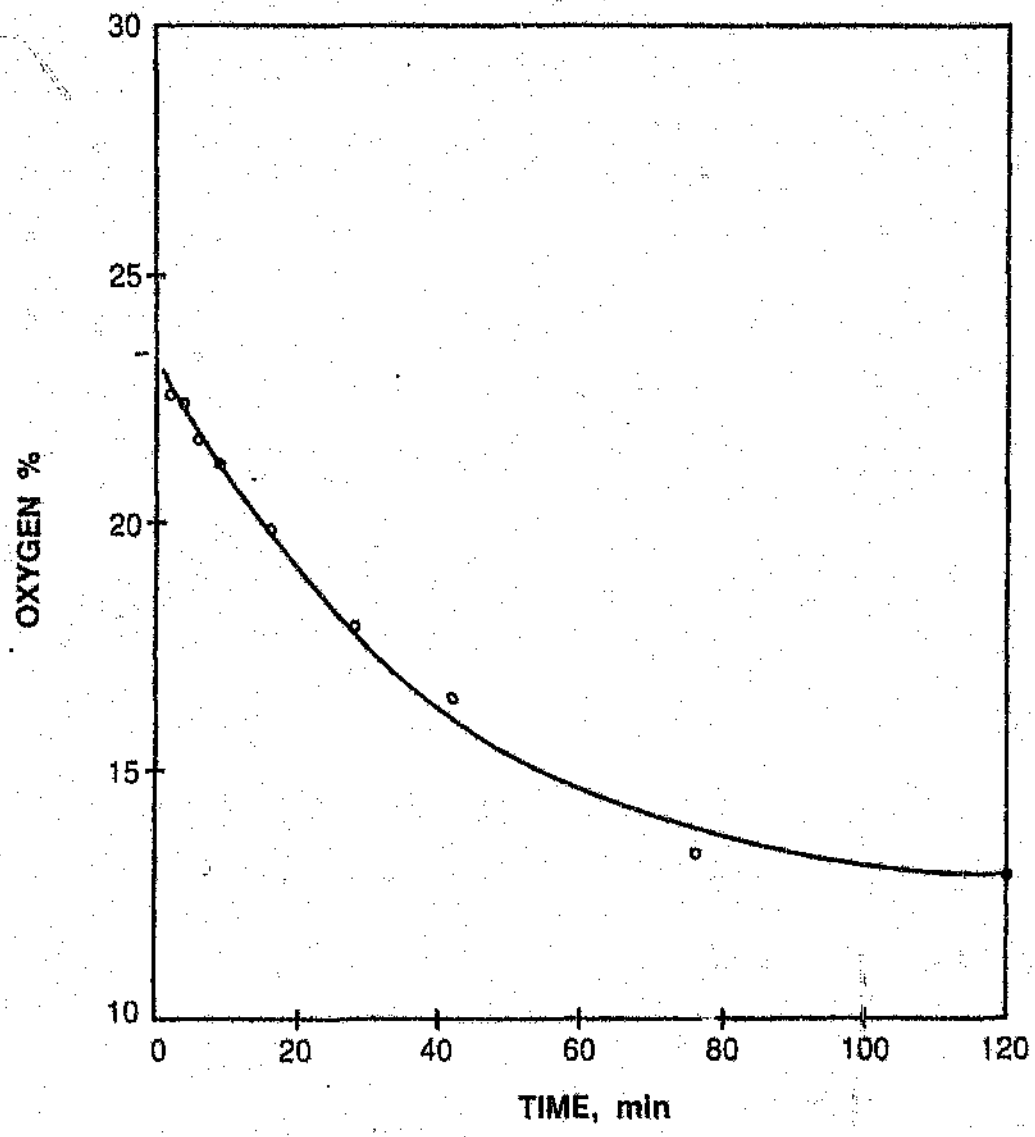


Figure 4.30 Oxygen content variation of the reaction mixture during the reduction at 1350 °C.

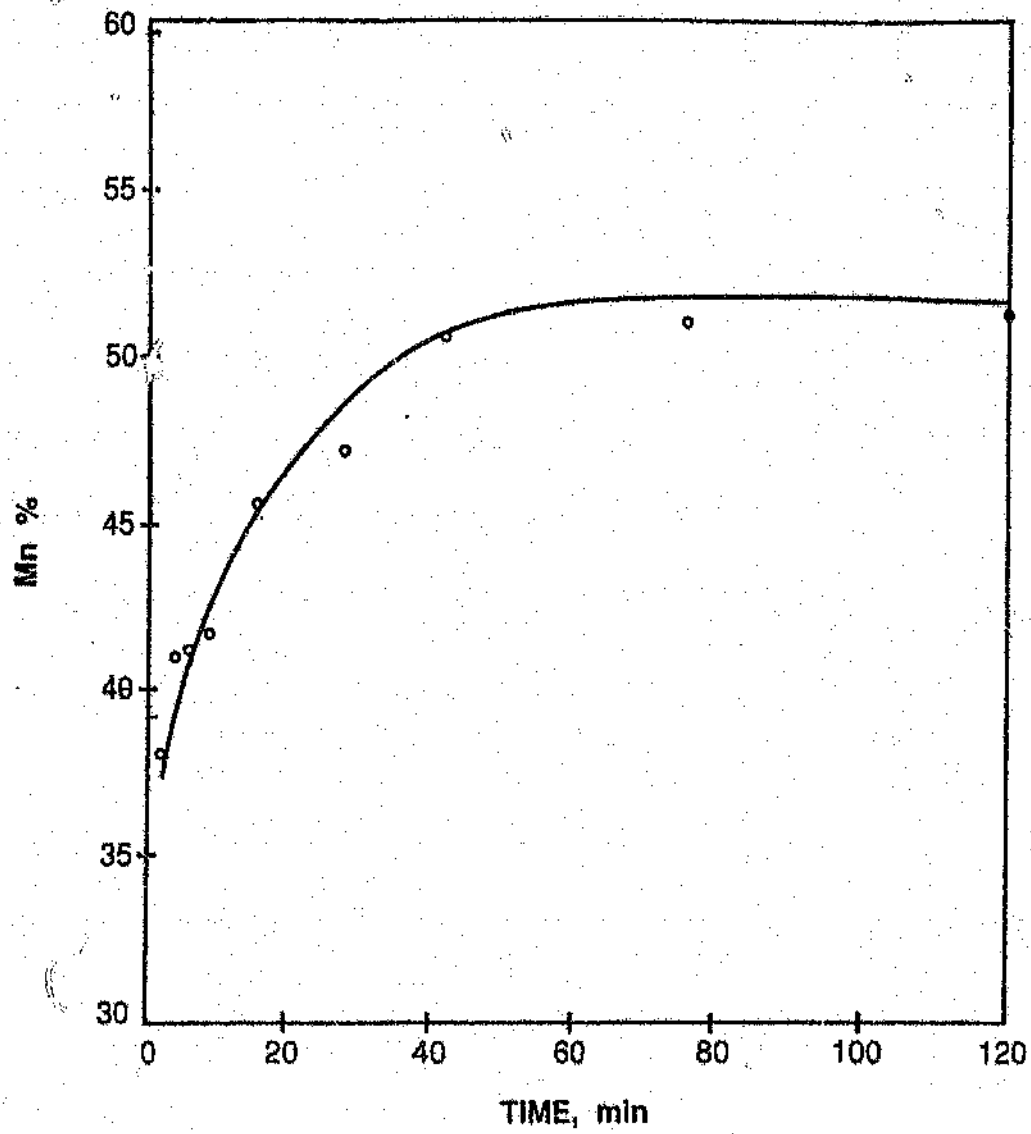


Figure 4.31 Manganese content variation of the reaction mixture during the reduction at 1350 °C.

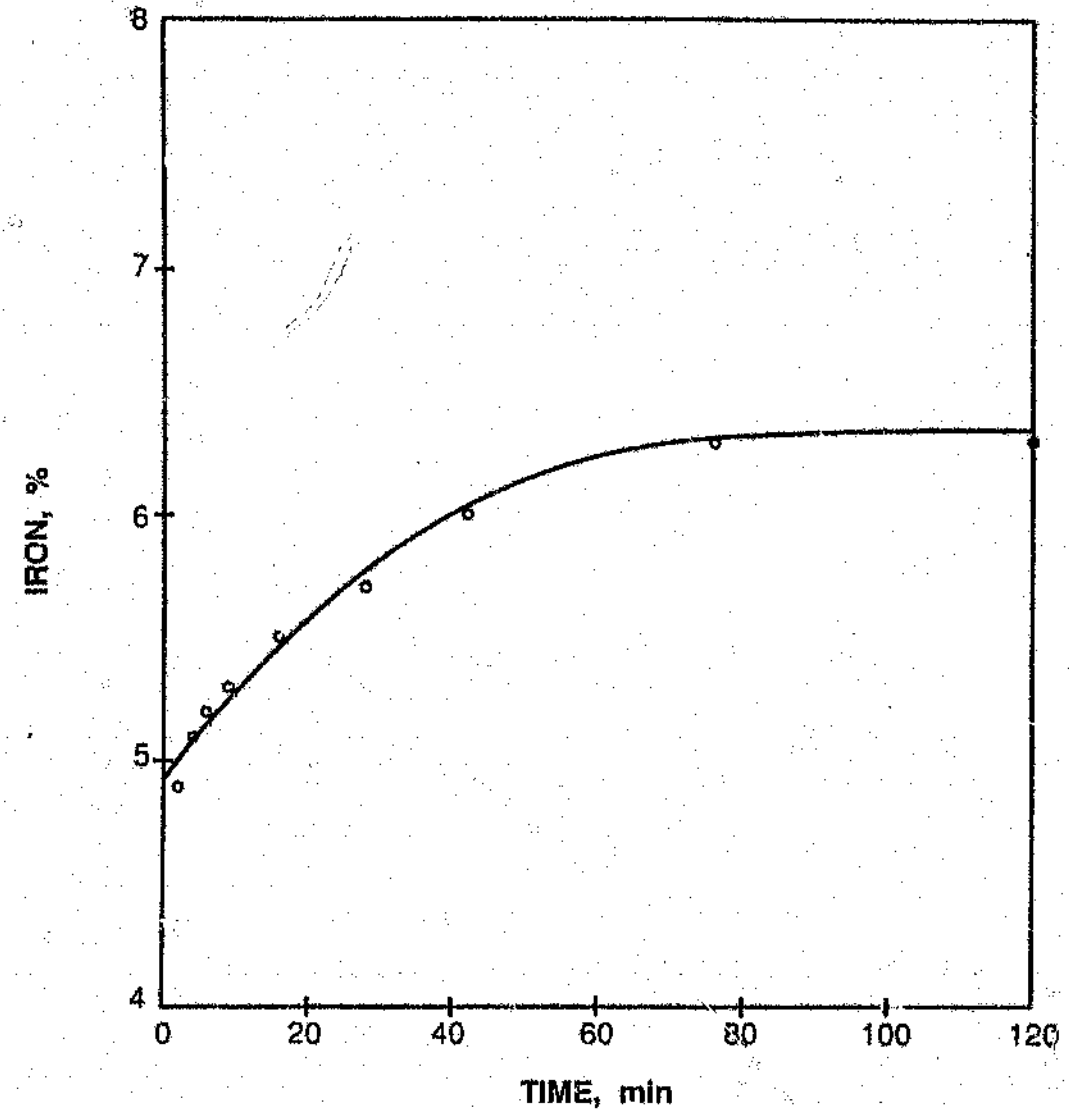


Figure 4.32 Iron content variation of reaction mixture during the reduction at 1350 °C.

## 4.3 The Reduction Mechanism

The experimental results are discussed in this section in order to explain the mechanism of reduction of Mamatwan manganese ore by carbon.

It was found that the rate of reduction is fairly high at the beginning and slows down as the reaction approaches completion revealing the possible contribution of more than one mechanism in the process. An examination of the kinetic curves for reduction versus time at 1350 $^{o}$C, 1300 $^{o}$C and 1250 $^{o}$C shows that there are three distinct stages during the reduction :

1) The initial stage during which the rate of reduction is very fast. i.e., at reductions of between 0 and 30 percent.

2) The second stage during which the rate of reduction decreases compared to the to first stage and is almost linear with respect to the time, i.e., at reductions between 30 - 70 and 30 - 60 percent at 1350 $^{o}$C and 1300 $^{o}$C respectively.

3) The third stage during which the rate of reduction is decreasing in parabolic manner and reaction eventually ceases; i.e., at reductions higher than the 70 percent at 1350$^{o}$C.

### 4.3.1 Theory of Oxide Reduction By Graphite

Efficient conditions for the reduction of metals from their oxides by carbon are to a great extend determined

by the mechanism of the following processes. It is generally accepted that reaction of many oxides with solid carbon starts in the region of temperature at which the reaction of gasification of carbon

$$CO_2 + C = 2CO \quad \ldots\ldots\ldots\ldots\ldots\ldots \quad 2.2$$

is barely proceeding. Kolchin (1968) discussed four possible mechanisms by which solid metal oxides could be reduced by carbon.

a) The oxide is reduced by carbonmonoxide which is formed by gasification of carbon by the carbondioxide as reduction product.

$$MeO + CO = Me + CO_2 \quad \ldots\ldots\ldots\ldots\ldots\ldots \quad 4.4$$

$$CO_2 + C = 2CO \quad \ldots\ldots\ldots\ldots\ldots\ldots \quad 2.2$$

b) The oxide dissociates into metal and oxygen with subsequent oxidation of the carbon.

$$2MeO = 2Me + O_2 \quad \ldots\ldots\ldots\ldots\ldots\ldots \quad 4.5$$

$$(m+r)C\ (s) + (m+r/2)O_2\ (g) = mCO_2\ (g) + rCO\ (g) \quad . \quad 4.6$$

c) The direct contact between oxide and carbon leads to the formation of a metallic layer by diffussion of carbon into the oxide through this layer.

$$(m+r)MeO\ (s) + (m+r/2)C = (m+r)Me + mCO(g) + (r/2)CO_2(g) \ldots \quad 4.7$$

d) The metal oxide vaporizes and reacts with solid

carbon

$$MeO\ (s) = MeO\ (g) \quad \ldots\ldots\ldots\ldots\ldots\ldots 4.8$$

$$(m+r)MeO\ (g) + (m+r/2)C = (m+r)Me + mCO\ (g) + (r/2)CO_2 \quad \ldots\ldots\ 4.9$$

Kolchin (1968) claimed that it is not correct to explain oxide reduction by a single universal theory. Even for a single metal oxide, different mechanisms may come into play at different stages and under different conditions. However the first mechanism become widely accepted as the most likely mechanism of reduction for the majority of oxides. Tien and Turkdogan (1977) state as the consensus of opinion that, when a mixture of a metal oxide and carbon is heated in an inert atmosphere, the reduction occurs by way of the carbonmonoxide species with the regeneration of carbon monoxide from the carbondioxide product gas.

In the reduction of MnO by carbon, a system of at least three components, namely, manganese, oxygen, and carbon exists. For a two dimensional representation of the stability fields of the phases in the system, two degrees of freedom are necessary, and these are most conveniently taken as oxygen potential and temperature. Therefore from the phase rule at a given oxygen potential and temperature, there may be three co-existing phases. Since one of these is always a gaseous phase, two condensed phases must be present in each stability field.

Each pair of condensed phases possesses a region of stability in the space between oxygen potential and temperature, and this is determined by the reactions between oxygen and two condensed phases. A curve can be drawn for each combination; on one side of the curve two of the three phases can co-exist; and on the other side another two of the phases can co-exist. In this way the entire space is divided into regions in each of which only one pair of condensed phases co-exists. A graphical representation of this type is known as a Pourbaix diagram.

Downing (1963) constructed a Pourbaix diagram for the Mn-O-C system with coordinates of temperature and oxygen activity as shown in Figure 2.25. The diagram shows the regions of stability for pairs of phases and it is clear that $Mn_2O_3$ and $Mn_3O_4$ are not stable in the presence of carbon at atmospheric pressure. $Mn_2O_3$ dissociates below 1000°C to give $Mn_3O_4$ which in the presence of CO should react spontaneously to yield MnO. The diagram also indicates that MnO and carbon should react to produce $Mn_7C_3$ above 1267°C with the following reaction:

$$7MnO + 10C = Mn_7C_3 + 7CO \quad \ldots\ldots\ldots\ldots\ldots \quad 2.5$$

for which according to Downing $\Delta G^\circ = 0$ at 1257°C

Whereas for the reaction:

$$MnO + C = Mn + CO \quad \ldots\ldots\ldots\ldots\ldots \quad 4.2$$

the free energy $\Delta G^\circ$ does not become negative until a temperature of 1420°C is reached. This means that

manganese metal cannot appear in this system until liquid state conditions have been reached, by which time manganese carbide forms.

As also can be understood from the The manganese-carbon phase diagram shown in Figure 2.23 liquid metal phase formation may be expected at any stage of the reduction of Mamatwan manganese ore particularly at 135[illegible]. Microphotographs of quenched reaction products in which metallic phase is seen smoothly shaped and rounded may support this idea. Although only $(Fe,Mn)_5C_2$ was detected as metallic phase by X-ray, microprobe analysis of some metallic phases indicates sufficient amount of carbon to form $(Fe,Mn)_7C_3$ phases. Therefore final reaction product of the reduction can be thought to be mix of both phase. This is also in accordance with the above discussion related to the Pourbaix diagram of Mn-C-O system.

### 4.3.2 First Stage of the Reduction

Examinations of the reduced samples under optical microscope revealed that no metallic phase was formed below approximately 30 percent reduction. Reduction without the formation of a metallic phase indicates that a change in the oxidation state of oxides occurs. Stoichiometric calculations show that for the complete reduction of $Mn_2O_3$ to MnO and $Fe_2O_3$ to FeO a total of 29.16 percent reduction is required. This calculated value is in very good agreement with the experimental 30 percent reduction level below which no metallic phase is observed. The chemical reaction taking place during the first stage of reduction is therefore

concluded to be reduction of higher manganese oxides to MnO and iron oxides to FeO. The possible reactions for $Mn_2O_3$ and $Fe_2O_3$ are

$$Mn_2O_3 + C = 2MnO + CO \quad \ldots\ldots\ldots\ldots \quad 4.10$$

$$Fe_2O_3 + C = 2FeO + CO \quad \ldots\ldots\ldots\ldots \quad 4.11$$

The reduction of braunite, $Mn^{2+}Mn^{3+}_6SiO_{12}$, probably proceeded by a mechanism similar to that proposed by De Villiers(8). The $Mn^{3+}$ ions were reduced to $Mn^{2+}$, which formed MnO and charge balance was maintained in the braunite lattice by an increase in the $Si^{4+}$ content. Under the strongly reducing conditions present in the ore/carbon mix, the $Mn^{3+}$ and $Fe^{3+}$ ions would have been reduced very rapidly to $Mn^{2+}$ and $Fe^{2+}$ respectively.

Of the various physical and chemical processes that are involved in the reduction of manganese ore intimately mixed with fine powdered graphite, the most important to be considered is the formation of carbon monoxide. Rao (1971) explained that carbonmonoxide formation can occur by one or more of the following mechanisms in such a mixture:

a) Oxygen of the entrapped air combining with carbon particles.

b) Carbon reacting with the oxygen released by the dissociation of manganese and iron oxides

c) Oxygen chemisorbed on carbon surfaces liberated as carbon monoxide

d) Direct reduction taking place at the points of contact between oxide and carbon particles.

Metal oxides in the ore can react easily with the carbon at ore-carbon contact points with the following reaction.

$$Me_2O_3 + C = 2MeO + CO \quad \ldots\ldots\ldots\ldots 4.12$$

where Me refers to manganese and iron

This reaction is very favoured thermodyanamically as is the subsequent reaction :

$$Me_2O_3 + CO\ (g) = 2MeO + CO_2\ (g) \quad \ldots\ldots\ldots 4.13$$

However the building up of carbon dioxide in the system would eventually stop the reaction. In the presence of carbon at elevated temperature the Boudouard reaction

$$CO_2 + C = 2CO \quad \ldots\ldots\ldots\ldots\ldots\ldots 2.3$$

is highly favoured. Every mole of $Me_2O_3$ reduced requires one mole of CO and generates one moles of $CO_2$. This one mole $CO_2$ will react with one mole of carbon to generate 2 moles of CO, thus doubling the amount of CO available in ensuring reducing conditions.

Reduction is initiated by reaction 4.12 and subsequently perpetuated by reactions 4.13 and 2.2 until all the manganese oxide and iron oxide has been converted to the MnO and FeO respectively.

### 4.3.3 Second Stage of the Reduction

When the oxygen is removed from the oxide, the ratio of metal/oxygen increases in the oxide. As the solubility limit of metal in the oxide reached and the oxide becomes super-saturated with liberated metal ions, the metal will start to precipitate. Nuclei of iron rich metallization can therefore commence as a result reaction

$$FeO + CO\ (g) = Fe(s) + CO_2\ (g) \quad \ldots\ldots\ldots \quad 4.14$$

This random nucleation may be due to the finely intergrown nature of the ore (De Villiers, 1971, 1973). Under highly reducing conditions, iron oxide is reduced to metallic state in a faster rate than the to manganese oxide (Lien, 1971). Figure 4.11 also shows the comparison of reduction rate and degree between iron oxide and manganese oxide and confirms the above conclusion.

Once such nucleation of metal has occurred, further removal oxygen and consequent creation of a concentration gradient of metal ions across the oxide lattice induces these ions to diffuse towards the sites of nucleation.

The metallic iron that is formed is an intermediate product and transforms to iron carbide by carburization as the reduction proceeds. Metallization starts mainly according to reaction (4.14) but at the same time the iron is most probably being carburized through the reaction,

$$3Fe(s) + C = Fe_3C( \quad \ldots\ldots\ldots 4.15$$

Tsylev (1963) states that it is possible that the solid state reduction of manganese oxides proceeds via an intermediate reducing agent such as $Fe_3C$. Once formed, the metallic nuclei grow by spreading over rounded MnO-rich oxide grains. The nuclei that appeared on the particles analysed by EDAX were found to have higher percentage iron, which is an indication of the reduction of $Fe^{+2}$. The reduction by carbon dissolved in iron or by iron carbide is important in initiating the reduction of MnO in the second stage of the reaction of the ore with carbon. Figure 4.14 shows the photomicrograph of a partially reduced ore particle in which the iron rich carbide phase is in intimate contact with the MnO-rich oxide grains.

Thermodyanamically iron carbide may reduce manganese oxide according to the reaction:

$$5MnO + 7Fe_3C = Mn_5C_2 + 21Fe + 5CO \ldots\ldots 4.16$$

Stoichiometric calculations based on chemical analysis of samples show that iron carbide can contribute to the reduction of MnO at the order of 7 percent over and above the already achieved reduction in the first stage. This effect can be seen clearly at 1100 °C curve just after the first stage (see Figure 4.2). At such lower temperature reactions, the second stage of reduction almost terminates with this carbide reaction (4.16). At elevated temperatures iron carbide reduction of MnO proceeds much more rapidly.

The carbon monoxide produced by reaction (4.16) or with the ways explained by Rao (1971) can react readily with manganese oxide in the particles and the reaction may proceed through the series of

$$MnO \longrightarrow Mn \longrightarrow Carbide$$

in the early minutes of second stage. Antonov and Chufarov (1961) indicated that the temperature for the reduction of MnO by graphite is lowered due to the transition of metallic manganese to $Mn_3C$. In such a case oxygen removal from the oxide would be by a gas/solid type reaction occurring mostly at MnO-metal interface. The process at the metal-oxide interface can be described as adsorption of the gaseous reductant at the interface and desorption of gaseous products from the interface according to

$$CO_{ads} + O_{lattice} = CO_2 \quad \ldots 4.17$$

After the reducing effect of iron carbide ends at temperatures higher than the 1200 $^oC$, the reduction reactions occurring at the interfaces of the solid phases will probably be

$$MnO + CO = Mn + CC_2 \quad ..... \quad 4.1$$

$$CO_2 + C = 2CO \quad ..... \quad 2.2$$

$$5Mn + 2C = Mn_5C_2 \quad ..... \quad 4.18$$

occurring side by side during the process. The solution loss or gasification reaction between $CO_2$ and carbon particles regenerates CO and tends to restore the

reducing potential of the gas phase. The linear relationship of reduction with time in this stage indicates that the supply rate of the reductant is equal to or greater than its consumption rate. In case the supply rate becomes less than its consumption, a change in the mechanism and rate of the reduction would be expected.

Experiments which have been carried out under $CO_2$ and CO atmosphere also proved that gaseous reactions are important in the reduction of manganese oxides in the second stage of process. In this stage the direct reduction contribution is regarded as relatively small compared to the magnitude of gaseous reduction.

In reality the manganese carbide formed by reaction (4.16) dissolves iron in it resulting in the formation of a mixed iron-manganese carbide.

### 4.3.4 Third Stage of the Reduction

Up to 1200 °C reduction was mainly limited to the second stage of the reaction. The much slower final reduction phenomenon observed at the lower reduction temperatures indicates that whereas some part of the reduction may have been due to either direct solid-solid, gas-solid or oxide-carbide reaction, the reduction of the residual oxide is accomplished by a different process at temperatures higher than 1200 °C which is more a function of temperature.

Examination of the kinetic curves at 1250 °C, 1300 °C and 1350 °C (see Figure 4.2) and EDAX analysis of

carbide phases formed in partially reduced samples show that the mechanism described above involving the second stage is valid up to approximately 60-70 percent reduction depending upon temperature. Carbon percent of the carbide phase starts to decrease after about 25 minutes and 32 minutes reaction time at 1350 $^{o}$C and 1300 $^{o}$C respectively revealing that the double carbide itself may act as reductant. Ashin et al (1961) propose that, over the temperature range from 1310$^{o}$C to 1400$^{o}$C, reduction of MnO by carbon occurs via carbon dissolved in the manganese product. Carbide covering the grains which still contain unreduced oxide can also be seen on microphotograph in Figures 4.18 and 4.19. Once the metallic phase has mostly covered the oxide phase gas-phase reaction is no longer possible and the reaction with carbon dissolved in carbide phase becomes dominant. In case of metallic carbide layer formation surrounding the oxide, the removal of oxygen from the oxide surface occurs by transport of the reductant in the carbide phase and the withdrawal of the gaseous product to the surface of the carbide layer through the pores and micro cracks according to the following reaction:

$$MnO + C\ (carbide) = Mn\ (carbide) + CO \quad .... \quad 4.19$$

As the carbon is consumed at the carbide-oxide interface, the carbon concentration decreases thus setting up a gradient of carbon in the carbide. EDAX analyses showed that the mixed carbide was progressively enriched in Mn during this stage. In his study Barcza (1971) proposed a similar reduction mechanism involving solid state reaction for chromite

reduction. It was stated that the mechanism involved the diffusion of carbon across the layer of product, which consists of mixed carbides of iron and chromium. Diffusion of carbon into the chromite particles occurred by diffusion along the surface and at the grain boundaries and by volume diffusion. The mixed carbide itself was shown to be reducing towards chromite and this provided the means by which carbon was transferred from the graphite particles to the reaction interface. This mechanism was adopted mainly on the grounds that pure CO failed to reduce the chromite at 1400°C in the absence of solid carbon.

Another reason for the decrease in the rate of reduction is probably due to the silicate phase coating the oxide particles. This effect reduces the area of contact between the oxide and the reducing agent especially towards end of this stage. The silicate phase formed as a result of the reaction between $SiO_2$, MnO and CaO. Therefore, the dissolution of solid MnO in the silicate phase and the reduction of manganeous oxide dissolved in the silicate phase by solid carbon dissolved in the carbide may become important at the later periods of the reduction. The overlap of the growing silicate pha can be seen in the photomicrograph of Figures 4.17 and 4.18.

$$MnO\ (slag) + C\ (carbide) = Mn\ (carbide) + CO \quad .. \quad 4.20$$

At 1350 °C reduction of MgO to Mg(g) also was observed and it was confirmed by the chemical analysis and x-rays of the white deposit condensed at the top of the crucible. This probably involved a vaporous mechanism

whereby the gaseous magnesium condensed as MgO at the top of the crucible due to possibly less reducing conditions at the top of the crucible.

# 5 MATHEMATICAL ANALYSIS OF KINETIC DATA

## 5.1 Introduction

The kinetics of many solid state reactions can be represented by the general equation $f(\gamma)=kt$ where $\gamma$ is the fraction reacted in time t and the function $f(\gamma)$ depends on the reaction mechanism and the geometry of the reacting particles. The solid state reactions are divided into three groups:

1) Diffussion controlled reactions 2)Phase boundary controlled and first-order reactions and 3) Nucleation and growth type reactions.

Difficulties arise, however when 1) the reaction mechanism differs when experimental conditions are varied 2) the mechanisms of the later stages of the reaction different from those followed initially, 3) induction periods occur 4) adsorbed gas prevents $\gamma$ from reaching unity 5) the surface area of the sample changes because of cracking and 6) heat transfer determine the rate of reaction. Furthermore, it is practically difficult to establish the zero time for the start of the reaction. The time required to attain isothermal conditions may be negligible compared to the time for completion of the reaction and yet may influence the shape of a reduction-time plot (Taplin, 1974).

Solid-gas reactions taking place on a surface of oxide are generally considered in a series of sequential

steps. The overall rate will be determined by the slowest of the process or processes in the series. The possible consecutive steps are:

a) transport of gaseous reductant from the bulk gas phase to the particle surface through a boundary gas film.
b) molecular diffusion of the gaseous reductant through the product layer to the reaction interface.
c) adsorption of the gaseous reductant at the interface.
d) reaction at the interface (reaction between adsorbed reductant and oxygen of the lattice).
e) desorption of gaseous products from the interface.
f) mass transport of metal and oxygen ions and transformations in the solid phase; formation and growth of the reaction products.
g) molecular diffusion of gaseous products through the product layer to the particle surface.
h) transport of the gaseous products from the particle surface through the boundary gas film to the bulk gas phase.

Steps (c) and (d) are the rate limiting cases for the chemical-controlled reactions whereas steps (a)-(h), (b), and (d)-(e) are for the diffusion-controlled reactions.

## 5.2 Review of Some Solid-State Models

### 5.2.1 Diffusion Model

When a solid non-porous reaction product is formed on the reacting solid, the kinetics of the reaction will

be governed by the resistance through the solid product layer. That is the transport of matter across the product layer. If the thickness of this product layer is y and w is the weight of the solid reaction product at time t, then y = kw where k is a constant. The diffusion through the solid product layer will be given by the equation,

$$dw/dt = \alpha(DAC)/y = (\alpha/k)(DAC)/w \quad \ldots\ldots\ldots\ldots\ldots\ldots \quad 5.1$$

where, A is the area of contact and $\alpha$ is the stoichiometry factor. In this special case C is constant, i.e when there is a continuous supply of the reagent and D is the diffussion coefficient of migrating species through the product layer, then

$$\int(dw) = (\alpha/k)DAC \cdot \int(dt) \quad \ldots\ldots\ldots\ldots\ldots\ldots\ldots \quad 5.2$$

$$w^2/2 = k't + \text{constant} \quad \ldots\ldots\ldots\ldots \quad 5.3$$

$$y^2 = 2kDt + \text{constant} \quad \ldots\ldots\ldots\ldots \quad 5.4$$

choosing the boundary conditions y= 0 When t= 0 gives

$$y^2 = 2kDt = k_p t \quad \ldots\ldots\ldots\ldots \quad 5.5$$

Equation 5.5 is the well-known parabolic rate law, where $k_p$ is the parabolic rate constant. Jander (1927) applied the parabolic law, developed for planar interface reactions, to powdered compacts.

Equation 5.6 given below is the Jander equation relating the fraction of reaction completed to time, where $k_j$ is the rate constant.

$$2k_j t = 2kDt/r_o^2 = [\ 1 - (1-R)^{1/3}]^2 \quad \ldots\ldots\ldots\ldots\ 5.6$$

where R is the fraction reacted, t is the time, $r_o$ is the initial particle size of the reacting species and $k_j$ is a constant containing the diffusion coefficient.

Dunwald-Wagner (1934) derived an equation for solid state reaction analysis, based on a solution to Fick's second law for diffusion into or out of a sphere of radius r at zero or uniform concentration at time t=0, with constant concentration of diffusing species at the surface

$$(1-R) = 6/\pi^2 \sum_n^{\infty} = 1(1/n^2)\exp(-n^2\pi^2 Dt/r_o^2) \quad \ldots\ldots\ldots\ldots\ 5.7$$

where n is an integer series.

Serin and Ellickson (1941) expressed the Dunwald-Wagner equation in terms of the fractional completion of the process.

$$k_{se}t = \pi^2 Dt/r_o^2 = \ln 6/\pi^2(1-R) \quad \ldots\ldots\ldots\ldots\ 5.8$$

where $k_{se}$ is the rate constant containing the diffusion constant.

### 5.2.2 Phase Boundary Model

When the diffusion through the product layer is so rapid that the reactants cannot combine fast enough at the reaction interface to establish equilibrium, the solid state reaction is phase-boundary controlled. According to Laidler (1958) when a discontinuous

product phase occurs, the rate determining step may be the chemical process occurring at the phase boundary. Under these circumstances, the rate is determined by the available interface area, and such processes are referred to as topochemical.

Equations relating reduction and time have been derived for simple geometrical systems assuming that 1) the reaction rate is phase boundary controlled 2) the reaction rate is proportional to the surface area of the fraction of unreacted material and 3) the nucleation step occurs immediately, so that the surface of each particle is covered with a layer of product. The models developed from the foregoing boundary conditions are termed phase boundary or contracting-volume kinetic models. For spherical particles:

$$k_{pb}t = kt/r_o = 1-(1-R)^{1}/3 \quad \ldots\ldots\ldots\ldots\ldots\ldots\ldots\ldots \quad 5.9$$

where, $k = -dr/dt$

$k_{pb}$ is the rate constant

### 5.2.3 Nuclei-Growth Model

The solid state reaction models thus far discussed have been based on the assumption that, initially surface diffussion rapidly coats the surface of the reacting particle with a continuous product layer. However, the subsequent rate of reaction can be taken to be the nucleation of product at active sites and the rate at which the nucleated particles grow. According to Welch (1953) such a mechanism is possible whenever the

product phase is partially miscible in one of the reactants. All of the nuclei growth equations developed are of the general form

$$\ln [1/(1-R)] = kt^m \quad \ldots\ldots\ldots\ldots\ldots\ldots 5.10$$

Where m is a parameter which is a function of 1) reaction mechanism 2) nucleation rate and 3) geometry of the nuclei and k is the rate constant.

If a solid state reaction can be represented by a nuclei growth model a plot of ln ln [1/(1-R)] versus lnt should yield a straight line with slope m and intercept lnk.

## 5.3 Analysis of Experimental Data

The mechanism of reduction of Mamatwan manganese ore was discussed in the previous chapter. The reduction of the ore was found to take place in three consecutive steps.

As a further test of the above conclusions, kinetic data were treated mathematically. For the data ranging from 0 to 30 percent reduction at the temperatures above 1200°C, the rate of reduction of oxide phase was defined as dx/dt where x is the fractional reaction and is equal to the slope of the curve for reduction versus time. The relationship between rate and T has usually been expressed as:

$$\text{Rate} = A \exp(-Q/RT) \quad \ldots\ldots\ldots\ldots\ldots\ldots\ldots\ldots 5.11$$

where, Q is the activation energy
R is the gas constant
T is the absolute temperature
A is the pre-exponential factor

It is evident that a plot of ln rate versus 1/T should give a straight line with slope equal to -Q/R. Such a plot is shown in Figure 5.1. Apparent activation energy for this stage of the reduction was found ~ 61.03 kJ which may indicate that this part of the process is controlled by gaseous diffusional processes across the porous oxide product layer. This is substantiated by the fact that a porous oxide product layer forms around ore grains (See Figure 4.28 ). The porosity of the product layer was confirmed qualitatively by image analysis. It is clear that the duration of this stage is too short to have a controlling effect on the total reduction rate.

When the reduction curves obtained above 1200$^{o}$C are examined carefully they are seen to be almost straight from about 30 level reduction to 70 percent reduction level at 1350 $^{o}$C and the curves become concave down thereafter. The reduction curves which are seen to be straight indicate that the rate of the reduction reaction is constant during this part of the process. This linear relationship of reduction with time shows that the diffusional process is not the rate limiting step in this stage, i.e. the supply rate of the reductant is equal to or greater than its consumption (Biswas, 1981).

After reducing the higher manganese oxides to MnO the reduction proceeds mainly according to the reactions:

$$5MnO + 9CO = Mn_5C_2 + 7CO_2 \quad \ldots\ldots\ldots\ldots\ldots 2.1$$

$$CO_2 + C = 2CO \quad \ldots\ldots\ldots\ldots\ldots 2.2$$

During the reduction, a clear interface develops between the carbide phase and the MnO (Figure 4.14). Since the solid carbon cannot diffuse in the ore, most of the reaction may be considered localized at $MnO/Mn_5C_2$ interface. The reactant CO gas and product $CO_2$ gas diffuses through the available porosities and microcracks of the product carbide layer. The rate of this reaction is constant provided that sufficient carbon is present to saturate the carbide layer. The rate was considerably effected by changing the gas atmosphere from argon to CO. At higher temperatures it can be expected that the rate of carbon gasification step is high enough. Since chemical reaction has higher activation energy than gaseous diffusion, the former will increase at a much greater rate with increase in temperature than the latter. Figure 4.2 shows remarkable effect of temperature on this stage. Therefore chemical reaction between oxide phase and reducing gas is most probably rate controlling step in this stage.

It was mentioned that the rate equation for an interfacial reaction is applicable to the carbothermic reduction of MnO (Terayama 1985; Terayama 1982). Therefore, by considering reduction mechanism it was decided that phase boundary model is applicable to the kinetic data.

$$(1 - (1 - R)^{1/3}) = kt \quad \ldots\ldots\ldots\ldots\ldots 5.9$$

where R is the fraction of reduction of oxide.

A plot of $(1-(1-R)^{1/3})$ vs t is shown in Figure 5.2. As seen in this figure, the plot is linear at the earlier stages, but this relationship holds no longer at the later stages where the measured fractional reaction becomes lower than the calculated values from equation 5.9. This deviation at the later stages is thought to be caused by the additional resistance which occurs when the oxide phase is completely covered by the carbide phase which makes difficult direct contact between oxide phase and reducing gas, i.e the chemical reaction rate exceeds the supply rate of the reductant agent. This is also an indication of a change in the mechanism. The slopes of the lines in the chemical control region start to decrease after the linear section with increasing degree of the reduction (i.e., the reduction becomes increasingly diffusion controlled) and a new mechanism which involves mixed kinetics of interfacial and diffusion is to be considered.

By using equation 5.9 and regression analysis of kinetic data in Figure 5.3 the rate constants for the temperatures 1350°C, 1300°C, and 1250°C were calculated for the linear portions. The values are tabulated in Table 5.1.

Table 5.1

Regression analysis of second stage kinetic data

| Temperature (°C) | Rate constant (k) | Correlation coefficient | Standard error estimate |
|---|---|---|---|
| 1350 | $7.301 \times 10^{-03}$ | 0.994 | 0.140 |
| 1300 | $3.948 \times 10^{-03}$ | 0.996 | 0.007 |
| 1250 | $3.201 \times 10^{-03}$ | 0.994 | 0.008 |

By using the values of k from Table 5.1, Arrhenius plot of the kinetic data for this stage was drawn which is shown in Figure 5.4. Apparent activation energy for the interfacial reduction reaction of MnO phase in the ore was determined from the slope of the line is 153.32 kJ. This value also suggested that reduction reaction proceeded chemically-controlled after about 4 minutes retention time. Lien et al (1971) reported that at higher temperatures ( > 1300°C ) the rate of reduction of FeO would be controlled by the reduction reaction of FeO by CO since rate of the gasification reaction is high at these temperatures.

As a further test of this conclusion, the experimental data of the last part the reduction were treated by some diffusion-controlled kinetic models. Modified

Dunwald-Wagner's equation which was expressed by Serin and Ellickson (1941) in terms of the fractional completion of the process is expressed as

$$k_{se}t = \pi^2 Dt/r_0^2 = \ln 6/\pi^2(1-R) \quad \ldots\ldots\ldots\ldots\ldots\ldots \quad 5.8$$

This equation was found to hold up for the latest part of the reduction. Figure 5.5 shows the replot of the experimental data according to the equation 5.8.

From the slopes of straight lines shown in the Figure 5.5, the rate constant, $k_{se}$, was determined from which the diffussion constant at each temperature was calculated by multiplying $k_{se}$ values with $r_0^2/\pi^2$ These values are given in Table 5.2.

Table 5.2

Diffusion values for third stage kinetic data

| Temperature (°C) | $k_{se}$ (slope) | D ($cm^2$/sec) |
|---|---|---|
| 1350 | 0.0480 | $3.76 \times 10^{-7}$ |
| 1300 | 0.0207 | $1.62 \times 10^{-7}$ |
| 1250 | 0.0105 | $8.23 \times 10^{-8}$ |

Activation energy of the reduction in this stage was found as 310.40 kJ. It was calculated from a plot of log D versus 1/T which is shown in Figure 5.6.

Although no data are available in literature for the diffusion coefficient of carbon in iron-manganese carbide and diffusion coefficient of $Mn^{+2}$ ions in manganese oxide, data are available for several metals in similar structures. The diffusion coefficient for carbon in iron (Elliott, 1963) is $10^{-5}$ $cm^2/s$ at 1400 $^oC$. In the same study (Elliott, 1963) it was also mentioned that diffusion coefficient of several divalent and trivalent metals in oxide structures vary between $10^{-9}$ and $10^{-7}$ $cm^2/sec$ at high temperatures. Therefore above calculated diffusion coefficient values can be attributed to the diffusion coefficient of metal ions in oxide phase. As a result it can be predicted that diffusion rate of manganese ions in oxide phase would be slower than diffusion rate of carbon in carbide phase and it is most probably the rate controlling step in this stage.

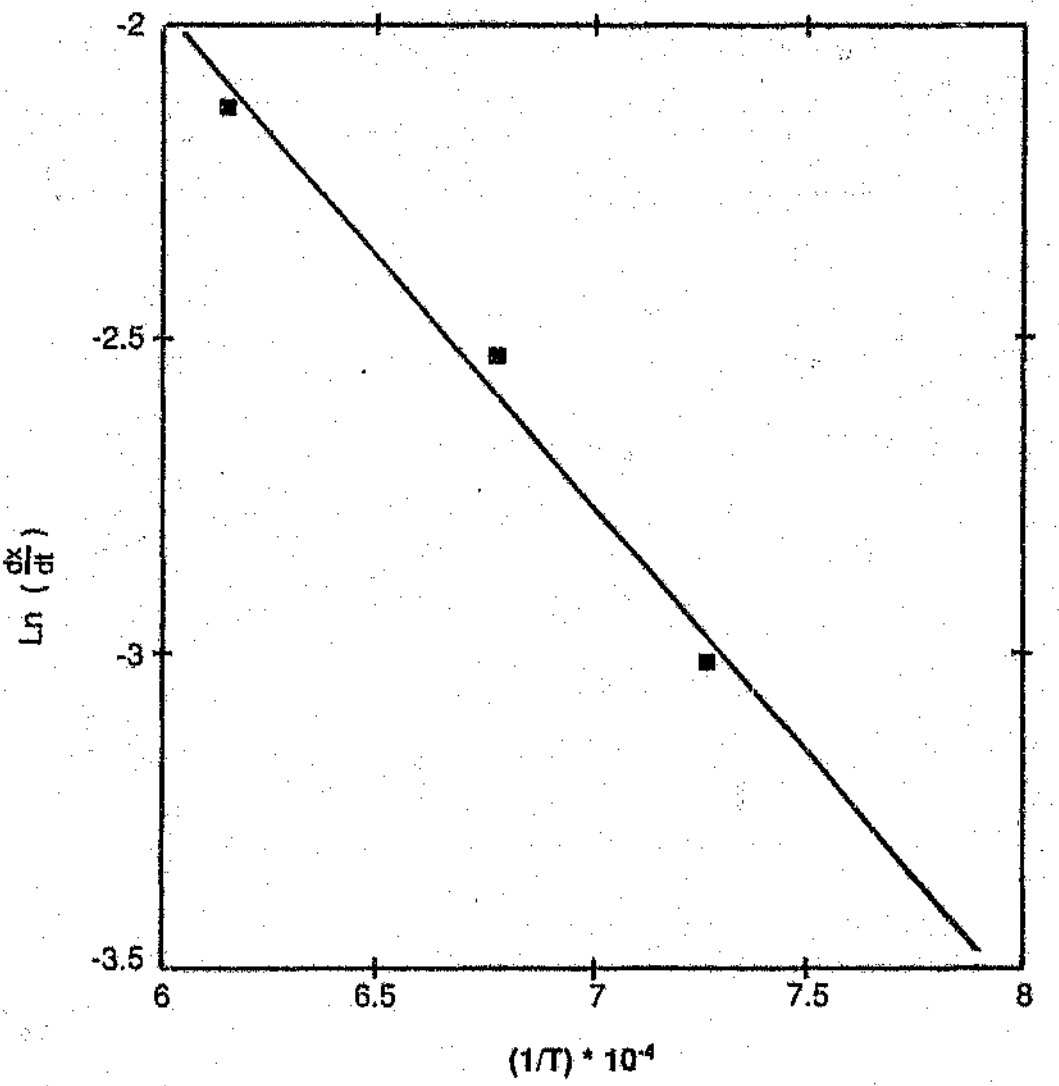


Figure 5.1 Arrhenius plot of the first stage kinetic data.

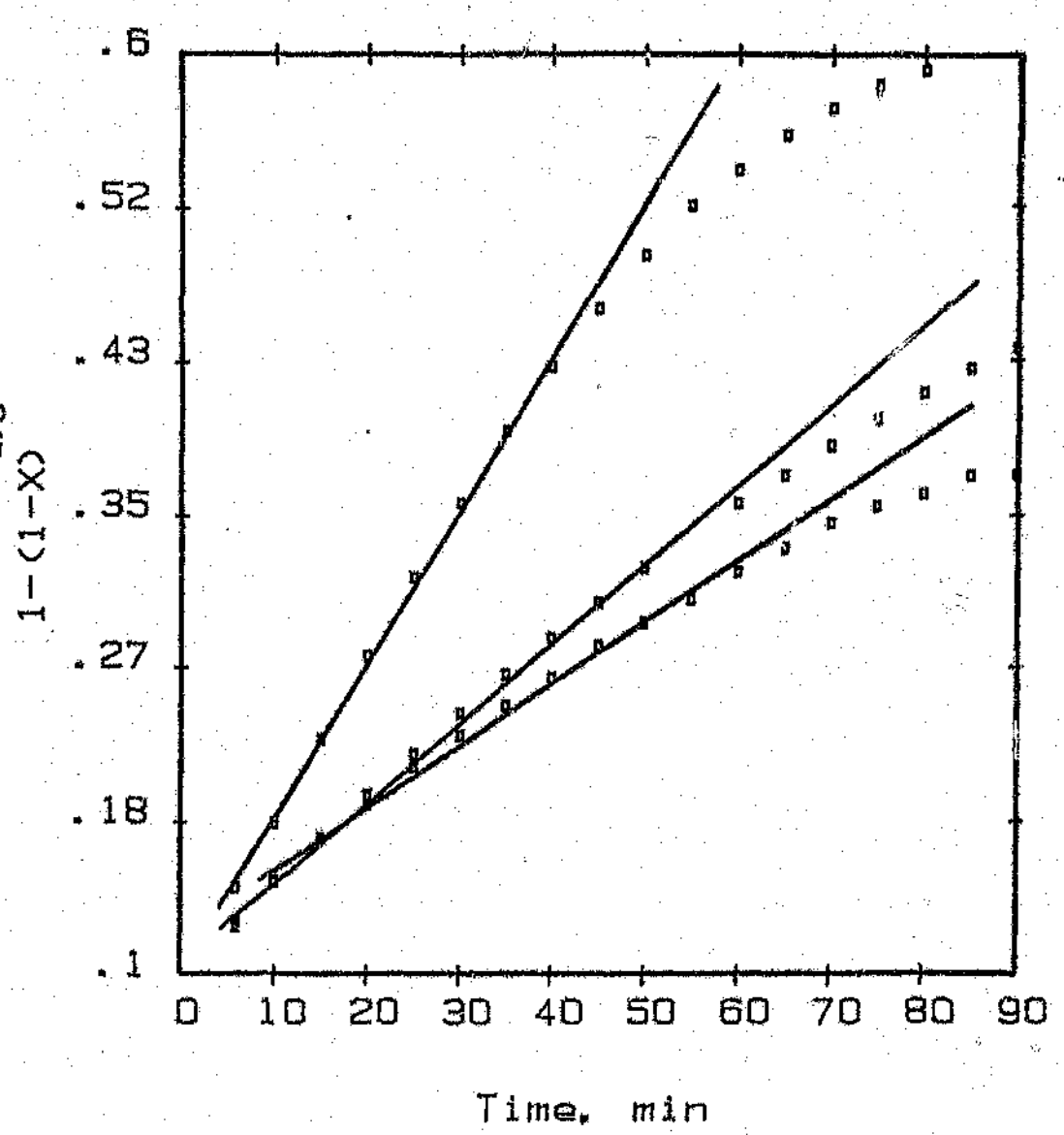


Figure 5.2 Application of kinetic data to Equation 5.9 after first stage of the reduction.

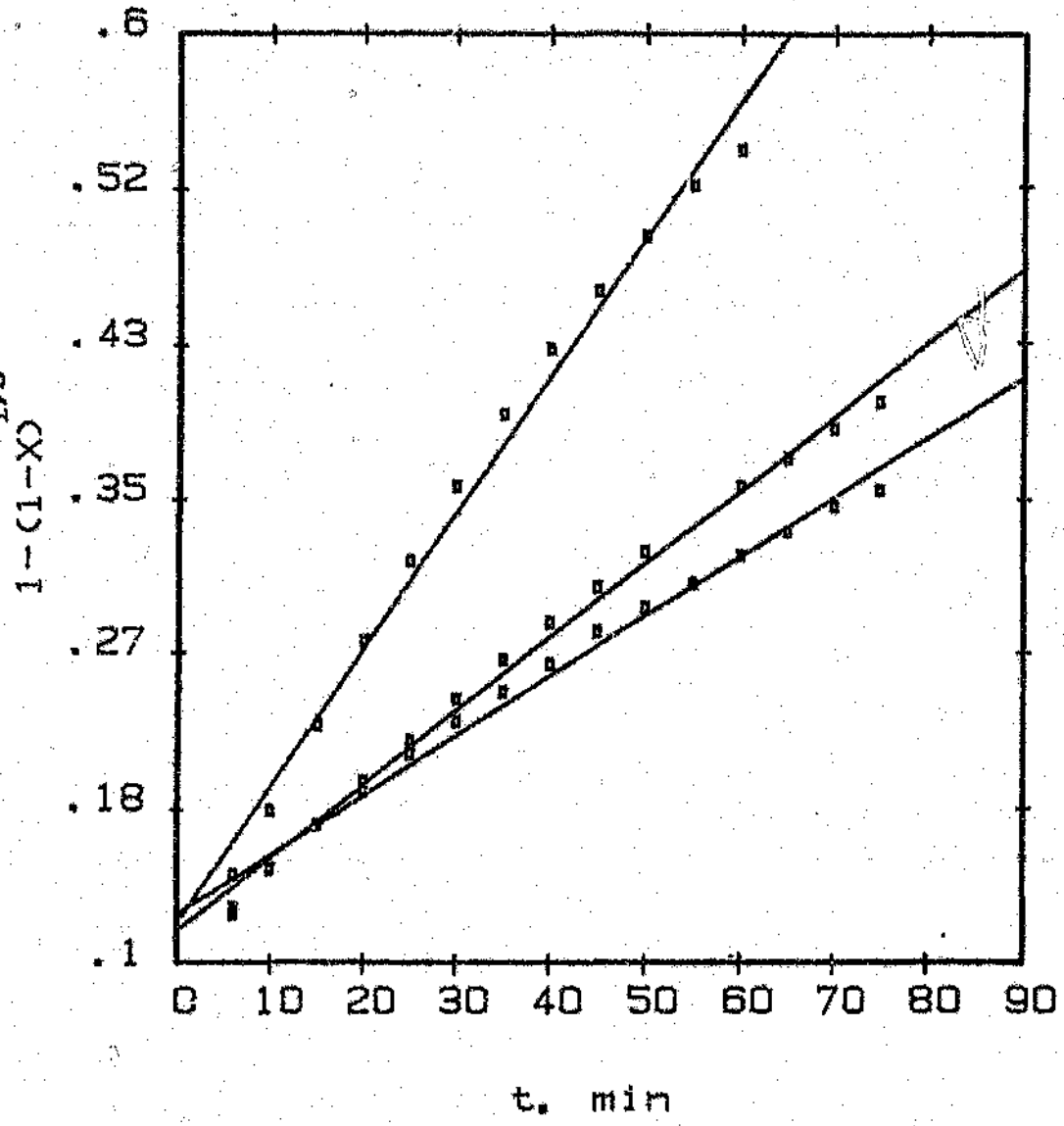


Figure 5.3 Regression analysis of the second stage kinetic data.

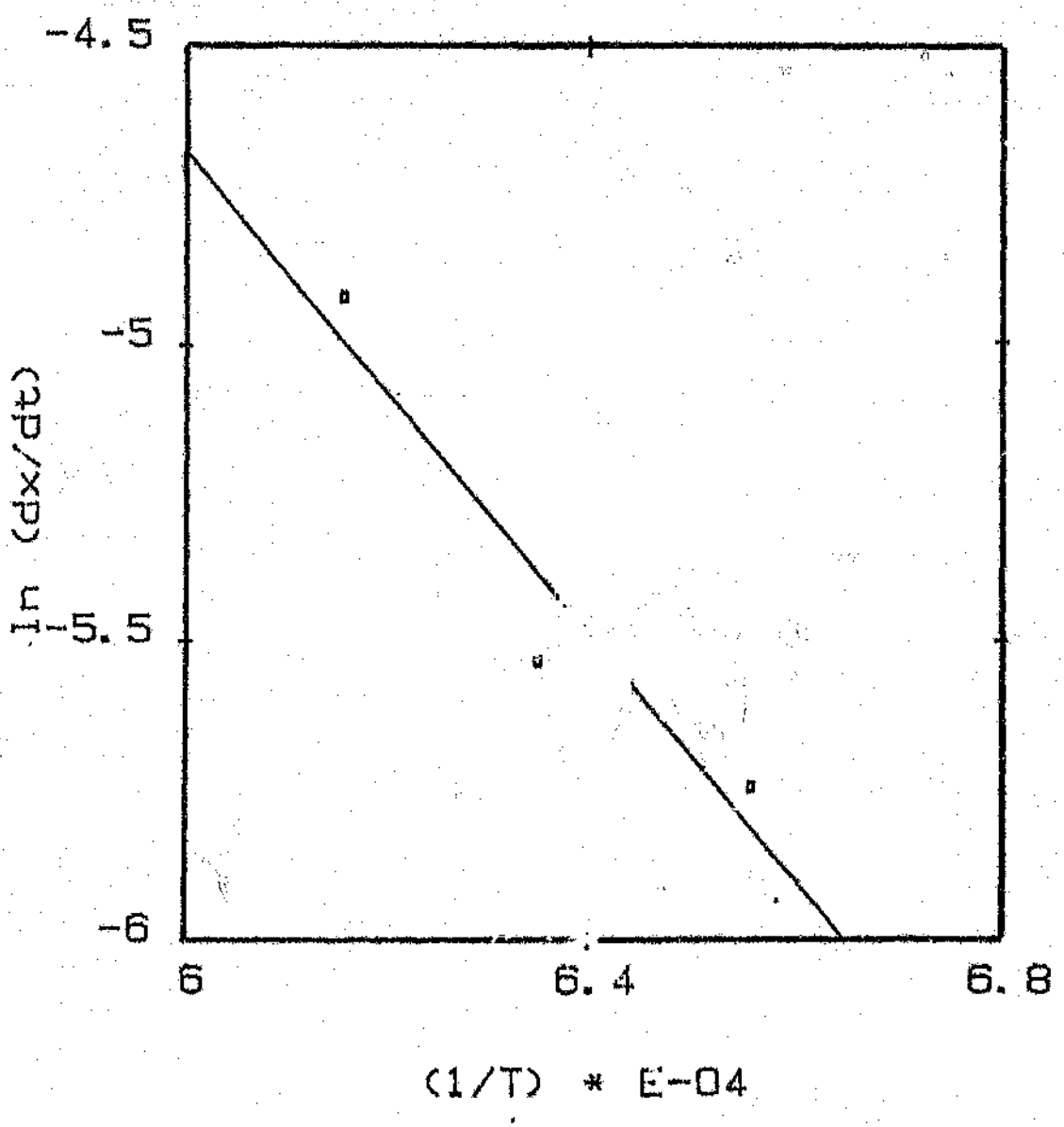


Figure 5.4 Arrhenius plot of the second stage kinetic data.

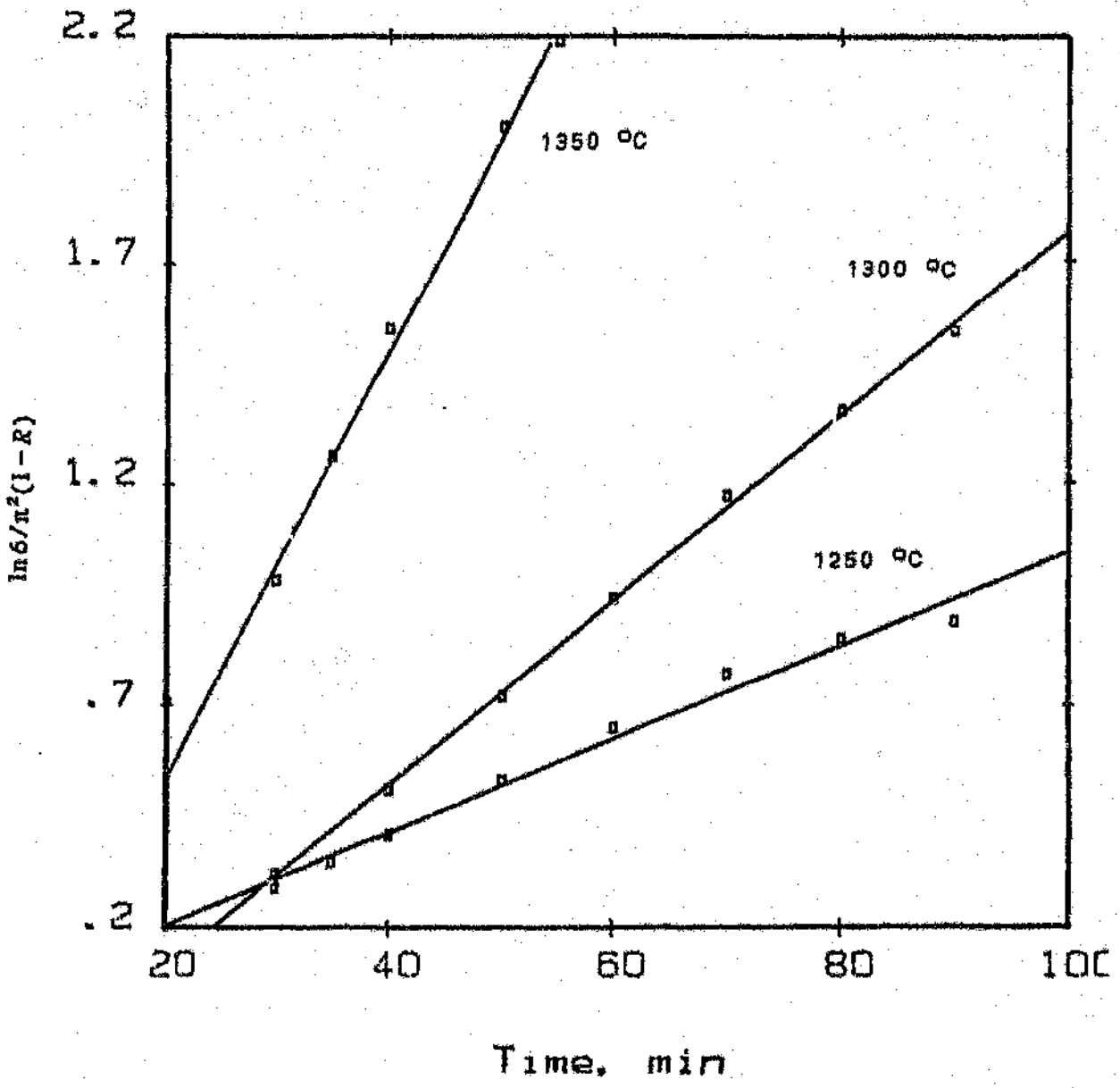


Figure 5.5 Application of equation 5.8 to the third stage kinetic data.

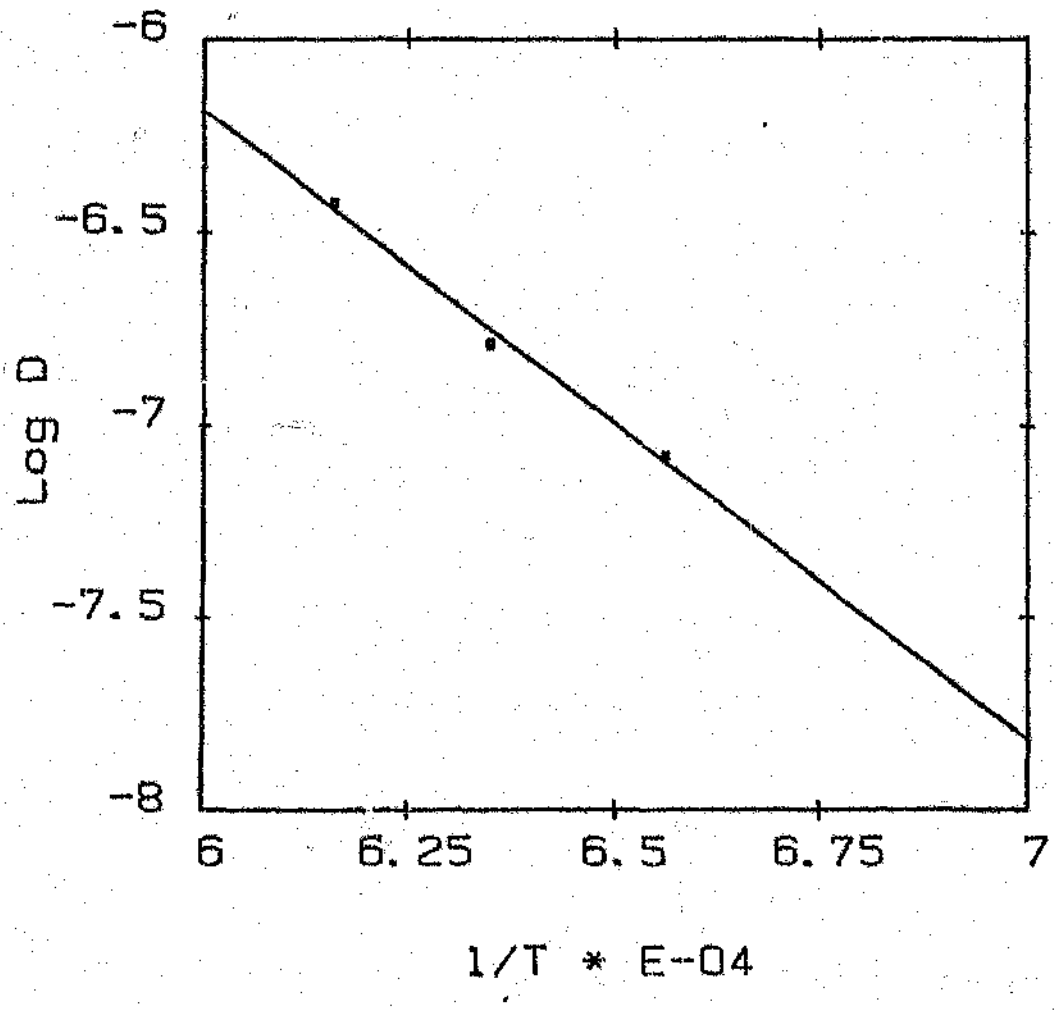


Figure 5.6 Arrhenius plot of the third stage kinetic data.

## 6 CONCLUSION

The mechanism and kinetics of reduction of the manganese ore from the Mamatwan ore mine has been studied by thermogravimetric (TGA) analysis, X-ray diffraction analysis (XRD), optical microscopy and energy dispersive analysis of x-rays (EDAX) between 1100°C and 1350°C with pure graphite under argon atmosphere.

During the preheating of the Mamatwan manganase ore a total mass loss of about 17.5 percent was observed. The rate and degree of reduction of preheated Mamatwan ore were found to increase with increasing temperature and decreasing particle size; markedly, at temperatures 1300°C and 1350°C with graphite under argon atmosphere. Reduction products were found as manganese-iron carbide mainly $(Mn, Fe)_5C_2$ and calcium silicate ($Ca_2SiO_4$) at 1300°C and 1350°C.

The reduction mechanism of Mamatwan ore was discussed in three consecutive stages. The first stages of reduction which was proposed to be taking place between 0-30 percent reduction ended after about 4 minutes reduction time at 1350°C. In this short period of reduction higher manganese oxides and iron oxide were reduced to their lower states by solid carbon or carbon monoxide gas. Reduction process was limited to this stage at 1100°C and 1200°C. Apparent activation energy was calculated as 61.03 kJ which was attributed to the gaseous diffusional processes across the porous oxide product layer.

The metallic nuclei were formed as randomly distributed small metallic globulus around the manganesous oxide areas inside of each manganese ore particle and each nucleus grew in size until a complete alloy coverage formed around each particle. This was proposed to be the second stage of reduction which took place between 30-70 percent reduction and was controlled mainly by interfacial chemical reaction. High degree of metallization and silicate formation with MnO dissolved in the silicate phase was observed at the end of this stage. Interfacial reaction model was applied to this stage and the apparent activation energy was found as 153.32 kJ.

In the last stage, reduction of remaining oxide by carbon dissolved in the carbide proceeded by a diffusional mechanism which was proposed to be taking place after 70 percent reduction. Very slow reduction was possibly due to the migration of $Mn^{+2}$ ions in oxide phase which was supported by the apparent activation energy of 310.40 kJ.

For further work on investigation of kinetics and mechanism of Mamatwan manganese ore, different reducing agents such as coal, coke, anthracite etc can be used to determine the effects of ash content, fixed carbon, volatile content on reduction. To determine the effects of agglomeration on reduction process, briquettes and/or spherical pellets as well as loose powder can be used. The proposed reduction mechanism and mathematical modelling can be tested by using a different approach to the problem such as larger scale testing on a pilot plant type of facilities.

## 7 REFERENCES


Antonov, V.K. and Chufarov, G.I. (1961) Reduction of MnO by solid carbon. Tr. Inst. Met. Akad. Nauk SSSR, Uralsk. Filial, no.7, pp.101-105.

Ashin, A.K., Rostovtsev, S.T. and Avdeev, V.F. (1964) Kinetics and mechanism of the reduction of manganese oxides with carbon. III. Reduction of Manganous oxide. Izv. Vyssh. Uchebn. Zavedenii, chern. Met. vol.7, no.10, pp.13-16.

Benz, R., Elliott, J.F. and Chipman, J. (1973) Solid phases of the Mn-C system. Met. Trans, vol.4, pp.1449-1452.

Barcza, N.A., Jochens, P.R. and Howat, D.D. (1971) The mechanism and kinetics of reduction of Transvaal chromite ores. Electric furnace proceedings, vol.29, pp.88-93.

Barnes, A.R. (1981) The prereduction and smelting of UG-2 chromite concentrates, Msc thesis, University of Witwatersrand.

Bystrom, A and Mason, B. (1943) The crystal structure of braunite. Arkiv. Kemi. Min. Geol, vol.16, pp.133-146.

Chipman, J. and Thomson, C.N (1952) ASM, 44, pp.1222-1224.

Davies, M.W and Richardson, F.D. (1959) Non-stoichiometry of manganous oxide, Trans. Farad. Soc, vol.55, pp.604-610.

de Villiers, J.P.R. (1975) The crystal structure of braunite with reference to its solid solution behaviour, Am. Min, vol.60, pp.1098-1104.

de Villiers, J.P.R. (1971) The geology and mineralogy of the Kalahari manganese field, north of Sishen, Cape province. S.A. Geol. Survey Memoir, no.59, pp. 1-84.

de Villiers, J.P.R. (1973) A mineralogical investigation of natural and heated Mamatwan manganese ore. Johannesburg. NIM, Technical memorandum. No. 1. 12pp

de Villers, J.P.R. (1973) A mineralogical investigation of natural and heated Mamatwan manganese ore, Johannesburg, NIM, Technical memorandum, Project 07772 no.1.

Dewar, K. and See, J.B. (1978) The influence of carbonaceous reducing agents on the rate of reduction of representative manganese and chromium ores, NIM, Report-no.1968.

Dollimere, D. and Tonge, K.H. (1971) Thermo-analytical behaviour of some synthetic manganese oxides, Therm. Anal. vol.2, Proc. 3rd, ICTA, Davos, pp.91-103.

Downing, J.H. (1963) Fundamental reactions in submerged arc furnaces. Electric furnace proceedings, pp.288-296.

Dressel, W.M. and Kenworthy, H. (1961) Thermal behaviour of manganese minerals in controlled atmospheres, U.S Bureau of Mines, Report of investigations 5761, pp.4-15.

Dunwald, H. Wagner C. (1934) Z. Physik. Chem., (Leipzig), B24, (1), p53.

Elliott, J.F. and Gleiser, M. (1963) Thermochemistry for steelmaking, vol.II. Reading, Mass., Addison-Wesley.

Featherstone, R.A. (1975) Application of Mamatwan Manganese ore, INFACON 74, Glen, H. (ed), Johannesburg, S.A inst. Min. Metall, pp.263-273.

Gericke, W.A. (1989) The establisment of a 500.000 T/A sinter plant at Samancor's Mamatwan manganese ore fines. Proceedings. INFACON-89. vol.1, 5th international ferroalloy congress, Held at Neworleans, Louisianne, USA, April, 1989, pp.24-33.

Glosser, F.P. (1962) J.Amer.Ceram. , 45, pp.242-249.

Grimsley, W.D. (1977) A study of the characteristics and mechanism of reduction of manganese ore by solid carbon. Msc. Dissertation, University of the Witwatersrand.

Hahn, W.C. and Muan, A. (1960) Studies in the system Mn-O. The $Mn_2O_3$ - $Mn_3O_4$ and $Mn_3O_4$ - MnO equilibria, Am. J. Sci. vol.258, no.1, pp.66-78.

Iida, S.O. and Inonou, O. (1962) Phy. Soc. Japan, vol.17, supp. B-1, p.281.

Isobe, M. (1951) Sci. Rep. Inst. Tohoku Univ. Ser, A,3, pp.540-620.

Jander, W. (1927) I.Z. Anorg. Chem., vol.163, 1/2, 1.

Jones, R., and Meichack, K. (1990) THERMO. A software for thermodyanamic calculations, Council for Mineral Technology, Pyrometallurgy division.

Kleyenstuber, A.S.E. (1982) A review of the geology and mining of the Kalahari manganese field, South Africa inst. min. Metall, Johannesburg, pp.213-220.

Kleyenstuber, A.S.E. (1979) 'n mineralogiese ondersoek van hoetemperatuur-reduksieprodukte van mangaanerts vanuit die Mamatwanmyn, Kalaharimangaanveld. M.Sc thesis (unpubl.) Rand Afrikaans Univ, Johannesburg, 125pp.

Kleyenstuber, A.S.E. (1984) The mineralogy of the manganese-bearing Hotazel formation of the proterozic Transvaal Sequence in Grigualand West, South Africa. Trans. geol. soc. S. Afr. 87, pp.257-272.

Klingsberg, C. and Roy, R. (1960) Solid-solid and solid-vapour reactions and a new phase in the system Mn-O, J. Am. Ceram. Soc, vol.43, no.12, pp.620-626.

Kolchin, O.P. (1968) The mechanism of reduction of metals from their oxides by carbon. Mekh. KInet. Vosstanov, metal. mater. Simp. (NIM translation no.244) pp.40-48.

Koursaris, A., Kleyenstuber, A.S.E. and Finn, C.W.P. (1983) A mineralogical investigation of the reduction of Mamatwan manganese ore with carbon, Spec. Publ. Min. Metal. Inst. S.A, 7, pp.375-382.

Koursaris, A. and See, J.B. (1975) Reactions in the production of high carbon ferromanganase from Mamatwan Manganese ore. NIM. Report-no.1975.

Kucukkaragoz, C.S. and Finn, C.W.P. (1983) The influence of reducing atmospheres, spinel compositions, and gangue components on the mechanism and kinetics of reduction of chromite fines and agglomerates, PhD Thesis, University of Witwatersrand.

Kuo, K. and Persson, L.E. (1954) A contribution to the constitution of the ternary system Fe-Mn-C, Isothermal sections at 1050°C, 910°C and 690°C, J. Iron steel Inst. vol.178, pp.39-44.

Laidler, R. (1958) United nations peaceful uses of atomic energy 2nd international conf., Geneva, proceedings, vol.20, pp.116-119.

Lien, H.O.,El-Mehairy, A.E, and Ross, H.U. (1971) A two-zone theory of iron oxide reduction. Journal of Iron and Steel Institute, July. pp.541-545.

McRae, L.B. (1981) The prereduction of Mamatwan-type ores. NIM. Report-no. 2020.

McRae, B.L. (1977) Proc. of the int. Symp. on Agglom, 2nd, Anlanta, Ga, Mar. 6-10, Publ. AIME, vol.1, pp.356-377.

Mikolajczak, L. (1974) Ferro-alloys review: Ferromanganase review, Met. Bull. Mon, no.2, pp.21-23.

Morral, F.R. (1984) Manganese - a chronology and bibliography, CIM bulletin, vol.77, no.86, pp.72-75.

Muan, A. (1959) Phase equilibria in the system manganese oxide-$SiO_2$ in air, Am. J. Sci, vol.257, pp.297-315.

Naruse, W. (1975) Manganese alloy production by the sintering process. INFACON 74, Glen, H. (ed), Johannesburg, S.A inst. Min. Metall, pp.69-76.

Nguyen, V.H. and Ryzhonkov, D.I. (1972) An investigation of the reduction of a mixture of wustite and manganese oxide by carbon. Steel in USSR. vol.2, pp. 178-180.

Pentz, R.D. (1970) 'n ondersoek na die veredeling van laegraadse mangaanerts met besondere verwysing na die reduseerbaarheid. M.Sc. Dissertation, Potchefstroom University.

Pilter, P. (1967) The reduction of metallic oxides with solid carbon, Kohasz. Lapok. vol.100, pp.303-308.

Pilter, P. (1967) The reduction of manganese oxides in solid state with carbon monoxide and hydrogen. Kohasz. Lapok, vol.100, pp.492-500.

Rankin, W.J. (1980) The kinetics of the reduction of manganese oxide by graphite. Journal of SAIMM, pp.239-250.

Rao, Y.K. (1971) Met. Trans, vol.2B. p.1439-1447, 1971.

Ribound, P.V. and Muan, A. (1963) melting relations of CaO-Manganese oxide and MgO-manganese oxide mixtures in air. J. Am. Ceram. Soc. vol.46, no.1, pp.33-36.

SAMANCOR (1979) Brochure describing the manganese and iron ore interests of the Samancor Group of Companies, SAMANCOR, Johannesburg, pp20.

Schurmann, E. and Geissler, K.I. (1977) Giessereiforschung, 29, (4), pp.153-159.

Schenck, S., Frohberg, M.G., and Steinmetz, E. (1963) Arch. Einsenhuttenwes.,34, pp.37-42.

Serin, B and Ellickson, R.T. (1941) J. Chem. Phys., vol.9, 742.

Serin, B. and Ellickson, R.T.J. (1977) Chem. Phys. 1941, vol.9, 742.

Shantarin, V.D., Shestakovskii, O.F. and Suchilnikov, S.I. (1972) Kinetics of the reduction of manganese concentrates with solid carbon. Communication.1. Steel in the USSR, pp.790-792

Soykan, O. and Eric, R.H. (1988) The solid state reduction characteristics of the Bushveld complex chromites PhD Thesis, University of Witwatersrand.

Taljaardt, J. (1982) Major manganese ore fields, Republic of South Africa, Unpubl. Rep. SAMANCOR, Johannesburg, pp7.

Taplin, H.J (1974) A unifying concept for the reaction kinetics of powders. Jour. Amer. Cer. Soc. vol.57, no.3, pp.140-143.

Terayama, K. and Masao, I. (1985) Study on reduction of manganese oxide with carbon by enffluent gas analysis method. Transaction of the Japan inst. of metals. vol.26, no.2, pp.108-104.

Terayama, K. and Ikeda, M. (1982) J.Japan Inst. Metals, 46, 1138 (in Japan).

Tien, R.H. and Turkdogan, E.T. (1977) Mathematical analysis of reactions in metaloxide/carbon mixtures. Metal. Trans, vol.8B, pp.305-313.

Tsylev, L.M. (1963) The smelting of ferroalloys in the blast furnace using oxygen enriched blast. Pergamon Press. p.14.

Van Hook, H.J. and Keith, M.L. (1958) The system $Fe_3O_4$-$Mn_3O_4$, Am. Mineral, vol.43, no.1, pp.69-83.

Volkert, G. and Frank, K.D. (1972) Metallurgie der Ferrolegierungen, (Eng. translation: NIM, Johannesburg, Tr-516.), pp.400-412.

Vogel, R. and Doring, W. (1935) Arch. Eisenhuttenwes., 9, (5), pp.247-252.

Welch, A.F.E. (1953) Solid-solid reactions, solid state chemistry, Ed. WE Garner. Butterworths sci. publ.

Yagihashi, T. Asada, K., Atarashiya, K., Ichinose, S. and Hanada, H. (1963) Properties and reduction of manganese ores. II. manganese ore reduction with CO gas or CO-$CO_2$ gas mixtures. Tetsu to Hagane, vol.49, no.8, pp.1059-1065.

**Author: Burucu E.**
**Name of thesis: Kinetics And Mechanism Of The Reduction Of Mamatwan Manganese Ore Fines By Solid Carbon.**

***PUBLISHER:***
**University of the Witwatersrand, Johannesburg**
**©2015**

***LEGALNOTICES:***

**Copyright Notice:** All materials on the University of the Witwatersrand, Johannesburg Library website are protected by South African copyright law and may not be distributed, transmitted, displayed or otherwise published in any format, without the prior written permission of the copyright owner.

**Disclaimer and Terms of Use:** Provided that you maintain all copyright and other notices contained therein, you may download material (one machine readable copy and one print copy per page)for your personal and/or educational non-commercial use only.

The University of the Witwatersrand, Johannesburg, is not responsible for any errors or omissions and excludes any and all liability for any errors in or omissions from the information on the Library website.